BELGIAN SCIENCE POLICY OFFICE
Second Multiannual Scientific Support Plan for a Sustainable Development Policy
SPSD II Global Change, Ecosystems and Biodiversity

Mud Origin, Characterisation and Human Activities
MOCHA

Contract EV/36/35A

Scientific Report Year 1 (01/04/2004 – 31/03/2005)

Characteristics of Cohesive Sediments on the Belgian Continental Shelf

Royal Belgian Institute of Natural Science
Management Unit of the North Sea Mathematical Models (MUMM)
Gulledelle 100, B-1200 Brussel

Universiteit Gent. Renard Centre of Marine Geology (RCMG)
Krijgslaan 281, S-8, B-9000 Gent

Katholieke Universiteit Leuven, Historic Geology Section (KUL)
Redingenstraat 16, B-3000 Leuven

Table of contents

1. Introduction

The report focuses on a description of the cohesive sediments on the Belgian Continental Shelf. These data will form the basis to trace the origin of the mud (see next scientific report), but also to define with more accuracy the parameters necessary for sediment transport modelling. The variability in mechanical and mineralogical composition and geological history will attract attention and reflect the different origins and the mixing of these sediments.

The report is divided in five chapters and consists of the **first part work package (Characteristics of the cohesive sediments**) of the project, which was essentially meant to review the existing knowledge on cohesive sediments in the Belgian coastal zone (figure 1.1), to classify the cohesive bottom and suspended sediments based on existing and new mineralogical, geological, paleontological and erosion data and to carry out field experiments. This part is the backbone on which the two other work packages will be based (analysis and interpretation of the data).

The report is divided - as far as possible – according to the task description of the project proposal. The second chapter is devoted to a review of the knowledge on cohesive sediments on the Belgian Continental Shelf. Focus was put on the dynamical/mechanical differences and on the distribution of cohesive sediment using recent and historical data sets (Gilson collection). The next chapter (3) is used to characterize the suspended particulate matter on the BCS according to floc size and SPM concentration variation during various time scales (tides, neap-spring and seasons). The analysis of suspended and bottom samples according to their clay minerals, microfossils and grain sizes is presented in chapter 4. In chapter 5 the cohesive bottom and suspended sediments are classified following their geology, their dynamic properties and their clay mineral and microfossil content.

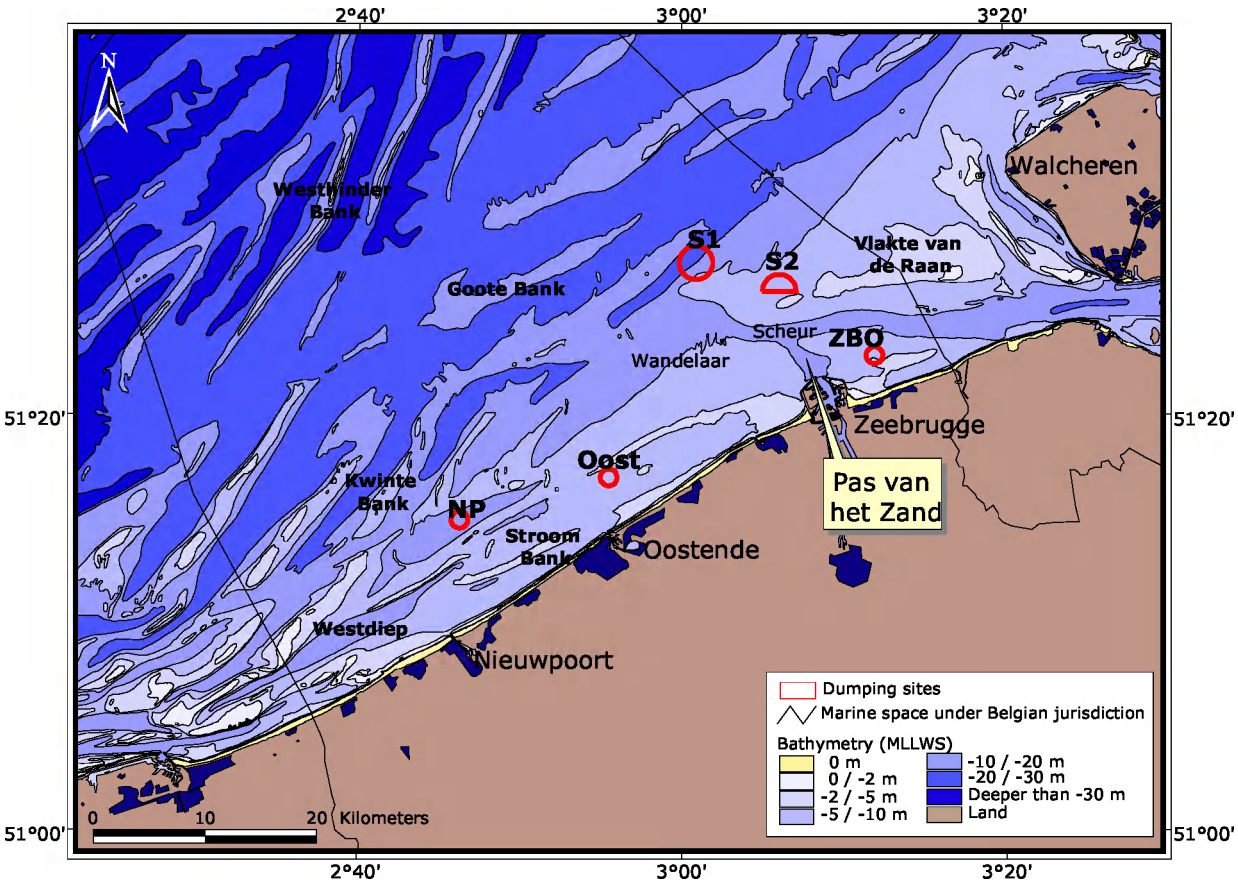

Figure 1.1: Belgian coastal area. On the map are indicated the dumping sites (S1: Br&W S1; S2: Br&W S2; ZBO: Br&W Zeebrugge Oost; NPO=Br&W Nieuwpoort; Oost: Br&W Oostende), the navigation channels (Pas van het Zand en Scheur) and other locations mentioned in the report.

1.1 Partnership

In this report the scientific results of the Mocha project for the first year are presented, for which the following partnership was set up:

Royal Belgian Institute of Natural Science,
Management Unit of the North Sea Mathematical Models: Michael Fettweis, Frederic Francken, Dries Van den Eynde
Invertebrate Department: Jean-Sébastien Houziaux

Ghent University, Renard Centre of Marine Geology
Vera Van Lancker, Samuel Deleu, Els Verfaillie and Isabelle Du Four

Katholieke Universiteit Leuven, Historic Geology Section
Noël Vandenberghe, Kathleen Fontaine

Reference to this report:
Fettweis, M., Francken, F., Van den Eynde, D., Houziaux, J.-S., Vandenbergh, N., Fontaine, K., Deleu, S., Van Lancker, V. & Van Rooij, D., 2005. Mud Origin, Characterisation and Human Activities (MOCHA): Characteristics of cohesive sediments on the Belgian Continental Shelf. Scientific Report Year 1, Belgian Science Policy, 70pp+app.

1.2 Aim and summary of the project

Along the Belgian coastal zone, but mainly concentrated between Oostende and the Westerschelde estuary mud deposits and high concentrations of suspended particulate matter (SPM) occur, making the Belgian coastal waters one of most turbid in the North Sea (values of a few hundred mg/l are common). The presence of mud fields and high turbidity in an energetic environment such as the Belgian Coastal Zone (BCZ) has been the subject of various studies the origin of the mud remains however still controversial. Different mud sources have been identified, such as the Dover Strait, the erosion of clay layers, the Schelde, but reliable quantitative data are often not available, especially for the smaller sources (erosion of clay, Schelde), which could be of importance on a regional scale. The –Mocha- project aims therefore at presenting different evaluation tools and strategies in order to study these different sources of mud on the Belgian Continental Shelf. Mud is transported by natural processes, such as tides, winds, but also human activities (dredging and dumping operations) have an important influence, therefore a twofold strategy is followed:

1. Investigating the contribution of the different possible sources of mud.
2. Investigating the influence of human activities (dredging, dumping and harbour extension).

During the first part of the –Mocha- project all the relevant information on the fine grained sediment transport system will be collected and critically analysed. This part will form the major part of this report. Together with the data measured during the project this information will provide arguments to trace the origin of the mud in suspension and on the bottom in the Belgian Coastal Zone. The newly gathered data on clay mineral associations, microfossils, mechanical and erosion characteristics may indicate the origin and pathways of the suspended load and the mud on the bottom. The mechanical (density, strength) and the grain size data together with the hydrodynamic results of numerical simulations leads to a classification of dynamical sediment types and can give an indication of the erosion behaviour of the muddy sediments.

The –Mocha- project aims to increase knowledge on the cohesive sediment distribution, transport system and on the different mud sources, which is especially important because of its

effect on the economy (dredging and dumping), the environment and as such also for setting up a framework for a sustainable management of the area. The information supplied can be integrated as part of the general and permanent duties of monitoring and evaluation of the effects of all human activities on the marine ecosystem to which Belgium is committed following the OSPAR-convention (1992). Harbour extensions, deepening of navigation channels and other large scale projects (windmill farms) will continue in the future and thus the choice of e.g. efficient (from an economic and a physical point of view) dumping sites with a low environmental impact is an essential part of the sustainable management of the Belgian EEZ.

1.3 Definitions

1.3.1 Cohesive sediment (mud and clay)

Cohesive sediments are built of particles which exert significant electrostatic forces on each other. They consist of a mixture of water, clay minerals, silt, carbonates, organic matter and sand and can occur as suspensions, fluid mud, freshly deposited and very soft to hard consolidated sediments. Cohesive sediments in suspension or suspended particulate matter (SPM) consist of loose aggregates or flocs of various sizes and densities. Deposits are called mud or clays. From a geotechnical point cohesive sediments may be described by their density (table 1.1) or their strength (table 1.2).

Table 1.1: Classification of cohesive sediment based on density (Coastal Engineering Manual, 2002).

Sediment description	Bulk density (kg/m^3)
Suspension	<1100
Fluid mud	1100
Freshly deposited mud	1300
Very soft consolidated	1500
Medium consolidated	1800
Stiff consolidated	1900
Very stiff consolidated	2100
Hard consolidated	2200

Table 1.2.: Classification of cohesive sediments based on strength and consistency (British Standard Inst.).

Consistency	Field indication	Strength (kPa)
Very soft	Extrudes between fingers	<20
Soft	Easily moulded in fingers	20-40
Firm	Moulded in fingers by firm pressure	40-75
Stiff	Cannot be moulded in fingers	75-150
Very stiff	Brittle or very tough	>150

The term **mud** is used for a water-rich sediment (with a grain size <62.5 μm) containing a considerable amount of fine fraction <2 μm and in that same fine fraction a considerable amount of clay minerals. The water contents are about 60-80 weight % and bulk density is <1800 kg m^{-3}. In sedimentology the term **clay** is used for the finest fraction, but no standard limits are defined (Folk scale: <2 μm, Wentworth scale: <4 μm).

In the bottom mud of the Belgian coastal zone the <2 μm fraction is about 30% (Gullentops et al., 1976) and in the Schelde river 8 to 25% (Chen, 2003). The sand fraction (>62.5 μm) in mud is generally lower than 5%. The average silt-clay ratio of the mud from the Belgian coastal zone is 0.92, see figure 1.2; this ratio is almost not influenced by the sand content (Francken & Fettweis, 2003). In the Scheldt estuary the silt-clay ratio is lower (0.66) and increases with decreasing sand fraction (Wartel et al., 2000).

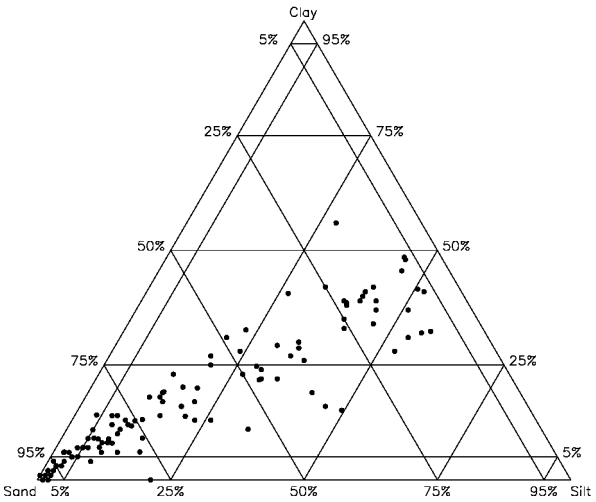

Figure 1.2: Distribution of bed samples from the Belgian coastal zone, (Folk scale; clay: <2 μm, silt: 2-62.5 μm; sand: >62.5 μm (from Francken & Fettweis, 2003)

There is a good chance that the <2 μm fraction in a sediment is positively correlated with the <62.5 μm fraction but the Pleistocene Eolian loam sediments e.g. consist dominantly of a size fraction between 62.5 and 2 μm. Therefore the simple criterion % <62.5 μm for the definition of mud may represent quite different types of sediments and has probably been introduced because of the technical simplicity of a sieve analysis.

Clay minerals and often calcium carbonate are present in the clay size fraction, and quartz and feldspars and minor muscovite as well as calcium carbonate grains are present in the silt and sand fraction. Organic matter is generally present.

The term **clay (sediment)** is used for the already compacted sediment layers, originally deposited as mud layers, occurring in the case of the Belgian North Sea at shallow depth under the sea bottom. These clay layers are either of Paleogene age containing about 20% weight of water, or from Quaternary age with higher water content; Holocene clay has a bulk density of 1500-1800 kg m^{-3}.

1.3.2 Clay minerals

Clay minerals are sheet silicates, displaying crystal lattice defects and substitutions, leading to a size of the mineral sheets generally smaller than 2 μm and to an electrical charge on the particles, which are compensated by exchangeable cations. The main groups of clay minerals which are of common occurrence in the North Sea and its surrounding are a kaolinite, an illite, a smectite and a chlorite group.

Characteristic for the **kaolinite group** minerals is the succession of sheet units consisting of one silica tetrahedral sheet linked to one octahedral sheet; the octahedral cation sites are occupied by aluminium (figure 1.3). Different types of kaolinites exist, which can be recognized by their degree of ordering in the crystal lattice. The distance between two successive units in the direction parallel to the sheets is slightly higher than 7 Å.

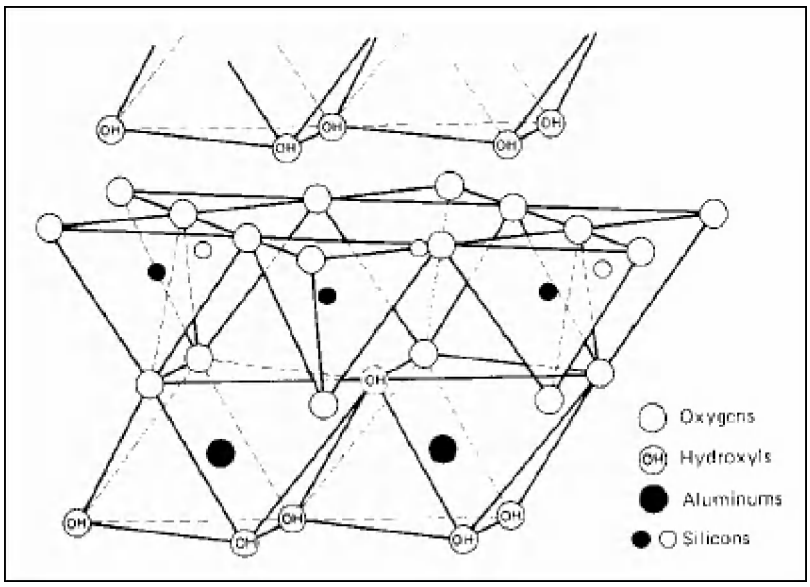

Figure 1.3: Structure of kaolinite (Course Civil and Environmental Engineering, University of Alberta)

Characteristic for the **illite group** minerals is the succession of sheet units consisting of a central octahedral layer linked above and below to the top of a silicate tetrahedral layer (figure 1.4). The cations in the octahedral layer can be variable. Fe rich varieties exist and the mineral glauconite is particularly rich in iron (glauconite grains are generally not pure mineral-glauconite). Illite is from a mineralogical point of view related to the large mica minerals muscovite and biotite. Compared to these minerals however, the clay-sized illite has more crystal defects, less potassium at the interlayer sites and a moderate exchange capacity. The distance between two successive units in the direction parallel to the sheets is about 10 Å.

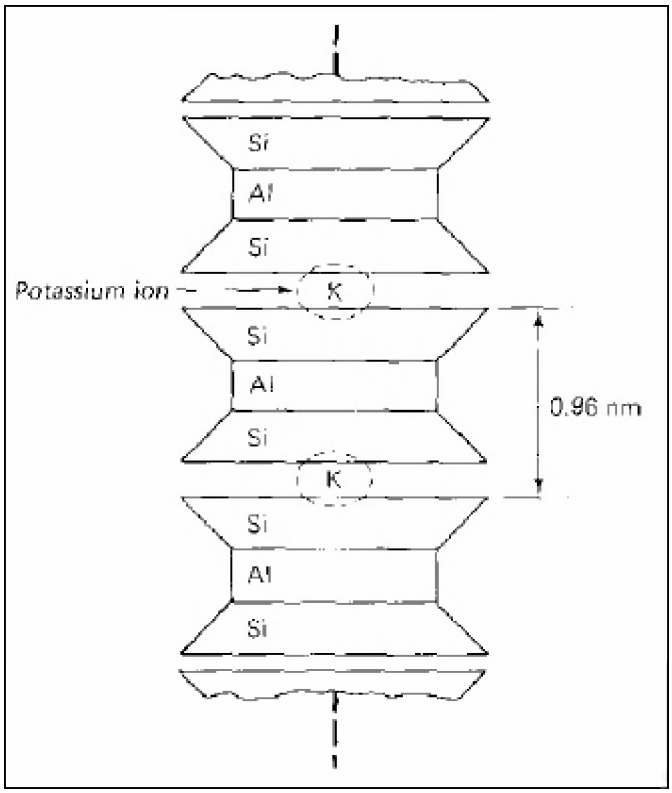

Figure 1.4: Structure of illite (Course Civil and Environmental Engineering, University of Alberta).

The **smectite group** has the same basic crystal lattice unit as illite, but the numerous crystal defects and substitutions in smectites are leading to a higher charge deficit, compensated by a large exchange capacity bringing a variety of hydrated environmental cations in between the crystal units. Therefore smectite minerals have an important swelling capacity. A variety of chemical compositions are possible. As in all clay mineral groups, both octahedral aluminium (montmorillonite) and magnesium (saponite) varieties exist, but particularly aluminium rich (beidellite), iron rich (nontronite) and other varieties exist. Smectites are generally identified by intercalating ethylene glycol molecules in the interlayer space expanding it to 17 Å between successive sheet units.

Vermiculite is a group name for clay minerals with a similar structure as smectite minerals but with an even larger charge deficit and exchange capacity. There also exists a variety of chemical compositions.

The **chlorite group** has a crystal structure of successive units consisting of a central octahedral sheet linked on both sides to the top of silicate tetrahedral sheets, as is the case with illites, but between each such unit another free lying octahedral sheet is present (figure 1.5). Generally in sediments chlorites are iron rich, but a wealth of chemical varieties exists due to substitutions and defects in all structural elements. The distance between two successive units in the direction parallel to the sheets is 14 Å.

Because of the similarities between the different clay minerals, nature has often made clay minerals consisting of randomly alternating crystal motifs described above. These minerals are named random mixed layers. The classical one is the illite-smectite interlayer, however within these interlayers also chloritic and vermiculitic components might be present. The relative proportion of these several components in the mixed layer mineral is very variable.

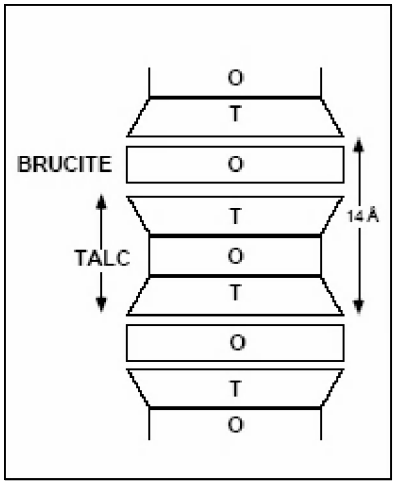

Figure 1.5: Structure of chlorite (Lecture 11, Aqueous Geochemistry, University of Calgary).

For the sake of completeness it should be mentioned that other clay minerals exist which are however not relevant for the discussion of North Sea mud: attapulgite, sepiolite, talc, pyrophyllite. Details of all clay mineral structures can be found in Brindley & Brown (1980).

In mud and clay sediments the clay size fraction consists of appreciable amounts of clay minerals and variable amounts of carbonate (see total carbonate maps Gullentops et al., 1976) and organic matter. Generally the clay size fraction represents less than 50 % of the sediment and the silt and sand sizes consist of quartz with some feldspar and minor muscovite. Shell carbonate fragments can be present in variable amounts.

1.3.3 Suspended particulate matter

Suspended particulate sediments are mixtures of minerals (clay minerals, quartz, carbonate) and organic matter (plant and animal detritus, bacteria, algae and other organic components). The characterizing feature of these matters is that the individual grains are too small to settle under their own weight. Due to their cohesive nature, the clay minerals together with organic matter may form aggregates or flocs, which are able to settle.

1.4 Abbreviations

BCS Belgian Continental Shelf
BCP Belgian Continental Plateau
BCZ Belgian Coatal Zone
HCMS High Concentration Mud Suspension
LISST Laser In Situ Scattering and Transmissometer
OM Organic Matter
SPM Suspended Particulate Matter

2. Cohesive sediments on the Belgian Continental Shelf

2.1 Cohesive sediments and their erosion/deposition behaviour

Erosion of mud is defined as the sum of the processes responsible for the resuspension and transport of particles attached to the bed. Mehta et al. (1989) and many others later distinguish between three types of erosion:

1. re-entrainment of a stationary high density mud suspension (fluid mud), with quick re-suspension of mud over the water column;
2. surface erosion, where mud particles are successively brought in suspension (freshly deposited-medium consolidated) and
3. mass erosion of fully consolidated deposits, which result in the formation of blocks or pebbles of clay delineated by cracks.

The erosion mechanism is called type I in beds with increasing bed shear strength with depth and type II in uniform beds. The resistance of the bed is expressed by a critical shear stress for erosion above which erosion starts and an erosion constant (Ariathurai, 1974). This critical shear stress approach is controversial as is e.g. reported by Wang (2003), who found from measurements that there is no threshold stress. He proposed a power law fit, that has however large scatters, indicating thus no definite relationship. The sand content of the mud has an important influence on the erosion resistance; Williamson & Torfs (1996) have found that with increasing sand content the erosion resistance increases.

The erosion of consolidated cohesive sediments depends on the natural structure of the sediment (fissures, fractures, amount of sand and silt, clay minerals) and is a result of the conditions during deposition and the subsequent altering. Consolidated deposits invariably exhibit a strong tendency to slake or disperse during rewetting (Bots, 1986). This together with the enlargement of cracks and fissures due to softening of the exposed layers by swelling may decrease their erosion resistance. Predicting the erosion resistance of consolidated cohesive sediments is not straightforward, because the geological history, the clay mineralogical composition and the silt and sand content influence the strength of the sediment. Erosion occurs as mass erosion, as the formation of small easily erodable flakes or as an erosion of type I, as is reported for a cohesive shoreline at Lake Ontario (Davidson-Arnott & Langham, 2000). Sand may act as an abrasive agent and increase the erosion. The shear stresses necessary to erode firm to very stiff clays are high and very variable, see e.g. Coastal Engineering Manual (2002). Gaskin et al. (2003) estimated the critical shear stress for erosion of the St Lawrence River clay banks as 6-20 Pa.

Deposition of cohesive sediments is often described as a function of the bottom shear stress, besides SPM concentration and settling velocity. Deposition starts when bottom shear stress is below a threshold value. In the equation of Krone (1962) this is expressed as a probability of the mud particles to be attached to the bottom, which varies linearly between 0 and 1. The Krone equation is valid for low suspended sediment concentrations (< a few g/l). It assumes that the sediment is in suspension or on the bottom, but it does not take into account the formation and transition between high concentration mud suspensions (HCMS) and fluid mud and the consolidation and bed formation.

In order to model more precisely the mud transport it is considered as unwarranted to simulate the erosion, transport and deposition processes with much detail (Gerritsen et al. 2000). This requires information on the vertical profiles of the bulk density, water content, organic content, biostabilisation or -destabilisation, clay and sand content and geotechnical parameters with a high spatial resolution and of an excess shear erosion formulae with a time-dependent expression of the erosion rate, as is described in Sanford & Maa (2001) or Aberle et al. (2004).

2.1.1 Dynamical/mechanical differences of cohesive sediments on the BCS

On the BCS different cohesive sediments from a consolidation, erosion or depositional behaviour can be identified. They are classified as stiff to very stiff consolidated, soft to medium consolidated, freshly deposited, fluid mud and suspension. This classification is also a reflection of their geological history: Tertiary and Holocene clay and recent mud. Cohesive sediments will be described such that the differences and similarities between the various cohesive sediments on the Belgian continental shelf (BCS) can be characterised on a physical basis.

Berlamont et al (1993) focuses on the parameters controlling the mechanical behaviour of mud, this is particularly useful because it comprises also the parameters necessary to simulate the cohesive sediment transport. In the paragraph we will present the cohesive sediments on the BCS principally based on a 'modelling' approach. This means that settling velocities, consolidation, rheological parameters of fluid mud, erosion and deposition parameters will be provided (when known).

2.1.1.1 Stiff to hard consolidated cohesive sediments

The Tertiary clays on the BCS are stiff to very stiff consolidated (firm to stiff consistency). They are generally covered by Quaternary sediments and in e.g. the swales the Quaternary cover may have a thickness of less than 2.5 m (Lanckneus et al., 2001). Van Lancker et al. (2002) mention the Westdiep swale where the clays of the Kortrijk formation are eroded and towards the east the clays of the Maldegem Formation arising e.g. in the Scheur. In the Flemish Bank region, Tertiary deposits may be eroded in the swales west of the Kwinte Bank. Further offshore the swales of the southern part of Hinder Bank region have a thin Quaternary cover. To the south and northeast of the Goote Bank no Quaternary deposits are found.

The erosion of these Tertiary clays occurs in the form of clay pebbles with a firm consistency; these have e.g. been found on the sandbanks and along the slopes of the Scheur (figure 2.4). Kornman & van Maldegem (2002) mention, that the dredged Boom clay, which has been dumped in the Westerschelde has a high erosion resistance.

2.1.1.2 Soft to medium consolidated cohesive sediments

Soft to medium consolidated cohesive sediments (bulk density ρ_b 1500–1800 kg/m^3) with variable sand content occur in the Belgian coastal zone and north of the Vlakte van de Raan and are generally of Holocene age (figure 2.1). These deposits correspond to the so called 'coastal mud fields'. The extension of these 'fields' has been mapped by amongst others Bastin (1974), Gullentops et al. (1976) and Fettweis et al. (2004). Missiaen et al. (2002) describe an area marked by poor seismic penetration due to gas formation in shallow peat layers; it corresponds quite well with the extension of the Holocene mud layers.

The Holocene was characterised by rapid sedimentation in mudflats and salt marshes, which followed the (relative) sea level rise and the morphology of the Pleistocene substratum (Baeteman, 1999). From about 3000 BP on the coastline started to retreat and these mud and peat layers were gradually flooded and eroded and form today part of the sea bed in the coastal zone. They are often covered by a thin layer (cm to several 10 cm) of very fine sand or muddy sand. Part of the mud can be covered or de-covered during severe hydrodynamic conditions. Erosion of the mud may be enhanced by the sand acting as abrasive agent.

No measurements exist of the erosion resistance (critical erosion shear stress, erosion constant) of these sediments. Fettweis & Van den Eynde (2003) have used a value of 2.0 Pa for the critical erosion shear stress in a cohesive sediment transport model of the BCS

Figure 2.1: Van Veen grab sample of Holocene layered clay covered by a thin layer (5 cm) of fine sand with patches of recent ('liquid') mud, west of Pas van het Zand, R/V Belgica campaign 2005/07.

Figure 2.2: Van Veen grab sample of recent mud (1 cm) on top of sand, R/V Belgica campaign 2003/04. (old dumping place Oostende)

Figure 2.3: Box core (completely filled, 50 cm) of very soft mud, which is gradually more compacted underneath and covered by a recent layer of 7-8 cm mud, R/V Belgica campaign 2003/04 (old dumping place Oostende)

2.1.1.3 Freshly deposited mud

Freshly deposited mud occurs on the BCS mainly in the man made environments such as navigation channels and harbours. Layers of about 0.5 m of fresh and very soft consolidated mud have also been found near the old dumping site of Oostende (Van Lancker et al., 2004), see figure 2.2 and 2.3. Very often the fresh mud is limited to a thin layer of maximum a few cm on top of the sediment bed (fluffy layer), see samples east and west of Zeebrugge, south of the Vlakte van de Raan, in the MUMM monitoring points 130, 230, 700, 702, in the swales between the sand banks. Kerkhofs (pers. comm.) mentions a freshly deposited mud field near the beach at Wenduine.

The erosion resistance of these mud layers is small (no quantitative data for the BCS exist) and as a consequence most of them are resuspended during storm events or during spring tides (Fettweis & Van den Eynde, 2003). Measurements of the critical shear stress for erosion (τ_{ce}) and deposition (τ_{cd}) have mainly been performed in laboratories; see e.g. Berlamont et al. (1993) who mention values for τ_{ce} of soft estuarine muds between 0.1-2 Pa and τ_{cd} of 0.05-0.2 Pa. Larger aggregates will generally begin to deposit at higher shear stresses of 0.2-1 Pa. The Fettweis & Van den Eynde (2003) have used 0.5 Pa and an erosion constant of 0.12×10^{-3} kg/m²/s in their cohesive sediment transport model of the BCS.

Ravens & Gschwend (1999) have measured the erodibility of sediments from the Boston harbour, the critical shear stress for erosion and the erosion rate were quite uniform ($\tau_c=0.1\pm0.04$ Pa, $M=3.2\pm0.2\times10^{-3}$ kg/m²/s).

2.1.1.4 Fluid mud

Various definitions of fluid mud are used; they are based on density, rheological behaviour or SPM concentration. They all have in common that fluid mud is described as a benthic suspension separated from the upper water column by a lutocline. In soil mechanics (Sills & Elder, 1986) this corresponds to the transition where pore water pressure and total vertical stress are equal (such as is the case in HCMS) and the situation where the pore pressure becomes less than the total vertical stress such that a structure to carry the weight of the sediments has developed.

The bulk density cannot be defined exactly, because it is a function of the material composition (sand or organic matter content). Values between 1030-1130 kg/m³ and even >1200 kg/m³ are mentioned in literature, having a SPM concentration >50g/l (e.g. Toorman, 1992). The transition between fluid mud and HCMS has been set at the rheological transition, which is non-Newtonian for fluid mud, but still Newtonian for HCMS (Verreet & Berlamont, 1989).

In turbulent flows with high concentration of mud (>10 g/l) drag reduction in the viscous sub-layer with respect to the apparent shear stress of the logarithmic layer in the upper water column may occur (Best & Leeder, 1993; Li & Gust, 2000; Toorman et al., 2002, Winterwerp et al., 2002b). The decrease of shear stress will in a tidal environment decrease the time available for erosion and increase time for deposition. Suspensions with high mud concentration will thus favour the deposition of mud; this could also explain the high deposition of mud in the navigation channels Pas van het Zand and Scheur Oost on the BCS.

Fluid mud and HCMS have been reported on the BCS in the Zeebrugge harbour and the navigation channel 'Pas van het Zand' (Strubbe, 1987). The reflection horizon of the high frequency (210 kHz) echo soundings can be interpreted as the transition between HCMS and water and the one of low frequency (33 kHz) as the transition between fluid mud and the consolidated mud bed (or sand bed). The transition between HCMS and fluid mud forms the nautical depth. The reflection of the echo soundings cannot be linked uniquely to the density of the mud, therefore the nautical depth in the dredging industry is determined using density measurements (Druyts, 2000). Dredging is carried out when the density of the mud above the minimum navigation depth is higher than a certain value. In the Zeebrugge this has been fixed

at 1150 kg/m^3 in Rotterdam at 1200 kg/m^3. No information on quantities, formation as a function of time (seasons, spring-neap cycles, tides, storms, salinity) or durableness, etc. have been found for the fluid mud layers on the BCS

2.1.2 Biological influence on erosion resistance

The effect of benthos on sediment stabilization (or –destabilization) in shelf seas is getting more attention (Friederichs, 2004). Macrobenthos is interacting actively with sediments by filtering the water, 'eating' the sediment and altering the erosion resistance or indirectly through affecting the hydrodynamics around the macrobenthic structures. The erosion resistance of the surface beds may increase (e.g. development of microbiological mats) as well as decrease. Reduction of erosion resistance has been ascribed to the development of biochemical surface layer and the feeding and reworking by marine worms (Lintern et al., 2002).

No or little information on benthic species distribution and frequency and their interaction with sedimentology is available from the mud fields on the BCS. The Holocene and the Tertiary clays are characterised by the *Barnea candida* macrobenthic community (Degraer et al., 2000), including also the introduced American piddock *Petricola pholadiformis*. The holes of these bivalves may also be used by the bivalves *Venerupsis senegalensis* and *Hiatella arctica* (pers. comm. F. Kerkhofs).

We have found white piddocks in consolidated mud layers in high numbers near the coast between Nieuwpoort and Oostende (R/V Belgica campaign 2002/14b) and east of the Pas van het Zand (R/V Belgica campaign 2002/06). The thin sand cover as found on the Holocene mud layers, limits the growth of the population and may explain the restricted and often ephemeral distribution in the Holocene layers.

The benthic communities in freshly deposited mud are even less diverse and consist mainly of worms such as *Capitella capitata* (the so called "Polydora mud", see fresh mud near coast of Wenduine) and - depending on the oxygen level and/or organic content - of bivalves living in the sediment such as *Macoma balthica* and *Abra alba* (Kerkhofs, pers. comm.).

2.2 Cohesive sediment distribution

2.2.1 MUMM mud chart

The map in figure 2.4 is based on the sediment samples taken by MUMM and shows the distribution of cohesive sediments on the BCS based on the descriptions of consistency (see § 2.1). Fluid mud is not indicated on the map, because not enough data exist concerning its distribution. This is probably also due to the sampling method (Van Veen grab or box-core). Thick layers of fresh mud have been found in the navigation channels, the Zeebrugge harbour and near the old dumping site of Oostende. The fresh mud in the rest of the area is only a few cm thick.

2.2.2 Bastin mud chart

Bastin (1974) made a sedimentological map based on the radioactivity of sediments, measured during several surveys in July-August 1964. For this reason a probe was developed which was dragged over the seabed. By measuring the gamma rays it was possible to differentiate between sand, sand & mud, clay and clay & mud. Moreover, sediment samples were taken during each campaign to validate the gamma ray results. The probe only measures at its bottom side and one should take in mind that this may cause a partly wrong idea of the recent mobile mud depositions.

The tracklines are perpendicular to the coast and are 13 km long. The total surveyed area is more or less 1000 km^2. Bastin (1974) defines mud as a light-packed mix of clay, silt, sand, chalk and organic matter with a high water content. Clay is defined as a more rigid and denser sediment and can have two origins: either compaction of mud layers or erosion of older eroded sediments. Sand and mud can be one of the following three types of sediments:

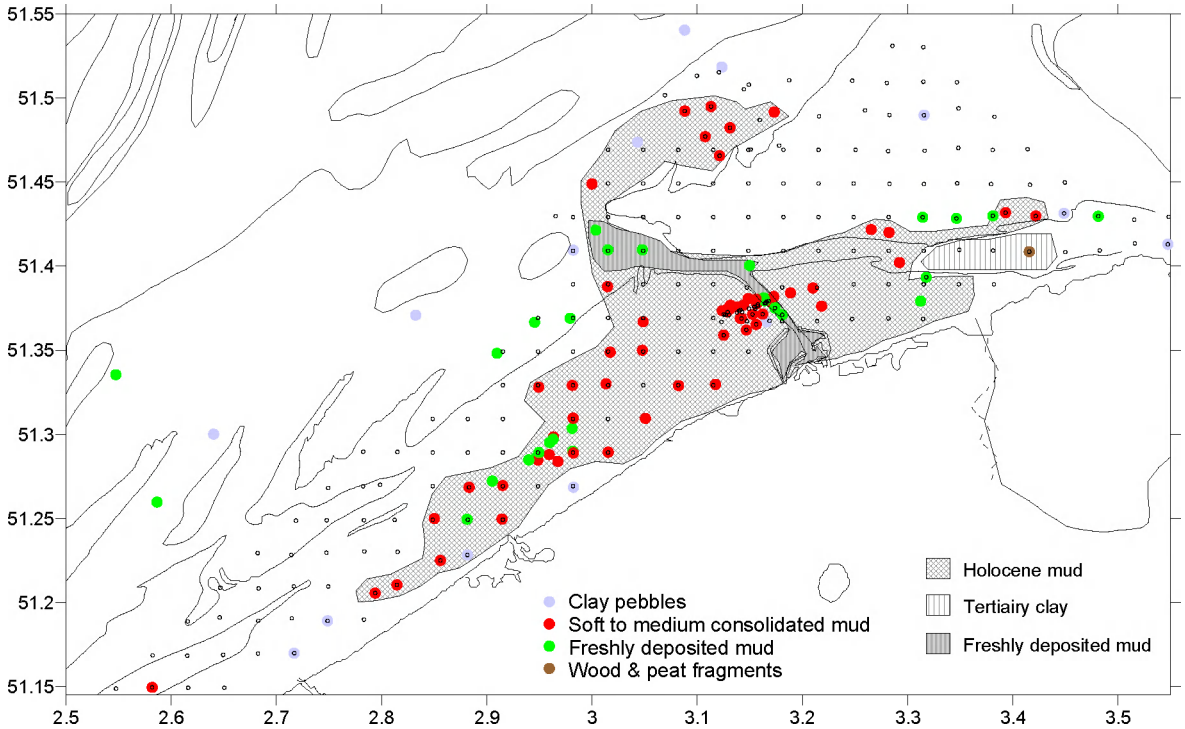

Figure 2.4: Distribution of cohesive sediments on the BCS. The small black dots indicates places where samples have been taken; if not coloured then they consist of sand; clay pebbles have been found in the light blue, Holocene clay in the red and fresh deposited mud in the green points. The wood and peat fragments are from Holocene age.

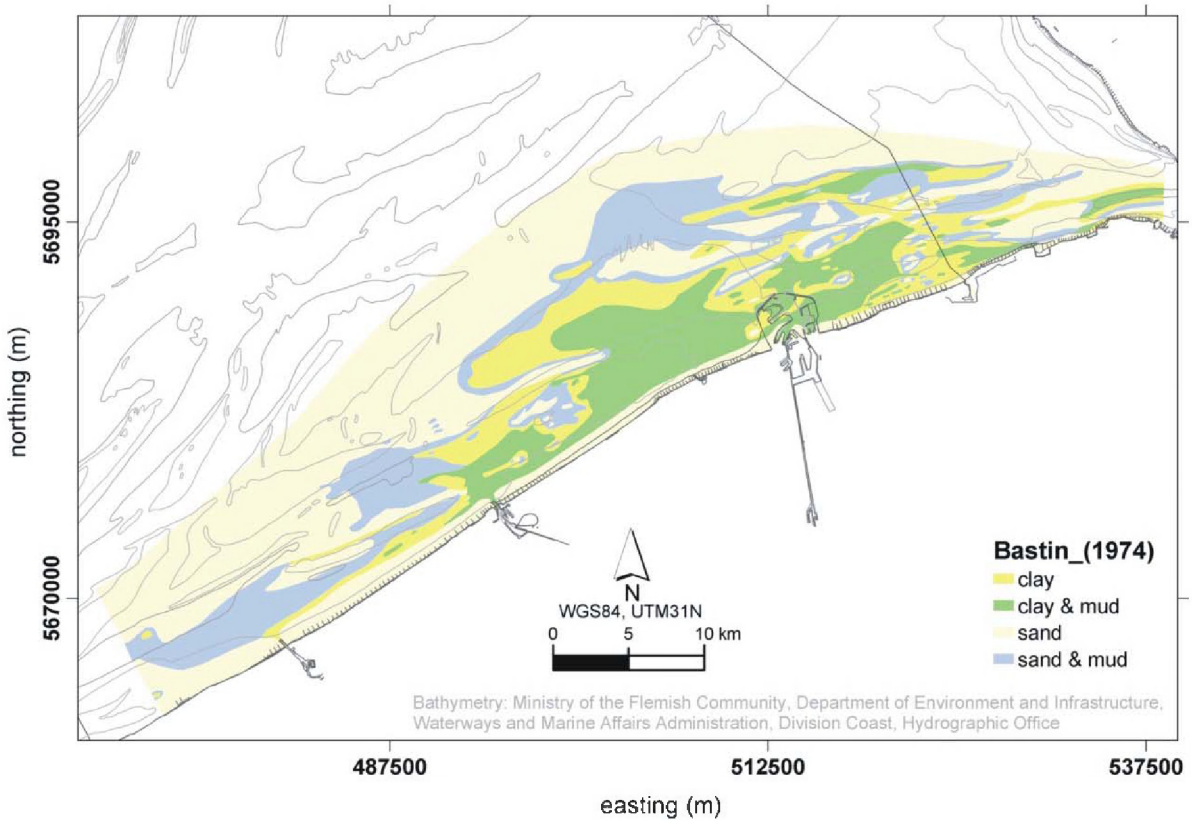

Figure 2.5: Distribution of the 4 sediment types defined by Bastin (1974) based on his gamma ray technique.

- Sand with a thin layer of mud on top: this facies is heavily influenced by wave and current conditions, e.g. near the Stroombank.
- Mix of sand with mud/clay: either by a simultaneous deposition or by diffusion of the mud layer into the underlying sand or by diffusion of elsewhere eroded clay which was transported on the sand and diffused into it, e.g. near Nieuwpoort.
- Layering of sand and mud/clay: due to the different ebb- and flood currents eroding and depositing sediment from different places, e.g. north of the Wandelaar Bank.

The sand cannot be further divided into coarse, medium and fine sand due to the limitations of the gamma ray technique.

The occurrence of clay & mud is especially concentrated between the Oostende and Zeebrugge harbours and east of the Zeebrugge harbour (figure 2.5). The distribution of clay and sand & mud is more or less adjacent to the distribution of the clay seawards. The distribution of sand is limited to the beach line and to the more offshore parts. Further on offshore Bastin (1974) supposed a continuation of the sand.

2.2.3 RCMG database

RCMG hosts a large database of samples (*SEDISURF*) taken over the course of the 1980's, 1990's and 2000's. The database is populated by more or less 6200 samples and most of them are Van Veen grabs taken by different institutes on different vessels. One of the problems with this large database is that every institute has its own definitions for silt-clay. Moreover there are a large number of zero values which either can be true values or errors. Before producing a relevant and reliable mud map, the database therefore needs to be carefully analysed and this will be done in the near future. At present a map of the median grain-size has been produced using multivariate geostatistics. This technique allows a sound interpolation of data whereby the underlying bathymetry is used as a second variable for the interpolation of the median grain-size.

2.2.4 Bathymetric evolution

A map of 1959 (sheet Vlaamse Banken, published by the Ministry of the Flemish Community, Department of Environment and Infrastructure, Waterways and Marine Affairs Administration, Division Coast, Hydrographic Office) representing soundings from 1953 to 1956 was digitised and is compared with the most recent bathymetric chart of 2003 (also sheet Vlaamse Banken, published by the Ministry of the Flemish Community, Department of Environment and Infrastructure, Waterways and Marine Affairs Administration, Division Coast, Hydrographic Office). The contour lines of 10 m depth are plotted in Figure 2.6. There are relative little morphological changes, nevertheless it is striking that the navigation channel towards the Zeebrugge harbour has been deepened due to dredging over the years. This resulted in dredging into the Paleogene layers (Bartoon). Another striking feature is the build-up near the S1 dumpsite due to continuous dumping activities.

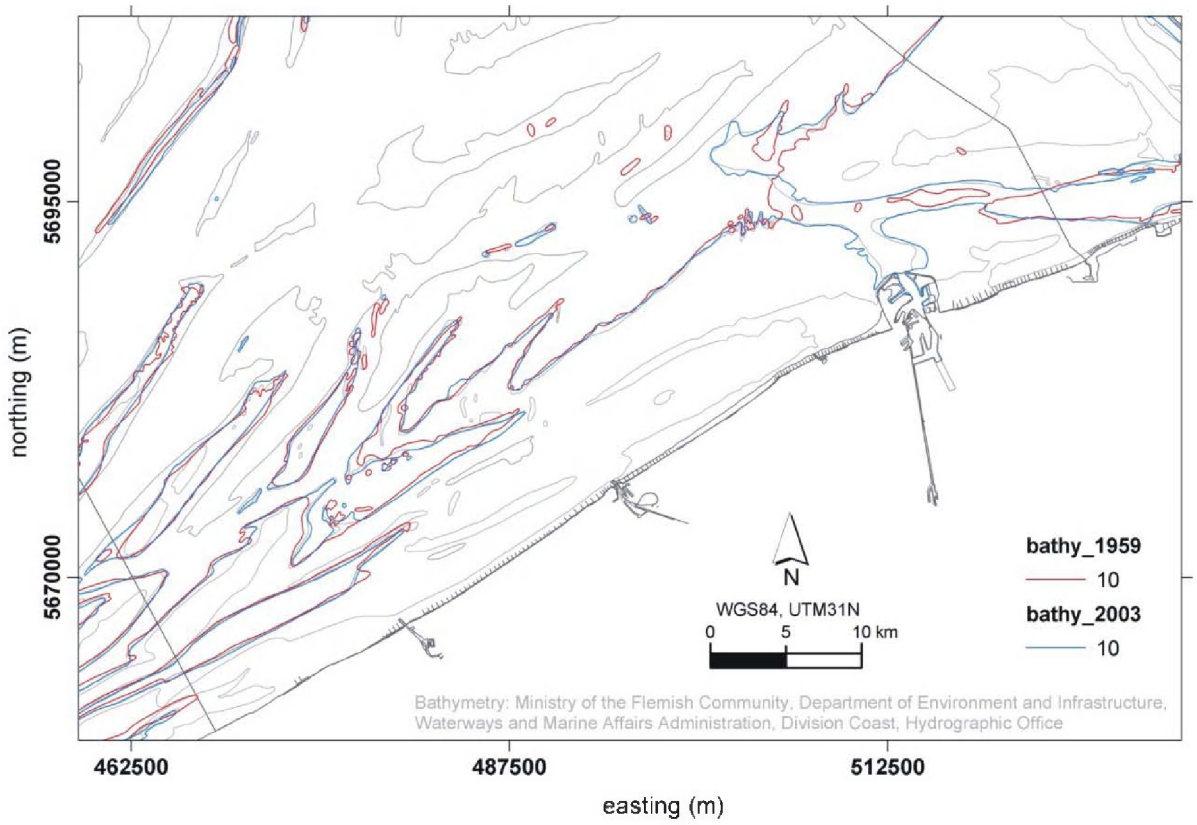

Figure 2.6: Bathymetry map showing the evolution of the 10 m depth contour from 1959 to 2003.

2.3 Historical data: Gilson collection

In 1899, Prof. Dr. G. Gilson started an ambitious sampling program focusing on nearly all compartments in the southern bight of the North Sea, mainly within the Belgian marine areas (van Loen et al., 2001). Gilson aimed at understanding how environmental parameters influence the distribution of marine species. He therefore included an exhaustive sediment sampling scheme to complement benthos sampling. Sampling information (instruments, geo-positioning, date, etc.) was generally well documented. Gilson's particular cup-shaped instrument was able to sample the first 10-20 cm of soft bottoms and allowed for some conservation of sediment layers in the sample (van Loen et al., 2001). 3000 sediment samples were collected until 1939, with 90% collected by 1911, later samples being more anecdotal. Gilson performed only several grain-size analyses of his samples. Only 700 sub-samples were kept until nowadays in the RBINS repositories. However, Gilson has provided a detailed description of the sediment hauled onboard for most of his samples. The level of detail of these descriptions is high and allows a standardization of their information content in the form of "data", which we primarily did to characterize benthic habitats. For about 500 samples, the original detailed description could not be recovered in the archives and only a summary was available. In these cases, the information is therefore truncated (e.g. "very fine, grey sand with surficial grey mud" becomes "fine sand with mud") and should be used with caution.

2.3.1 Sample selection and methods.

We focus our attention on the coastal sampling grid of Gilson (figure 2.7), other samples being more spread in offshore areas. 1956 sediment descriptions were considered valid in this area in terms of either sedimentological information content and geo-referencing accuracy.

Different methods have been tested so far to code Gilson's texts into quantitative data. For the purpose of this project, we have addressed the question of cohesive sediments (Gilson does

not make a difference between 'mud' and 'clay') and sand content of the surface sediments by aggregating specific informations: main nature of sediment (sand, mud); presence of mixed mud and separate mud layer in sand samples; presence of mixed sand and pure sand layers in mud samples. Other constituents like gravel or shell debris were not considered. In a first step, mud and sand content was ranked accordingly to four categories: pure sand; sand with mud; mud with sand; pure mud.

Thanks to additional semi-quantitative indications provided by Gilson (e.g. "*very thick* mud layer"), this basic mud/sand proportion scale was manually adjusted where possible with steps between the 4 main subdivisions. This adjustment is subjective and it induces a bias in the mud content ranking since not all descriptions contain semi-quantitative information. However, this strengthens the overall pattern and allows monitoring local heterogeneities that would not appear based solely on the first rough classification. The obtained values were then normalized to obtain a scale of mud content. Typical values resulting from this stepwise treatment of Gilson's descriptions are illustrated in table 2.1. Further data verification, geostatistics and interpolation methods could provide more accurate results. For this first mid-term report, we used the "kriging" interpolation method with default parameters to identify major trends derived from Gilson's observations.

Table 2.1: Steps taken to convert Gilson's text into "mud content" (1. category ranking; 2. sub-ranking using available semi-quantitative information; 3. normalization), illustrated with values obtained for some typical cases. The "mud content" reflects the suggested proportion of mud in sand after all coarser constituents have been.

Sampling_NR	Date	Gilson's description	Category	mud/sand rank	mud content
G5434	11/10/1911	sable grossier, coquilles	pure sand	4	0.00
G4087	28/07/1906	Sable fin, petits grumeaux de vase noire et de vase grise	sand with mud (trace)	3.75	0.08
G5420	25/09/1911	sable assez fin, légèrement vaseux	sand with mud	3.5	0.17
G2096	31/07/1902	sable gris très néritique; morceaux de vase noire dure.	sand with mud	3.25	0.25
G5442	20/10/1911	sable vaseux gris, coquilles, vase grise	sand with mud	3	0.33
G3232	17/09/1904	sable moyen très vaseux gris, très néritique, grossier	sand with mud	2.75	0.42
G2662	9/06/1903	Vase grise pure ; sable gris fin (à parts égales)	Mud with sand	2.5	0.50
G1273	29/07/1901	vase grise très sableuse	Mud with sand	2.25	0.58
G5602	13/10/1913	Vase sableuse, beaucoup; vase noire; vase grise de surface	Mud with sand	2	0.67
G1887	11/04/1902	sable grossier très néritique, un peu; vase noire très dure, en morceaux, beaucoup ; vase grise	mud with sand	1.75	0.75
G5424	25/09/1911	Vase noire sableuse; un peu de sable gris-jaune	Mud with sand	1.5	0.83
G1673	20/09/1901	vase noire ; un peu de vase noire sableuse	Mud with sand	1.25	0.92
G0070	12/06/1899	Vase noire bleuâtre	Pure mud	1	1.00

This data processing does not give any indication on the nature of mud within the sediment. According to Gilson's observations, mud can be mixed to sand, form a separate surface or deep layer, or even form patches of varying sizes within heterogeneous sediments. Only on several occasions does Gilson give an indication of the vertical order of different observed layers. However, Gilson often provides additional information on the mud aspect: "pieces" or "lumps", "hard", "liquid", "grey", "black", "surficial", etc. On the other hand, Gilson also occasionally provides indications on the "hardness" of the sampled bottom as observed with a sounding weight.

Models developed at MUMM attempt to describe the patterns of mud deposition and erosion in this hydrodynamical complex area. A major question addressed by this project is to track mud "origin" and behaviour to feed management-oriented models. We therefore tentatively examined some aforementioned parameters within Gilson's descriptions to check whether these could suggest hypotheses on long-term changes. Running models taking into account physical changes in the environment (like bathymetric changes associated with emergence of harbours and navigation channels) might provide a validation of such hypotheses. In order to perform long-term comparisons with mud deposition or erosion patterns provided by contemporary data, we have tentatively coded this information as well to monitor occurrences of "soft" or "hard" mud areas. Use of these data must be performed with care since we cannot make the as-

sumption that Gilson always recorded them accurately, while a part of the descriptions is only available in a summarized form.

Four items related to cohesive sediment consistency and/or erosion/deposition processes have à priori been extracted:

1. Occurrence of "rolled mud balls" (i.e. clay pebbles) in the sample, indicative of eroded and transported clay.
2. "Hard mud" from both bottom soundings and descriptions (breaking into "pieces" in hands), indicative of (at least) medium consolidated cohesive sediments. Probably Gilson meant Holocene clay as is shown in figure 2.1, the clay is layered and breaks into pieces.
3. "Liquid" and/or "surface" mud, flowing through fingers, indicative of freshly deposited mud.
4. "Soft mud", most probably indicative of freshly deposited thick mud layers (see navigation channel towards the harbour of Oostende) or soft consolidated cohesive sediments which were formed through rewetting of the more consolidated Holocene clays (see figure 2.3).

2.3.2 Relative mud content index

Despite questions on "data" accuracy, the developed approach provides a consistent general map of mud content along the Belgian coast as well as along the mouth of the Westerschelde estuary (figure 2.7). High content of cohesive sediments are mainly located between Oostende and Zeebrugge, which is consistent with observations made more recently (see figures 2.4 & 2.5). In front of the western and central Belgian coast, two bands of much lower mud content can be observed, which corresponds with the Wenduine and Nieuwpoort Bank, this indicates that the 'mud fields' are older than the sandbanks. Higher mud contents are also found in deeper areas, as along the island of Walcheren (Deurloo and Oostgat gullies), north of the Vlakte van de Raan and along the southern flank of the Goote Bank. In front of the Western coast and in the southern part of the Westhinder Bank, a slight but significant amount of mud is found in the swales between the banks, where gravel is also present. On the Vlakte van de Raan large mud-free areas are found, which is in full agreement with contemporary data.

2.3.3 "Hard" and "soft mud"

When considering the four items related to cohesive sediment consistency, we observe again a patchy distribution (figure 2.8). As mentioned earlier, we do only consider positive indications as "data" (i.e. absence of a parameter might be due to inaccurate recording). However, we can draw areas where respectively "hard" (i.e. at least medium consolidated) cohesive sediments and "soft" cohesive sediments dominate. The more consolidated cohesive sediments have mainly been observed east of Zeebrugge. In front of Zeebrugge and more to the west "softer" mud was observed, possibly indicative of freshly deposited mud or rewetted Holocene clay.

Interpretation of "liquid mud" occurrences must be performed with caution, since fresh mud deposition/resuspension can occur cyclically through tides and small amounts can be deposited for short periods. However, several occurrences are recorded around the Westpit area (north of the Vlakte van de Raan), where mud content is high, which corresponds to contemporary observations. The latter is an interesting observation, because it proves that these mud deposits are not due to the important mud dumpings occurring currently on the B&W S1 dumping place.

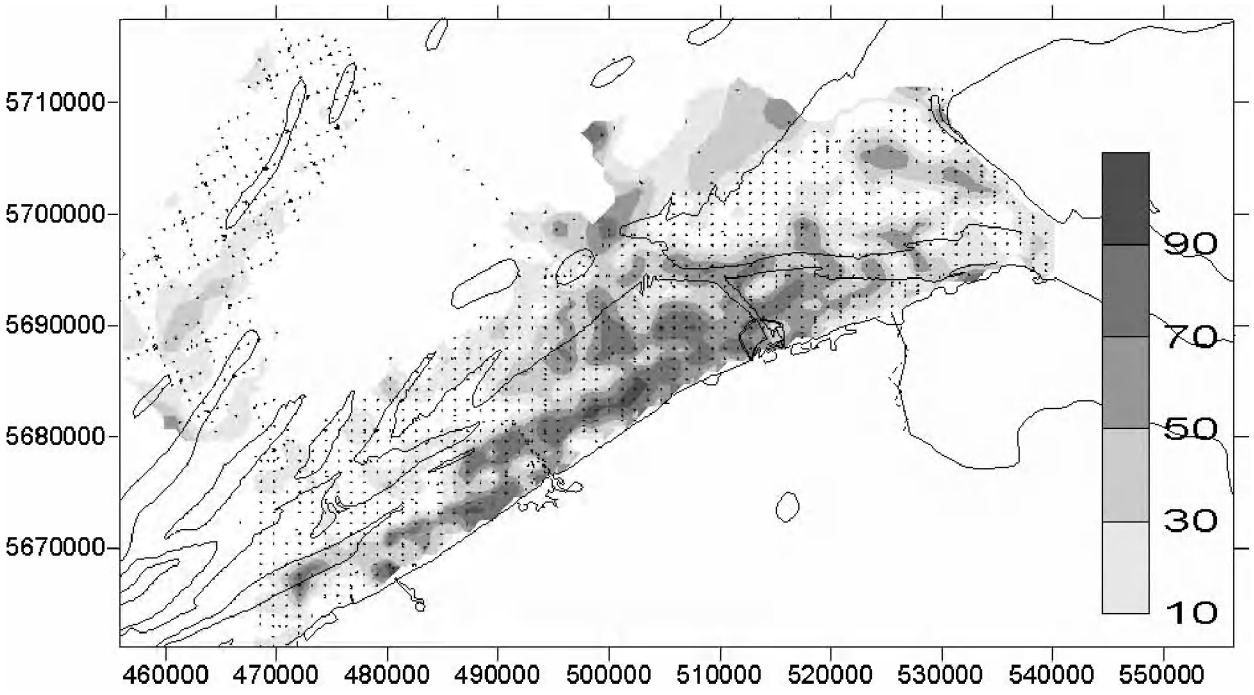

Figure 2.7: Mud content (in %) of surface sediments as inferred from Gilson's sample descriptions. The content is calculated by comparing relative mud and sand proportions according to original descriptions, all other constituents being excluded of the analysis. Interpolation (Kriging) was made within Gilson's sampling grid (one dot = one sample) to visualize the general pattern. The result was superimposed on modern coastline and 20 m MLLWS isobath data. (UTM projection 31N, ED50 European Datum).

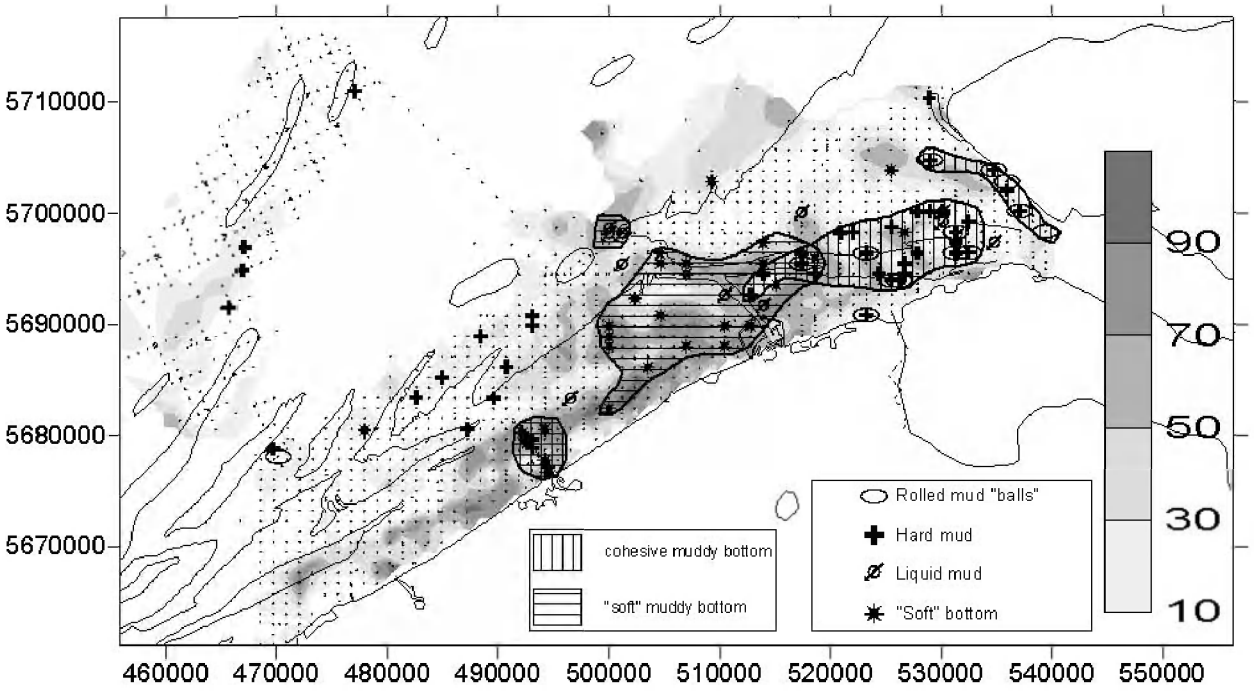

Figure 2.8: Plot of different mud parameters extracted from Gilson's descriptions. Areas where respectively "soft" and "hard" mud tend to dominate were drawn manually (UTM projection 31N, ED50 European Datum).

2.3.4 Discussion

When comparing these results with a recent map of mud distribution (figures 2.4 & 2.5), the overall pattern is very consistent, although of course absolute mud contents should not be directly compared. As can be expected, major changes are to be searched in the Zeebrugge harbour area and in navigation channels where high amounts of mud accumulate nowadays. Additional information provided by Van Mierlo or other authors before the construction of the first part of the Zeebrugge harbour and the dredging of the Pas van het Zand channel would help to evaluate the changes through time more accurately.

"Soft mud" could suggest fresh mud deposition, although the exact meaning of this parameter cannot be evaluated accurately. Occurrence of "hard mud" in the Scheur (Tertiary or Holocene clay) fit contemporary observations during capital dredging of this navigation channel. Erosion of these consolidated clay layers appear in the form of clay pebbles which have mainly been found by Gilson in the vicinity of "hard" mud.

In front of Oostende we observe the co-existence of "hard" and "soft mud". In this area, Gilson has increased the sampling effort in order to know whether the impact of mud dumping by harbour dredgers resulted in an increase of mud amounts on the bottom. So far, we did not find any conclusion regarding this topic in his papers and archives.

In a letter to Gilson by an officer of the "Administration des Ponts et Chaussées", 1913, relative to mud dumping on the North slope of the Wenduine Bank (by Nieuwpoort and Oostende harbour dredgers), we find indications that the dumped mud was quickly eliminated by tidal currents and storms:

- *[Charles Verstraete] m'a dit [...] que des prélèvements d'échantillons de fond effectués par vous et lui sur le talus Nord du banc de Wenduyne, près des bouées de dragages, permettaient de croire que les produits que l'on y déverse ne s'y maintenaient pas et étaient enlevés presque immédiatement.*
- *Cela me paraît plus que vraisemblable [...]*
- *Ne vous semble-t-il pas que c'est une dépense inutile que d'aller porter à 7 ou 8 kilomètres au large les produits de dragages, et que déversés dans la grande rade d'Ostende ils n'ajouteraient pas grand-chose à l'énorme quantité de vase qui se ballade en mer et dont une partie vient se déposer devant les ports ?*
- *Eventuellement je ferai usage de votre opinion et me permettrai d'en citer la source.*

This letter suggests that early information on mud dredging and dumping should be available in archives of the "Administration des Ponts et Chaussées". So far, we do not know what Gilson's opinion on this topic was. This old observation supports the view that mud found in front of the central and western coast is of Holocene origin and that these old mud layers are exposed to the surface depending on hydrodynamics, weather conditions and sand transport.

2.3.5 Conclusions

Coding of Gilson's information provide "qualitative" but valuable information on the nature of surface sediments, which can in turn be used to support validation of hypotheses on mud origin and behaviour. The data available so far show some trends confirming hypotheses based on numerical models and recent data, i.e. changes in local mud deposition occur mainly around Zeebrugge and in artificial, deepened navigation channels, due to changes in local hydrodynamics.

Interesting to the historian is the fact that Van Mierlo (1897; 1908) had foreseen a fast filling of Zeebrugge harbour with mud before its construction begun, which led him to fight against this project. A detailed analysis of the hydrographical and sedimentological changes around Heist after construction of the first Zeebrugge harbour, at the turn of the 20th century, can be found in Van Mierlo (1908). Van Mierlo (1899) also provided the first sedimentological map of the BCS (based on about 300 sample descriptions), this map was reproduced in van Loen et al. (2001).

3. Suspended particulate matter on the BCS

3.1 Floc size and settling velocity

A floc is defined as an aggregate of fine cohesive sediments and organic matter. It is well known that the SPM transport is affected by the formation and break-up of aggregates (flocculation), because it may vary the settling velocity of the particles (Van Leussen, 1994). Flocculation is a function of the overall hydrodynamic and biological environment and also of the physical, chemical and biological characteristics of the particles, such as the SPM and organic matter concentration, the size, cohesiveness and form of the particles (Berlamont et al., 1993). Mainly turbulence and to a much lesser extent Brownian motion and differential settling are the responsible physical agents (Van Leussen, 1994). Due to turbulence the particles may collide and will flocculate, large turbulent motion however results in disruption of the aggregates.

In tidal areas flocculation effects may vary in space and time as a result of turbulence stress and floc history. The residence time of the flocs has furthermore to be sufficient long (order of hours) such that the flocs can attain their equilibrium size. This is particularly relevant at low turbulent levels, at small sediment concentration and/or very shallow water (Winterwerp, 2002). Deposition and resuspension of fine grained sediments may affect the size of the particles, e.g. by break-up of the aggregates during resuspension (Fugate & Friederichs, 2003) and/or changes in the structure of the aggregates due to consolidation. The occurrence of phytoplankton and its associated mucus finally is a crucial factor controlling the aggregate size, because these organic components are larger and stickier than the lithogenic components (Hamm, 2002). In the absence of phytoplankton the aggregation efficiency will be lower and the aggregate size significantly smaller (Ziervogel, 2003).

The settling velocity determines the deposition rate and depends on the size and density of the mud flocs. Large flocs are more porous and may contain more organic material, whereas small flocs may have densities of approaching those of sand grains. The floc density and size can be related by using a fractal model (Kranenburg, 1994); Winterwerp (2002) based his flocculation and settling velocity model on this fractal approach of mud flocs. The settling velocity increases first with increasing SPM concentration, when at a certain SPM concentration (a few g/l) a maximum in settling velocity is reached and hindered settling occurs.

3.1.1 Measurements of floc size

The LISST 100C uses laser diffraction technology (see §4.2.2) to measure particle size distributions between 5-500 μm of the SPM and measures the transmission coefficient (Agrawal & Pottsmith, 2000). The volume concentration is calculated (by the instrument) using these measured parameters together with an empirical volume calibration constant and the assumption that the particles are spherical. The LISST works well in resolving uni-modal and multimodal silicate particle distributions, which are separated by at least 1 Φ (Traykovski et al. 1999). Gartner et al. (2001) have shown under laboratory conditions that the LISST underestimates mono-sized particles by about 10% and that this error tends to increase as particle size increased. This is partly due to the logarithmic spaced ring detectors of the instruments; large particles are thus not well represented. Aggregates are slightly flattened, because they are complex associations of lithogenic and organic particles (Van Leussen, 1994; Mikkelsen & Pejrup, 2001), which may thus influence the measured size distribution. It has been shown that diffraction patterns are formed by the flocs and aggregates itself and not by the primary particles from which the aggregates are built of (Van Leussen, 1994) and that no multiple diffraction occurs in an aggregate (Agrawal & Pottsmith, 2000). Multiple diffraction results in a shift towards smaller size classes and can become important when the transmission is lower than 30% (Traykovski et al., 1999). The presence of particles coarser than the size range of the instrument changes the size distribution measured by the LISST. Traykovski et al (1999) have shown

that with the LISST 100C particles larger then 250 μm are registered in the 500 μm class. The results of LISST measurements should therefore be interpreted as an index for comparing size distributions rather than relying on their exact values (Fugate & Friederichs, 2003).

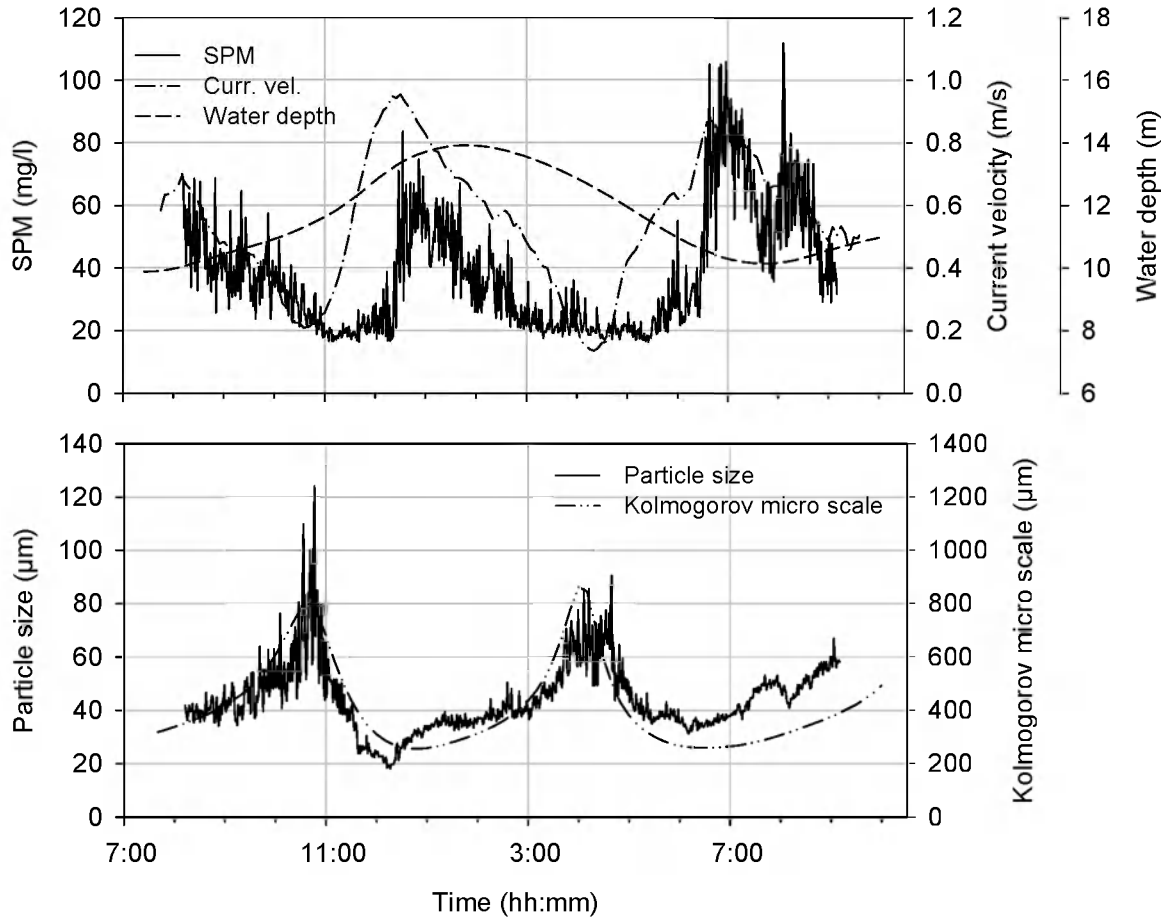

Figure 3.1: Zeebrugge site, through tide measurements from 8 September 8h00 PM until 9 September 9h00 AM 2003 (R/V Belgica campaign 2003/22): (a) SPM concentration (mg/l), water depth (m) and vertical averaged current velocity (m/s) and (b) averaged particle size (μm) and Kolmogorov microscale of turbulence (μm, model result). Measurements have been taken at about 3 m above the bottom (from Fettweis et al., 2005).

Measurements of floc size using the LISST 100C (Agrawal & Pottsmith, 2000) and of SPM concentration have been carried out in (near Zeebrugge and Oostende) and just outside the high turbidity zone (Kwinte Bank), see figures 3.1 & 3.2. Since no direct measurements of settling velocity have been carried out the fall velocity was calculated indirectly, following a method presented by Mikkelsen & Pejrup (2001) using the averaged floc size, the SPM volume concentration and the SPM concentration (Fettweis et al., 2003).

An interesting result is that the particle size of the aggregates in the coastal turbidity maximum zone was smaller (average: 44-65 μm) and the effective density higher (400-1800 kg/m^3) than more offshore at a site situated near the edge of the turbidity maximum (average: 122-198 μm; 200-800 kg/m^3), this in contrary with measurements from the Tamar estuary (Winterwerp et al., 2002a). The settling velocity on the Kwinte Bank was during a tidal cycle between 1.8 and 8.2 mm/s (mean: 3.8 mm/s) and near Zeebrugge 0.3-2.3 mm/s (mean 0.9 mm/s). These results underline the suggestion of van der Lee (2000), saying that the settling velocity depends only indirectly on SPM concentration. The processes responsible for the occurrence of differences in aggregate size have been ascribed to – beside minor differences in hydrodynamic between the two areas - differences in availability of suspended particulate organic carbon (POC) with respect to SPM, which is higher outside the coastal turbidity maximum

(Fettweis et al., 2005) and possibly also to the presence of different types of suspended matter with respect to mineral composition on the Belgian North Sea continental platform (see §4.4). POC is regulating floc growth, because of its cohesive properties. In the high turbidity zone the POC is more quickly saturated by the less cohesive lithogenic fraction and growth of aggregates is therefore limited.

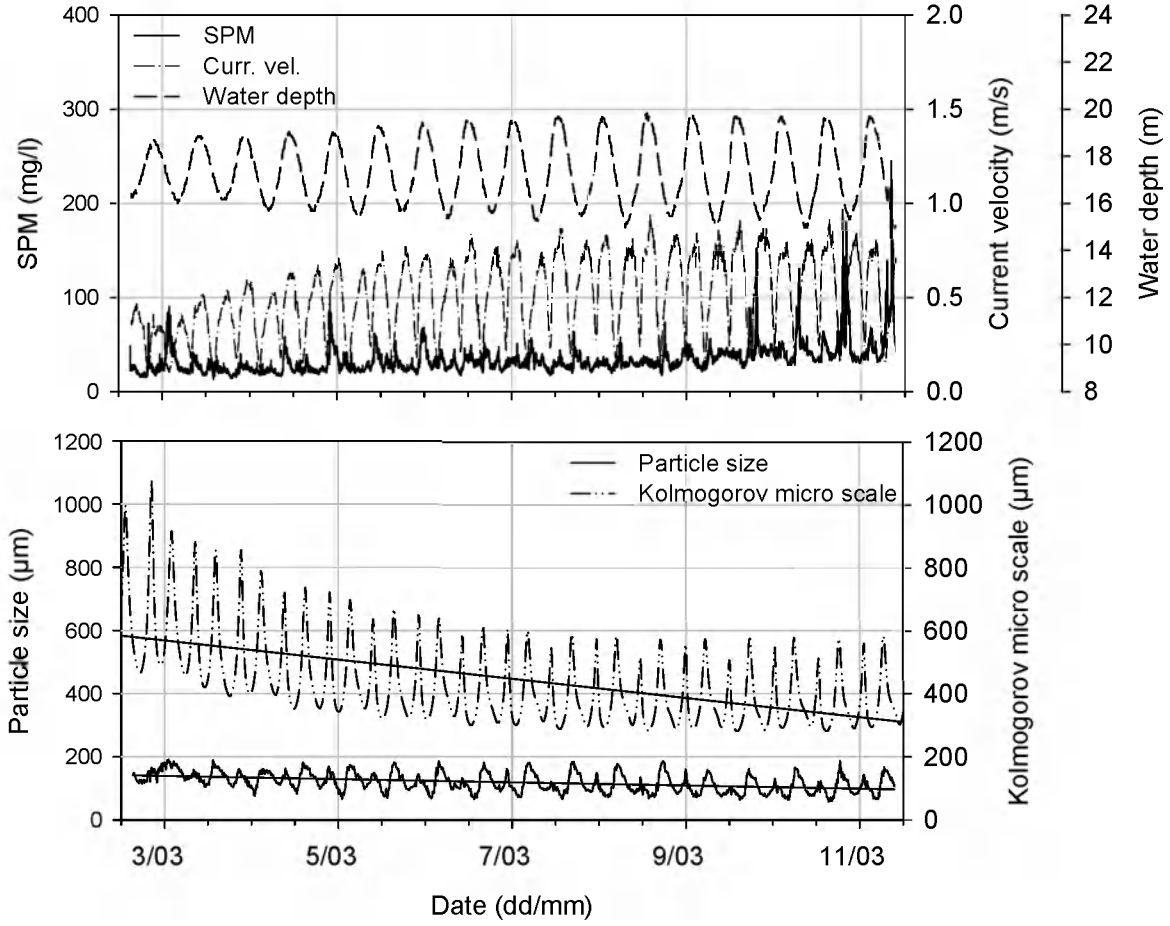

Figure 3.2: Kwinte Bank site, tripod measurements of 2-11 March 2004 (2004/05): (a) SPM concentration (mg/l), water depth (m) and vertical averaged current velocity (m/s) and (b) averaged particle size (μm) and Kolmogorov microscale of turbulence (μm, model result). Measurements have been taken at 0.8 m above the bottom (LISST) and 1 m above the bottom (OBS). The slope of the regression line for particle size is -7.13 and for Kolmogorov microscale -20.12. (from Fettweis et al., 2005).

3.2 Through tide SPM concentration measurements on the BCS

The process of resuspension/transport/deposition will result in mixing and fractioning of the sediments and as a consequence depends on the sediments which are supplied and on the hydrodynamic conditions. SPM concentration measurements (through tide and long term) have been carried out on the BCS using the R/V Belgica and a stand alone benthic lander (tripod). A list of them is given in table 3.1, the figures with the results can be found in appendix. I.

The measurements show that the SPM concentration in the coastal zone and more off shore varies strongly. Tidal variations are clearly detectable. In the coastal zone (B&W Oostende, Pas van het Zand, B&W Zeebrugge Oost, Scheur E, Vlakte van de Raan) the SPM concentration is usually high with occasionally low values. Maxima vary between 8-592 mg/l and minima between 1-99 mg/l. More off shore the concentration are during most of the measurements low, with occasionally higher values. SPM concentration maxima are between 5-340 mg/l and minima between 1-44 mg/l. The peaks in SPM concentration are coupled to the peaks in current

velocity and occur after the maxima in current velocity (Fettweis et al., 2002). The occurrence of a time lag in suspended sediment transport is well known (Bass et al., 2002; Dyer, 1995; Hoitink et al., 2003) and is related to the fact that the re-suspended mud needs a certain time to be distributed over the water column. Van Parys & Pieters (2001) observed this process near Zeebrugge, where the mud bed starts to be re-suspended when the tidal current increases to 0.15 m/s, but only when the current velocity was >0.5 m/s the increase of SPM concentration could be measured near the surface.

Table 3.1: Max and min SPM concentration during through tide measurements. Also indicated are the time relative to HW and the averaged wind speed & direction. Tide is the tidal amplitude: NT=neap tide, AT=average tide, ST=spring tide. The measurements are grouped according to locations (see fig 1-8 in app. 1). The measurements with the SBE09 are at about 3 m above bottom and with the SBE19 system at 3 m under sea surface.

Cmp	Instr	Tide	SPM Max		SPM Min		Wind		
YY/Nr			Time	mg/l	Time	mg/l	m/s	°	
B&W Oostende (fig I-2)									
99/07	SBE09	NT	-0.15	203	-7.57	20	3.8	98	E
	SBE19		-1.13	110	-7.35	21			
02/27-a	SBE09	AT	-2.08	55	-8.18	14	4.9	272	W
	SBE19		-2.02	54	-9.43	2			
03/04-b	SBE09	ST	±-4	>300	-6.48	54	2.4	132	SE
	SBE19		±-4	>300	-6.40	59			
01/06-b	SBE09	AT	-9.45	592	-0.98	53	6.7	203	SSW
	SBE19		-9.40	535	-0.67	49			
Pas van het Zand (fig I-3)									
01/06-a	SBE09	AT	-6.92	509	-1.65	28	3.2	150	SSE
	SBE19		-6.58	401	-1.70	28			
02/27-b	SBE09	NT	-5.12	121	-3.63	29	7.2	159	SSE
	SBE19		-7.40	110	-1.13	18			
03/04-a	SBE09	ST	±-7	>300	-1.15	39	9.1	101	E
	SBE19		±-7	>300	-1.07	37			
03/22	SBE09	AT	5.12	106	-2.20	17	6.0	30	NNE
	SBE19		5.20	106	-2.18	15			
B&W Zeebrugge Oost (fig. I-4)									
00/08	SBE09	ST	6.40	600	-0.87	44	4.3	36	NE
	SBE19		-1.55	618	-1.03	41			
00/14	SBE09	NT	5.80	215	8.02	16	9.6	252	WSW
	SBE19		8.95	368	8.07	64			
00/26	SBE09	AT	5.90	232	3.43	40	12.7	241	WSW
	SBE19		5.95	236	10.35	35			
Scheur E (fig I-5)									
00/31	SBE09	AT	5.73	24	-1.93	8	10.2	144	SE
	SBE19		-4.82	26	-11.67	15			
02/01-a	SBE09	AT	1.18	309	3.37	10	9.3	61	ENE
	SBE19		6.80	275	3.42	20			
02/01-b	SBE09	AT	1.63	306	2.18	99	15	24	NNE
	SBE19		1.65	365	-0.63	78			
02/06-a	SBE09	AT	-5.62	160	2.90	16	2.8	52	NE
	SBE19		1.05	118	3.10	24			
02/14-a	SBE09	ST	4.12	35	3.42	4	9.0	246	WSW
	SBE19		9.22	56	3.42	1			
01/17-a	SBE09	AT	0.17	59	-2.62	6	3.5	316	NW
	SBE19		6.38	61	8.55	13			
Kwinte Bank (fig. I-6)									
03/15	SBE09	AT	1.35	5	4.52	2	3.5	36	NE
	SBE19		4.50	24	4.75	1			
03/17	SBE09	NT	5.75	5	-13.60	2	5.8	353	N
	SBE19		-	-	-	-			

03/25	SBE09	ST	-8.18	58	-6.53	6	11.2	255	WSW
	SBE19		-2.62	47	-7.37	7			
Off shore (fig. I-7)									
00/19	SBE09	NT	-1.47	19	1.63	3	12.8	261	W
	SBE19		-1.20	22	1.72	8			
02/14-b	SBE09	ST	-1.08	10	-8.20	2	5.8	311	NW
	SBE19		-8.85	10	-8.88	1			
99/17	SBE09	ST	2.62	20	-0.60	7	4.6	267	W
	SBE19		2.80	8	-3.13	5			
01/29	SBE09	ST	-3.87	180	-1.08	34	9.1	39	NE
	SBE19		6.90	283	-1.42	23			
02/06-b	SBE09	ST	-2.25	75	4.00	1	6.9	37	NE
	SBE19		-2.20	77	4.10	9			
Vlakte van de Raan (fig. I-8)									
01/01	SBE09	AT	10.97	340	6.12	39	7.7	197	SSW
	SBE19		11.02	268	6.15	44			
01/17-b	SBE09	AT	9.03	8	-1.27	1	5.6	185	S
	SBE19		2.85	13	-1.22	7			

3.3 SPM concentration distribution on the BCS

The Belgian and southern Dutch coastal waters are an effective trap for fine grained cohesive sediments, resulting in the formation of an area of high SPM concentration. The formation of a coastal turbidity maximum has been ascribed to the governing hydrodynamic conditions, which are such that the residual water transport is reduced resulting in a congestion of the sediment transport in the area (Fettweis & Van den Eynde, 2003). Accurate knowledge of the SPM transport system is especially important because of its effect on the economy (dredging and dumping), the environment and as such also for setting up a framework for a sustainable management of the area.

The first studies on the suspended fine-grained sediments have been published by Van Mierlo (1899). The attention on this subject was redrawn in the seventies using measurements and modelling (Bastin, 1974; Nihoul, 1975; Gullentops et al. 1976; Eisma & Kalf, 1979) when the port of Zeebrugge was extended and the navigation channels deepened. The SPM concentration has a characteristic distribution in the Belgian-Dutch coastal zone, which is due to the hydrodynamics, the prevailing winds, the input of suspended matter into the area mainly from the English Channel and the resuspension and/of erosion of (recent and old) fine grained sediments (Fettweis & Van den Eynde, 2003). Seasonal averaged SPM concentration maps have been constructed from the measurement data, which have been downloaded from the BMDC database (http://www.mumm.ac.be/datacentre), see figure 3.3. On smaller time scale variation occur as a function of tides (§3.2), neap-spring tidal cycles, storm events and possibly also to wind influences in analogy with salinity variations in the Belgian coastal zone (Lacroix et al., 2004).

3.4 Use of satellite images to retrieve SPM concentration distributions

SPM surface concentration maps can be retrieved from satellite images. The advantage of satellite data is their geographical extension, the disadvantage is the relatively low time resolution and the fact that only cloud free conditions and surface waters are mapped. For the Belgian/Dutch coastal zone SeaWiFS images have been successfully used. The methodology and results are presented in Van den Eynde et al. (2005) and are briefly summarised below.

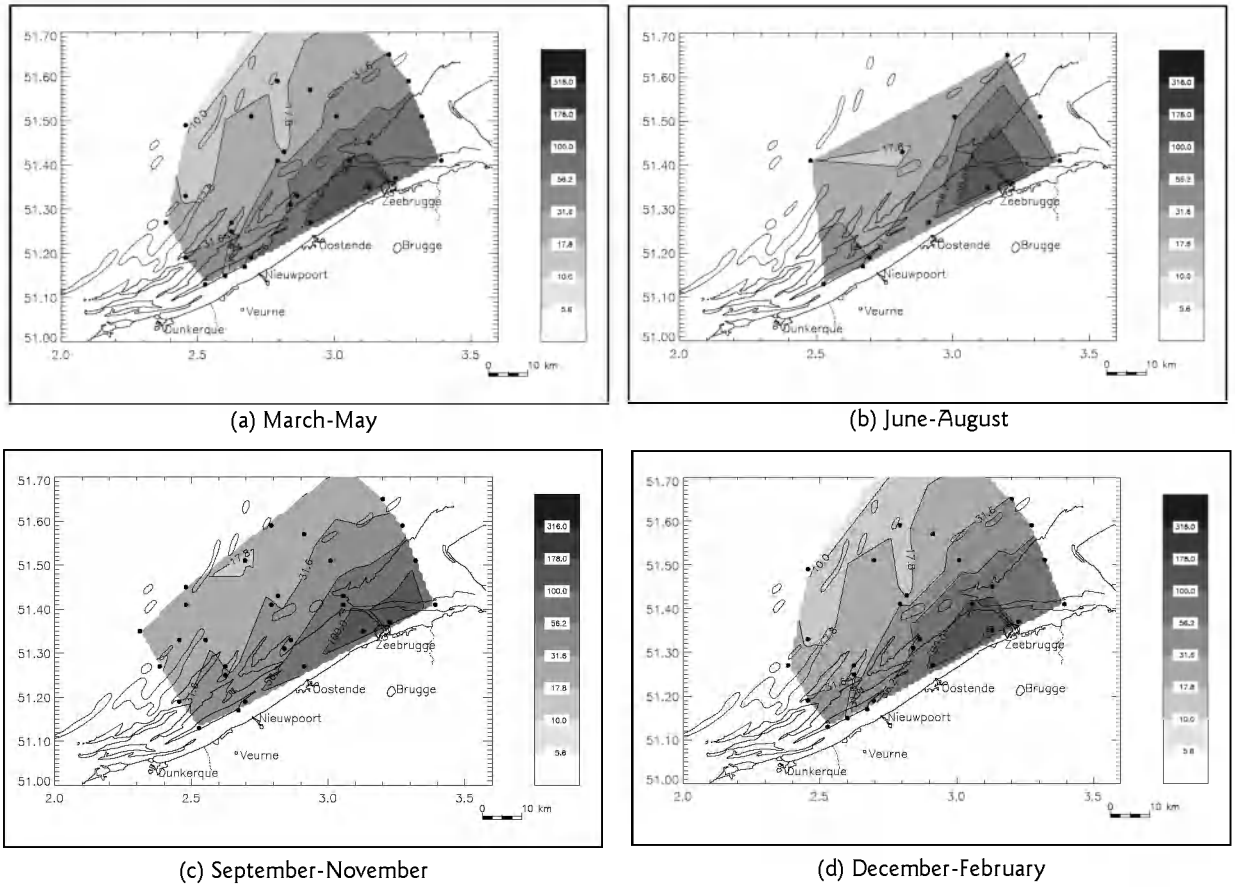

(a) March-May

(b) June-August

(c) September-November

(d) December-February

Figure 3.3: Suspended particulate matter concentration (mg/l), The map has been constructed using the arithmetic mean of minimum 10 samples per point of MUMM's monitoring data (1977-1996). Also indicated is the 10 m depth contour.

3.4.1 Calculation of surface SPM concentration from SeaWifs images

The SeaWiFS imagery uses the Top Of Atmosphere (TOA) radiance measured at the sensor level. Processing is needed to calculate the SPM concentration at the water surface. First the various atmospheric contributions to the TOA radiance, i.e. light scattering by air molecules and aerosols, absorption by oxygen and ozone and the sky glint, have to be removed to produce the reflectance at the sea level. This was carried out using the SeaDAS software algorithm extended to turbid waters. The description of this algorithm can be found in Ruddick *et al.* (2000). Next, a hydro-optical model (Nechad et al., 2003), designed for Belgian waters is used to convert the reflectance at the sea level into SPM surface concentrations.

3.4.2 SPM concentration from in situ measurements

Knowledge of resuspension, transport and deposition of fine grained sediment is important to understand the variations in SPM concentration observed in satellite images. This knowledge is provided from in situ measurements carried out with the R/V Belgica from 1999 to 2002.

The turbidity in the water column was measured with an Optical Back Scatter (OBS) sensor, mounted on a Rosette water sampling - SBE09 SCTD system. Data were acquired every half second. Every hour a vertical profile was measured. Furthermore every 20 minutes, a water sample was collected at about 3 m above the bottom using the 10 litre Niskin bottles of the Rosette water sampling system. These water samples were used for gravimetrical determination of the SPM concentration. The vertical profiles cover the water column from about 3 m above the bottom to about 1 m below the sea surface. In order to take into account the entire profile, including the lowest layer in which the highest concentrations are expected, an extrapolation is made using a theoretical profile (Van Rijn, 1993).

The vertical profiles reveal that the surface SPM concentration as well as the stratification is

high only for about 2 hours during ebb and flood (about 1/3 of the tidal cycle). During the rest of the tide the measured SPM concentration and stratification are much lower and correspond to a background value, which is high (50 mg/l) in the high turbidity zone (Oostende and Zeebrugge area). For all the profiles the depth-averaged and the surface SPM concentration were calculated, together with their ratio. In the near-shore Zeebrugge and Oostende area a clear cycle can be observed: 1 hour before high water and around low water, the ratio between the depth-averaged and the surface SPM concentration increases to about 2 and about 1.5 respectively. In the Oostende area the ratio around low water increases to almost 2.2. In the offshore area, on the other hand, the ratio between the depth-averaged and the surface SPM concentration stays constant over the entire tidal cycle and is limited to values below 1.1. Only one hour after high water, does the ratio increases to about 1.25.

3.4.3 Seasonal and depth-averaged SPM concentration maps

In order to obtain depth-averaged SPM concentrations from satellite measured surface SPM concentration maps, corrections have been applied. The ratio between the surface SPM concentration and the depth-averaged SPM concentration varies during the tidal cycle. During the background period, the ratio between the surface SPM concentration and the depth-averaged SPM concentration is almost equal to one and the surface SPM concentration, derived from the satellite images, will represent well the averaged SPM concentration. During the periods with higher stratification, however, this ratio can be higher than 2.2 and the satellite images underestimate the depth-averaged SPM concentration. Furthermore, this correction factor varies over the BCS. Therefore different correction functions have been setup (see Van den Eynde et al. 2005).

The corrected satellite images are then used to calculate a season-averaged SPM concentration, the results are presented in figure 3.4. The influence of seasons is clearly visible: the SPM concentration is lower during spring and summer and higher during autumn and winter. This seasonal variation is due to variation in import of suspended matter through the Strait of Dover, of higher frequencies of storms during the winter period and thus higher resuspension and maybe also to temperature effects on the settling velocity of the particles. A particle with a fixed size and density settles faster in warm water than in cold water (Krogel & Flemming, 1998) resulting thus in less favourable depositional condition in winter than in summer.

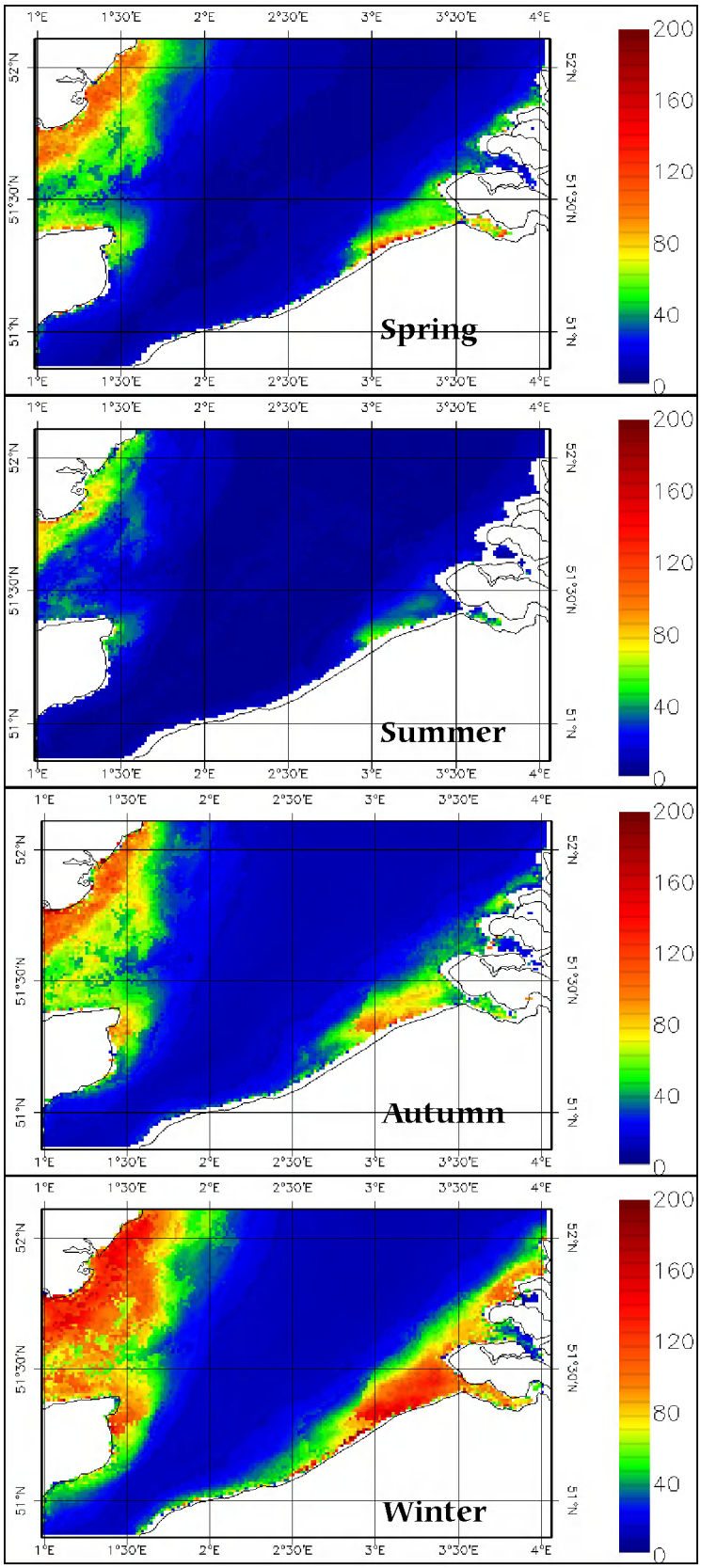

Figure 3.4: Seasonal and depth averaged SPM concentration (mg/l) derived from 370 SeaWiFS images (1997-2002) and in situ measurements. (Correction to obtain depth averaged SPM concentrations has only been applied to the B/Nl coastal waters, in the rest of the domain the SPM surface concentration values are displayed).

4. Analysis of clay minerals, microfossils, grain sizes of selected bottom and suspension samples

4.1 Clay mineralogy and microfossils as provenance indicators for the North Sea mud: a critical review

Clay minerals in recent deposits such as the North Sea mud are almost exclusively detrital. They have been eroded from older rocks exposed in the drainage area of the rivers supplying sediments to the sea or from coastal cliffs. In addition, clay minerals in the drainage area can be eroded from the present top soils; clay minerals in top soils reflect a climatic signature superposed on the parent clay mineral composition (see e.g. Chamley, 1989). In the case of recent North Sea mud, it can be safely stated that the detrital signature of the eroded geological formations will be dominant over the temperate-climatic effect on the mineralogy in the top soils around the North Sea. The different possible sources for the clay minerals in the North Sea mud are summarized below.

1. If the suspensions enter via the Strait of Dover they may have been derived from the Atlantic waters, from erosion of English and/or French coasts or from river input in the Channel (English and French side). These possibilities are summarized in figure 4.1.

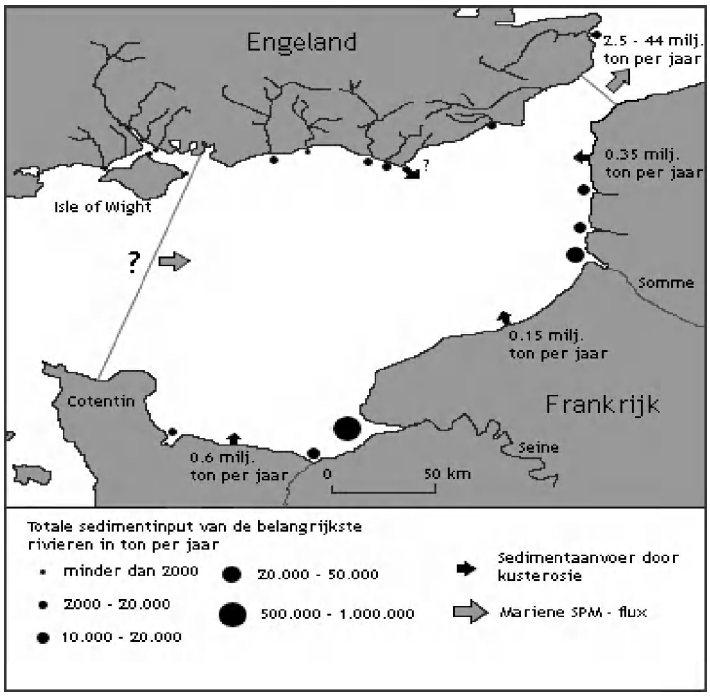

Figure 4.1: Different sources of suspended sediments in the English Channel and the sediment flux through the Strait of Dover (from Velegrakis et al., 1999).

2. Erosion in the Belgian part of the North Sea from pre-recent Cenozoic substrate of the North Sea. Such erosion might involve Ieper Group clays, clayey sands and clays of the Tielt & Maldegem formations and Holocene clays (Duinkerke clays). Even winnowing of the Pleistocene fluviatile and eolian sand cover of the North Sea could be a major mud source.
3. Mud can also enter the North Sea via the Schelde estuary as suggested by some satellite observations of the SPM concentration (figure 3.4). Other studies suggest that a large volume of mud transported in the river system is deposited on salt marshes (Temmerman, 2003). Sels (1997) has shown the active local erosion and sedimentation in the Schelde estuary and in the North Sea in front of the estuary during the last decades.
4. Large quantities of mud are dredged in relation with the continuous access of the Zeebrugge harbour; the dump sites to the north of Zeebrugge (figure 1.1) might become resuspended.

The presence of a mud bottom in the sea existed however before the harbour works first started, as is documented by reports of the early 20th century. Sels (2003) has calculated form differential depth maps the sedimentation and erosion sites around the dumping sites.

5. Although not favoured by many, an entry via northern, north-western part of the North Sea does not seem to be entirely excluded from the start.

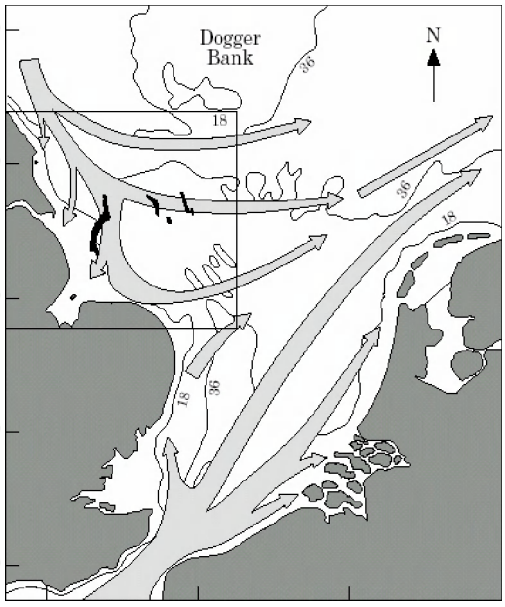

Figure 4.2: Major residual circulation in the North Sea (from Proctor et al., 2001)

Although some data are available on the clay mineralogical composition of these potential source areas, quantitative data are lacking with regard to eroded volumes involved and also the quantitative clay mineralogical composition is at best semi-quantitative and generally very poorly comparable between laboratories. Data on the clay mineralogical composition of the different potential sources are dispersed in the literature.

However, seen the different potential sources of the mud, it is expected that different clay mineral associations could be found on the Belgian platform, pointing to the provenance areas. Indeed, a preliminary study of the clay mineralogy in the southern North Sea shows a smectite dominated association but also shows some variability (Irion & Zöllmer, 1999), see fig.4.3. In this study intensities were modulated by parameters to quantify the clay mineral compositions. Therefore it seems justified to expect objective statements on clay mineral variations in the Belgian North Sea from a rigorously quantitative analysis and a relative dense and well planned sampling grid.

In order to explore further the information on provenance, an until now unused method will be tried out, namely the study of reworked microfossils. It is reasonable to expect that with the minerals also microfossils have been eroded from the source rocks and that although these microfossils are so much more fragile than minerals, some might have survived and leave a trace of the origin of the sediment.

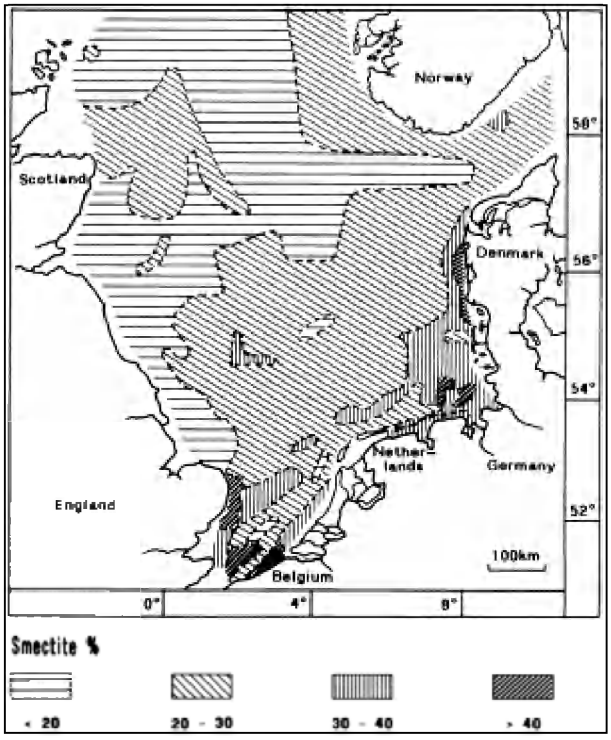

Figure 4.3: Smectite content in surface sediments of the North Sea (from Irion & Zöllmer, 1999).

4.2 Analytical Method

The XRD technique which has been applied for clay mineral analysis is described in appendix II.

4.2.1 The problem of quantitative clay mineral analysis

After the identification of the different minerals present according to the criteria outlined in appendix II (§ II.3), quantification of these minerals is required and unfortunately no generally accepted standard procedure exists for quantifying clay minerals. On the contrary, a variety of quantification methodologies have been proposed in the literature.

In the present research on North Sea mud, a method has been chosen reporting all clay minerals in relative proportion to each other using Mineral Intensity Factors (MIF) and normalized to 100% (Moore & Reynolds, 1997; Kahle et al., 2002). The simplified basic quantitative diffraction equation (Moore & Reynolds, 1997):

$$U_i = (1/V_i)^2.(1/\rho_i)\,|F_i|^2.(1+\cos^2 2\theta_i).(1/\sin 2\theta_i) \qquad (4.1)$$

with U_i = a constant for a specific diffraction peak I,
V_i = volume of the unit cell of the mineral producing peak I,
ρ_i = density of the mineral producing peak I,
F_i = structure factor of the mineral producing peak I,
can be used to demonstrate the relationship between the intensity of a diffraction peak and the weight fraction of a mineral:

$$I_i = K.Wf_i.U_i.(1/\mu) \qquad (4.2)$$

with I_i = intensity of the diffraction peak I,
K = a constant,
Wf_i = the weight fraction of mineral I,
μ = mean mass-absorption coefficient,
and the relationship between peak intensities of two minerals (I) and their relative weight presence (W) modulated by their mineral intensity factors (U):

$$I_1/I_2 = (Wf_1/Wf_2).(U_1/U_2) \qquad (4.3)$$

In this equation (U1/U2) is a constant and indicated as the Mineral Intensity Factor (MIF). If the relative weight fraction of each mineral can now be calculated using their peak intensity and their MIF. Assuming that all minerals in the sample are known, then

$$W_1 = (I_1/MIF_1)/\Sigma^n_{i=1}(I_i/MIF_i) \quad \text{for n mineral phases present} \qquad (4.4)$$

Widely varying MIF's are cited for the different clay minerals in the literature (Kahle et al., 2002) and the values traditionally used in our laboratory for the relevant minerals in North Sea mud are given in the table 4.1.

Table 4.1: Mineral Intensity Factors (MIF) used in the Historic Geology Section of the KUL.

	Smectite	Chlorite	Illite	Kaolinite
1/MIF	0.25	0.34	1	0.7

The intensities on the diffractograms are measured estimating the surface covered by the peaks. In a first step the background is reconstructed at the peak position. The peak height is now measured as well as the peak width at half height; both values are multiplied to represent the peak surface. For smectite, kaolinite and illite this surface determination is done on the respectively 17, 7 and peaks of the EG samples. For chlorite no intensities were calculated as the concentrations present in the samples are very low or absent, and therefore also do not interfere with the kaolinite determination.

4.2.2 Grain-size analysis by laser diffraction

All grain-size analyses are performed using a Malvern Mastersizer S long bed laser diffractometer. Laser light is interfering with particles and different theoretical models relate absorption and dispersion of light as a function of the size of particles. An array of optical sensors measure the diffraction patterns produced by the grains and convert these patterns into a volumetric size distribution of the grains in a sample.

The light source is a 2 MW He-Ne laser with 633 nm wavelength. The light bundle has a diameter of 28 mm and is polarized. The optical unit consists of 48 sensors: 42 sensors for recording the diffraction patterns, one central detector sensor, 2 sensors for aligning, 2 sensors for direct reflection measurement and 1 laser monitoring sensor. For this project the measuring range is set at 0.05-900 μm.

The raw data are transformed into size distributions using the Malvern software. The software uses Mie-theory for spherical particles. The turbulent sample flow leads to a volumetric size distribution estimate.

In comparison with the traditional settling techniques in columns or in automated sedigraph-type apparatus, based on Stokes law, the maximum size of the fine platy clay fraction population defined as 2μm equivalent-spherical diameter in Stokes law, becomes about 8 μm using the diffraction method (Konert & Vandenberghe, 1997). Therefore in this study, the clay fraction of a sediment is defined by $<8\mu$m.

4.3 Size analysis of suspended matter at two locations

4.3.1 Choice of the measurement locations

In situ measurements of suspended matter particle sizes using the LISST 100C at the Kwinte Bank (in front of Nieuwpoort) and near Zeebrugge, showed differences in size distribution (see §2.1.3). The differences could point to the presence of different types of suspended matter on the Belgian North Sea continental platform. At the one hand a background suspension clearly visible outside the direct coastal area as at the Kwinte Bank and on the other hand suspended matter in the turbulence maximum of the direct coastal zone. To test if the size differences of the flocs correspond to either changes in the size distribution of the individual composing grains (after floc destruction) or to the degree of flocculation of the same fundamental grains,

laboratory laser size analysis and clay mineral analysis have been performed to complement the in situ laser size measurements.

4.3.2 Basic data from the in situ size measurements using LISST

Above the sandy part of the Kwinte Bank two LISST in situ measurements were carried out during two different sampling campaigns (see also §3.1). Slightly different size results are obtained (table 4.2). However a remarkable feature of the size distribution seems to be the bimodal nature of the floc size distribution: 50 μm and 300-500 μm modal sizes in campaign 2003/15 and 10 μm and 200-500 μm modal sizes in campaign 2003/17. Modal sizes of 500 μm point to the possible occurrence of even larger flocs. On the contrary the sampling during campaign 2003/22 to the west of Zeebrugge over a medium consolidated mud bottom covered by fine sand with patches of liquid mud a unimodal size distribution is measured with 50 μm modal size. The bottom mud samples consist of almost equal part of silt and clay fractions with a median size of ±30 μm (Fettweis et al., 2003).

In the Zeebrugge sample, calculated effective densities of the flocs are high: 300-2000 kg/m^3; total suspension load is between 20-100 mg/l; particles are small: 20-90 μm and the settling velocities are small: 0.3–2 mm/s. In the Kwinte Bank samples, effective densities are smaller: 200-800 kg/m^3; total suspension load is limited to 3-9 mg/l; particle sizes are between 100-250 μm and the settling velocities are 2-10 mm/s.

Table 4.2: The sedimentological characteristics of the suspended particulate matter and the sediments on the bottom at the two measuring stations. In situ particle size distribution measured by LISST 100C..

Station	Zeebrugge	Kwinte Bank	
Campaign Nr.	2003/22	2003/15	2003/17
Suspension			
Averaged SPM conc. (mg/l)	35	<10	<10
Maximum floc size (μm)		> 500	> 500
Averaged floc size (μm)	44 μm	158	198
Modus (μm) at	50	50 300-500	10 200-500
Effective density of flocs (kg/m^3)	700-2000	200-800	-
Bottom sediment			
Mud content (%) in bottom	65	<1	
D50 of bottom mud (μm)	30	±200	

4.3.3 Size analysis with the laboratory laser diffractometer

For comparison reasons, samples were taken of the suspended matter near Zeebrugge and over the Kwinte Bank using a centrifuge. The Kwinte Bank sample was taken during a through tide measurement during campaign 2003/15; the centrifuged sample has been frozen, one week later it was defrosted and further kept at room temperature in closed sample bag. The Zeebrugge sample was taken during campaign 2003/22; it was not frozen and further kept in the same way as the Kwinte Bank sample. Both samples have not been completely dewatered or rinsed before transfer to the sample bags and therefore have been preserved in sea water. Care was taken not to squeeze of compress the sample bags.

In order to measure as closely as possible the natural distribution three analyses types have been applied. A first sub-sample was analyzed as it came out of the sample bags without any further treatment. In a second analysis, a sub-sample of 10 g was shaken overnight in water and splitted twice. A third analysis was performed on another 10 g of sample which was treated by boiling and adding dispersant and further splitting twice; in this last treatment it was hoped to decompose the floccules to their fundamental composing grains. For each analytical step a repeat analysis was done. In addition another grain-size analysis was carried out af-

ter carbonate and organic matter removal using dispersant. Carbonate content of the samples was determined by weight loss after HCl (1.5N) addition and organic matter content by weight loss after 24 hours heating between 190 and 387 °C. Repeat analyses are labelled 1 and 2 in table 4.3.

Direct analysis data show large differences and in particular the 5% coarse percentile data suggest the data to be unreliable because of secondary aggregation during the preservation period of the sample. Analysis in water shows a better repeatability. Both samples have a large clay fraction. The 5% coarse percentile of the Kwinte Bank sample is 48 μm and of the Zeebrugge sample 65.5 μm. The Kwinte Bank sample shows a non repeatable third coarse population (43% with mode at 114 μm).

Table 4.3: Grain size analysis of suspended matter using laser-diffractometry. Repeat samples are labelled 1 and 2.

	Zeebrugge		Kwinte Bank	
Belgica campaign	2003/22		2003/22	
Repeat sample	1	2	1	2
O.M. (%)	4.23		5.37	
CaCO3 (%)	36		40	
Direct analysis				
Number of populations	2(3)	2	3	2
Boundary (μm)	1.0	0.8	0.6 + 70	0.7
Mode (μm)	0.50+0.36 (7.5%) 18.13 (92.5%)	0.35 (8.5%) 15.27 (91.5%)	0.52 (6.0%) 8.43 (88.5%) 113.11 (5.5%)	0.52 (8.5%) 6.94 (91.50%)
5% biggest fraction (μm)	88.5	56.5	76.5	36
Clay content (%)	32.0	43.0	47.0	59.0
Analysis with water				
Number of populations	2	2	3	2
Boundary (μm)	0.8	1.0	0.8	0.8
Mode (μm)	0.35 (8.5%) 10.92 (91.5%)	0.50 (9.5%) 9.31 (90.5%)	0.35 (3.5%) 10.60 (53.5) 114.35 (43.0%)	0.35 (3.5%) 8.49 (96.5%)
5% biggest fraction (μm)	65.5	65.0	48.0	48.0
Clay content (%)	44.0	45.0	46.5	50.5
Analysis with peptisant				
Number of populations	2	2	2(3)	3
Boundary (μm)	0.9	0.8	0.9	1.0
Mode (μm)	0.35 (6.5%) 13.48 (93.5%)	0.35 (6.0%) 16.68 (94.0%)	0.36+0.50 (6%) 14.90 (94%)	0.36+0.50 (7%) 12.03 (93%)
5% biggest fraction (μm)	48.5	41.5	66.0	76.0
Clay content (%)	31	31	34	35
Analysis after removal of OM and CaCO3				
Number of populations	2	2	1	1
Boundary (μm)	32	31		
Mode (μm)	7.43 (78%) 53.09 (22%)	7.50 (77.5%) 52.87 (22.5%)	7.07	7.50
5% biggest fraction (μm)	196	103	41.4	48
Clay content (%)	45.5	44.5	55.5	53.0

Dispersant is supposed to break down the floccules. The Zeebrugge sample only shows minor differences with the in-water analysis: a slight increase in size is observed. The Kwinte Bank sample loses the coarse 114 μm mode population which is added to the 10 μm population in the same way as did the repeat in-water analysis. Both samples show after dispersant addition a decrease in the clay fraction content, a somewhat unexpected result. After removal of carbonates and organic matter, the clay fraction appears similar as in the in-water analysis. However the other descriptive grain-size parameters become quite different. In the Zeebrugge sample the 5% coarse percentile size doubles compared to the dispersant only treatment and the main modal size decreases to 7 μm instead of 13 μm but a new population appears with modal size 53 μm. There is no obvious explanation for this result.

The Kwinte Bank sample is now characterized by a unimodal size distribution with mode of about 7 μm whilst the 5% coarse percentile and the clay fraction percentage are roughly comparable with the in-water analysis.

The clay mineral composition of the Zeebrugge and Kwinte Bank suspended matter is similar as shown in table 4.4.

Table 4.4: Results of clay mineralogical analysis (% of clay minerals)

Station	Illite	Smectite	Kaolinite	Chlorite	Position Sm	v/p
Zeebrugge (SPM0322_TT20)	53.5	25.9	20.6	+	16.89	0.1
Kwinte Bank (SPM0322_KW)	60.5	20.0	19.5	+	16.83	0.1

4.4 Clay mineralogy of North Sea mud: bottom sediments and SPM

4.4.1 The sampling strategy and sample locations.

Based on the discussion on possible sources of mud as reported in §4.1 additional samples have been collected for this study, both in suspension and in the bottom sediment. The samples are listed in the table 4.5. In the left column the areas suspected as mud source are listed, in the second column the location code of the samples has been given, additional remarks are given in the third column and in the last column it is indicated if suspension or/and bottom samples have been taken. Suspended sediment samples have been collected using the on board centrifuge.

The locations of bottom and suspension samples collected in campaign 2003/22 in the North Sea are indicated in figures III-1, III-2, III-3 (appendix III). In order to estimate the influence of the tidal cycle, at one location TT20, suspension samples have been collected every two hours (samples TT20-1 to TT20-7, in campaign 2003/22).

In order to control the mud mineralogy arriving in the North Sea through the Schelde estuary several bottom and suspension samples have been analysed, the location of which is indicated in figure III-4 (appendix III) to gain some insight into the time evolution of the clay mineralogy, samples from a shallow borehole in the Paulina mud plate have been analysed the recent stratigraphy of which has been studied by (Temmerman, 2003).

The bottom samples have been taken either using box cores or Van Veen sampler. The lithology of these bottom samples has been described in tables in appendix III.

A last sample set was collected at and around the Nieuwpoort harbour. The samples have been provided by the Afdeling Waterbouwkundig Laboratorium en Hydrologisch Onderzoek of the Ministry of the Flemish Community. The sample set was used to test in a well defined area the clay mineralogy of the incoming sea water and of the incoming fresh water in the harbour which is experiencing important mud sedimentation rates. Sample locations are shown in figure III-5 (appendix III).

Table 4.5: Suspended and bottom samples. Suspended samples have been collected with the centrifuge. (B/6=dumping site Br&W Zeebrugge Oost, B/9=dumping site Br&W Oostende), see figures in app III for location map.

Possible source	Location	Re-mark	Bot-/susp	R/V Belgica campaign
Strait of Dover	SPM0403_Cap Griz-Nez, SPM0404_Calais-Dunkerque		Susp.	2004/03
	BC0322_115bis; SPM0322_115BIS		Bot+susp	2003/22
Erosion of Tert. & Quart. clays	Kwinte Bank: BC0322_KW1→BC0322_KW7		Bottom	2003/22
	Kwinte Bank: SPM0322_KW	track	Susp	2003/22
	Oostdyck: BC0322_OD3, BC0322_OD4		Bottom	2003/22
	Zeebrugge: BC0227_ZB1, RK0227_ZB3, RK_0227_ZB5		Bottom	2002/27
	Oostende: BC0304_OE10, BC0227_OE13, BC0304_OE14		Bottom	03/04; 03/22
Schelde	Westerschelde: S4-S12	Track	Susp.	2004/09
	Zeeschelde: S18-S22	Track	Susp.	2004/09
	VV0409_S4, VV0409_S12, VV0409_S18, VV0409_S22		Bottom	2004/09
	BC0322_250, BC0322_700, BC0322_702		Bottom	2003/22
	SPM0322_250, SPM0322_700		Susp.	2003/22
Dredging and dumping	Zeebrugge: BC0227_ZB6,	B/6	Bottom	2002/27
	BC0322_700; SPM0322_700	B/6	Bot+susp	2003/22
	Oostende: BC0304_OE10, BC0227_OE13, BC0304_OE14	B/9	Bottom	02/27 03/04
	BC0322_130, SPM0322_130	B/9	Bot.+susp	2003/22
Northern BCS	SPM0322_421-435-800, SPM0322_Bf (Birkenfels)	Track	Susp.	2003/22

BC=Box Core, RK=Reineck Core, VV=Van Veen grab

4.4.2 Identification and quantification of the clay minerals present

The results of the clay mineral identification and the quantification, as described above in the section on methodology, are presented in the tables 4.6-4.14 below. The relative contents of the total clay minerals are expressed as percentages and for chlorite the estimation is expressed as: - = absent, + en ++ = traces, +++ = a few percent.

Also the exact peak position and the v/p-ratio shape of the smectite peak after ethylene glycol saturation are reported. Diffractogram expressions of three different v/p values in the samples are shown in figure 4.4. The peak shape of d(001) of illite is always narrow and consequently no open illite is present.

The quantitative data have been represented graphically as circles with a diameter proportional to their content and positioned on the map with their centre at the sample location, see figures IV-1 – IV-12 (appendix IV).

Table 4.6: Clay mineralogy of bottom samples from the BCS. (BC=BoxCore sample), see figure III-1 for location map

Sample	Illite	Smectite	Kaolinite	Chlorite	Position Sm	v/p
BC0322_**115bis**	60	18	22	+	17.1	0.0
BC0322_**130** top	47	29	24	-	18.7	0.2
BC0322_**130** bottom	54	27	18	+	17.3	0.3
BC0322_**230**	89	1	9	+	16.8	0.4
BC0322_**250**	49	17	34	+	17.2	-0.2
BC0322_**330**	18	80	1	-	17.1	0.5
BC0322_**700**	47	28	25	+	17.1	0.2
BC0322_**702**	43	31	25	+	17.5	0.4
BC0322_**MC5** top	50	37	12	-	19.9	0.3
BC0322_**MC5** clay flakes	53	29	18	-	17.7	0.4
BC0322_**KW4**	64	8	28	-	17.0	0.1
BC0322_**KW7**	80	4	16	-	17.6	0.2

Table 4.7: Clay mineralogy of suspension samples on the BCS, see fig III-2 for location map.

Sample	Illite	Smectite	Kaolinite	Chlorite	Position Sm	v/p
SPM0322_**115bis**	62	17	21	-	17.1	-0.3
SPM0322_**130**	52	25	23	+	17.4	-0.2
SPM0322_**250**	50	13	37	-	17.3	-0.3
SPM0322_**330**	52	27	21	+	17.2	-0.1
SPM0322_**421-800-435**	66	6	28	-	17.0	-0.5
SPM0322_**BF**	53	19	28	+	17.7	0.0
SPM0322_**KW**	58	20	22	+++	19.0	-0.5

Table 4.8: Clay mineralogy of bottom samples in the vicinity of Zeebrugge (BC=BoxCore, RK=Reineck Core sample), see figure III-1 for location map.

Sample	Illite	Smectite	Kaolinite	Chlorite	Position Sm	v/p
BC0227_**ZB1**	56	28	17	+	16.9	0.2
RK0227_**ZB3**	62	26	12	+	17.2	0.2
RK0227_**ZB5**	83	5	12	-	15.1	-0.3
BC0227_**ZB6** top	60	14	27	-	17.2	0.2
BC0227_**ZB6** bottom	59	13	29	+	17.7	0.2

Table 4.9: Clay mineralogy of bottom samples in the vicinity of Oostende (BC=BoxCore sample), see figure III-1 for location map.

Sample	Illite	Smectite	Kaolinite	Chlorite	Position Sm	v/p
BC0304_**OE10**	55	6	39	-	14.7	-0.3
BC0227_**OE13** top	64	11	26	-	15.7	-0.4
BC0227_**OE13** bottom	71	1	28	+	14.5	-2.0
BC0304_**OE14** top	67	18	15	+	17.1	0.0
BC0304_**OE14** bottom	69	6	25	-	17.0	-0.3

Table 4.10: Clay mineralogy of suspension samples from the Dover Strait, see figure III-3 for location map.

Sample	Illite	Smectite	Kaolinite	Chlorite	Position Sm	v/p
SPM0403_**Cap Gris-Nez**	59	13	28	+	17.1	-0.3
SPM0403_**Calais-Dunker.**	65	3	31	0.0	15.8	-0.3

Table 4.11: Clay mineralogy of bottom (VV=Van Veen grab) and suspension samples (SPM) from the Schelde estuary (VV=Van Veen grab), see figure III-4 for location map.

Sample	Illite	Smectite	Kaolinite	Chlorite	Position Sm	v/p
VV0409_**S4**	15	77	8	+	17.2	0.5
VV0409_**S12**	44	39	17	-	17.0	0.2
VV0409_**S18**	49	20	31	-	17.3	0.0
VV0304_**S22**	51	18	31	+	16.8	0.0
SPM0409_**S04-S12**	48	32	20	-	17.1	0.2
SPM0409_**S18-S22**	45	29	27	-	17.1	0.2

Table 4.12: Clay mineral in suspended samples (every 2 h) during a through tide measurement near Zeebrugge (0322_TT20 8-9/09/2003), see figure III-2 for location map.

Sample	Illite	Smectite	Kaolinite	Chlorite	Position Sm	v/p
SPM0322_**TT20-1**	53	24	23	+	17.5	0.2
SPM0322_**TT20-2**	36	33	31	+	17.2	0.1
SPM0322_**TT20-3**	55	20	25	+	16.9	-0.2
SPM0322_**TT20-4**	52	24	24	-	17.1	-0.2
SPM0322_**TT20-5**	60	12	28	+	17.1	-0.5
SPM0322_**TT20-6**	57	17	26	++	17.4	0.0
SPM0322_**TT20-7**	55	20	25	+	17.0	-0.3

Table 4.13: Long term clay mineralogical variation in bottom samples from the Schelde estuary (Paulinaschor), see figure III-4 for location map.

Sample	Illite	Smectite	Kaolinite	Chlorite	Position Sm	v/p
P01 18-20cm	46	48	36	+	17.4	0.0
P01 27-28cm	66	6	29	+	17.0	-0.1
P01 41-42cm	71	2	26	+	16.7	-0.3

Table 4.14: Clay mineralogy of bottom samples from the Yzer basin and the harbour of Nieuwpoort), see figure III-5 for location map.

Sample	Illite	Smectite	Kaolinite	Chlorite	Position Sm	v/p
Yzer Lo-Fintele	42	44	15	-	16.9	0.2
Kanaal Ieper-Yzer	49	30	22	-	16.9	0.0
P1	47	33	20	-	16.9	0.2
P2	82	6	12	-	14.6	-0.3
P3	62	15	23	-	15.2	-0.3
P7	61	10	29	-	15.2	-0.2
P8	71	7	22	-	16.0	-0.3
P9	55	16	29	-	14.7	0.0

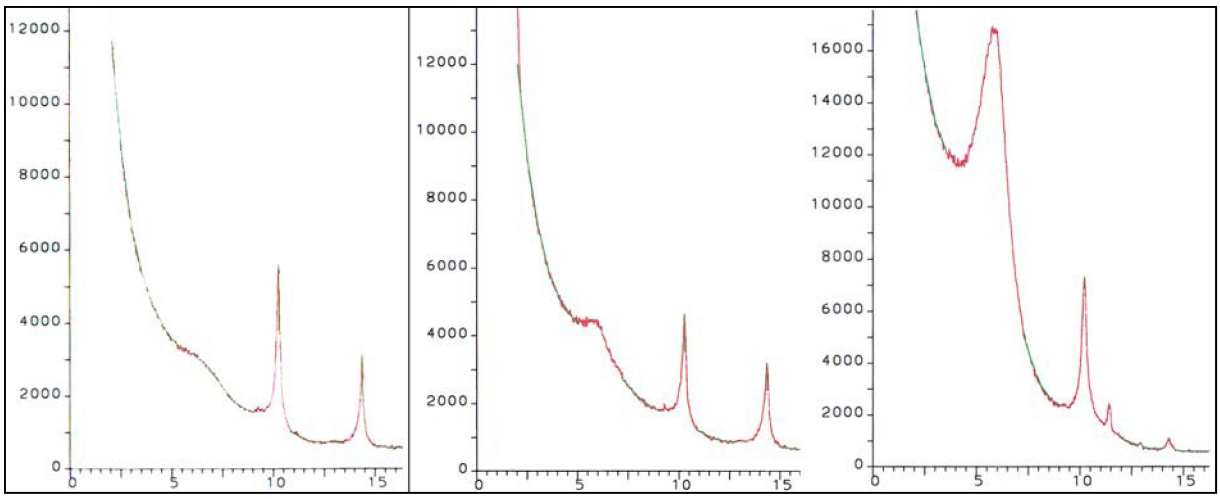

Figure 4.4: Diffractograms of samples BC0322_330, SPM0322_BF and BC0227_OE13 after glycolisation. The v/p ratio of the smectites are respectively 0.5, 0.0 and -0.4 (from left to right).

4.5 An exploration into the use of reworked microfossils as provenance indicators of North Sea mud

Microfossils in the mud sediments will be on the one hand dominated by the recent micro-organisms that rain down through the water column in the sediments together with the clay floccules but on the other hand also a limited number of older fossil micro-organisms will be included in the mud, eroded from the same sources as the detrital clay particles. Therefore microfossils can also be provenance indicators in the same way minerals can be. In this reconnaissance study a limited number of samples have been analyzed.

4.5.1 The preparation of microfossils from North Sea mud

Nannoplankton

A few gram of a carbonate containing sample is shaken in water: some drops are smeared on a glass plate, evaporated and covered with Canada balsam and a thin cover-glass. The nannoplankton is then identified under the microscope with magnifications of 1000, in normal and polarized light.

Organic walled microfossils

Samples are treated with HCl for carbonate removal, and in several further subsequent steps with HF to separate silicates from the organic matter, rinsed, further acid treated under heating and then centrifuged to separate the organic walled microfossils. A drop of this residue, sieved on a 30 μm mesh, is mixed with molten glycerin, covered with a glass slide and warmed till 60°C. The samples are studied under a microscope with magnification of 400-1000 and transmitting light.

Foraminifera

Carbonate containing samples are mixed with water, wet sieved over a 63 μm mesh, eventually further washed with Na_2CO_3 and treated with H_2O_2 (10-30%). The foraminifera are density separated from the silicates in CCl_4 and further sieved on a 125 μm mesh. This fraction is the studied under the microscope.

4.5.2 Microfossils in North Sea mud

4.5.2.1 Nannoplankton

Samples from suspension and bottom samples have been investigated, qualitatively and quantitatively, taking into account only complete specimens and not fragments although these are abundantly present in some samples. The specimens identified are described below.

4.5.2.1.1 Zeebrugge area and Oostende dumping site

BC0227_ZB1 Top: Abundance nannoplankton: 5 ex/mm² glass-slide (very rich in diatoms: 18 specimen/mm² glass-slide), with the following provenance:

- Cretaceous forms: 65%
- Paleogene forms: 11%; with *Isthmolithus recurvus*, *Reticulofenestra umbilica*, *Coccolithus formosus* and *Dictyococcites daviesii*, the occurrence of both species points to NP21 zonation (Earliest Oligocene) and sequence Ba3 (Bassevelde 3) or PRI 3 (Vandenberghe et al., 2003).
- *Coccolithus pelagicus*: 11%; large specimen, probably of recent origin
- rest: small *Prinsiaceae*: 11%, probably recent or sub-recent forms.

RK0227_ZB3 Top: Abundance nannoplankton: 6 ex/mm² glass-slide, with the following provenance:

- Cretaceous forms: 81%
- Paleogene forms: very scarce (<1%) with *Reticulofenestra umbilica* and *Braarudosphaera bigelowii*, pointing to latest Priaboniaan

- rest: *Coccolithus pelagicus*: 7%; large specimen, probably recent forms
- small *Prinsiaceae*: 11%, probably recent or sub-recent forms.

RK0227_ZB5 Top: Association with some Cretaceous coccoliths and with *Coccolithus pelagicus:* difficult to interpret the meaning of the association.

BC0227_OE13 Top: Abundance nannoplankton: 4 ex/mm² glass-slide, with following provenance:

- Cretaceous forms: 87%
- Paleogene forms: 4%; amongst which *Reticulofenestra umbilica*, *Coccolithus formosus*, *Dictyococcites bisectus* and *Dictyococcites daviesii*, pointing to nannofossil zone NP21 (Earliest Oligocene) sequence Ba3 (Bassevelde) or PRI 3 (Vandenberghe et al., 2003).
- Rest: *Coccolithus pelagicus*: 4%; large probably recent forms
- small *Prinsiaceae*: 4%, probably recent or sub-recent forms.

BC0227_OE13 20-30cm: Abundance nannoplankton: 1 ex/mm² glass-slide, with following provenance:

- Cretaceous forms: 92%
- Paleogene forms: <1%; some specimen of *Reticulofenestra umbilica* pointing to the Earliest Oligocene.
- rest: *Coccolithus pelagicus*: 8%; large probably recent forms.
- small *Prinsiaceae*: 0%

4.5.2.1.2 Nieuwpoort and west coast

BC0322_KW7: Abundance nannoplankton: 2 ex/mm² glass-slide, with the following provenance:

- Cretaceous forms: 72%
- Paleogene forms: 0%
- rest: *Coccolithus pelagicus*: <1%; a few large specimen, probably recent forms
- small *Prinsiaceae*: 27%, probably recent or sub-recent forms.

SPM0322_KW: Abundance nannoplankton: 26 ex/mm² glass-slide, many small coccoliths:

- Cretaceous forms: 6%
- Paleogene forms: <1%, with some small *Reticulofenestra spp.*, but no typical Priabonian-Earliest Oligocene forms
- rest: *Coccolithus pelagicus*: <1%; some large specimen probably recent forms; small *Prinsiaceae*: 93%, probably recent or sub-recent forms.

SPM0322_115bis: Abundance nannoplankton: 35 ex/mm² glass-slide, many small coccoliths:

- Cretaceous forms: 19%
- Paleogene forms: <1%, with some small *Reticulofenestra spp.*, but no typical Priabonian-Earliest Oligocene forms.
- rest: *Coccolithus pelagicus*: <1%; some large specimen of probably recent origin
- small *Prinsiaceae*: 79%, probably recent or sub-recent forms.

BC0322_115bis: Abundance nannoplankton: <1 ex/mm² glass-slide, percentages only indicative because of to poor associations:

- Cretaceous forms: 80%
- Paleogene forms: *Braarudosphaera bigelowii*: 10%, pointing to coastal influence
- rest: small *Prinsiaceae:* 10%, probably recent or sub-recent forms

4.5.2.1.3 MUMM monitoring points

SPM0322_130: Abundance nannoplankton: 5 ex/mm² glass-slide, with following provenance:

- Cretaceous forms : 75%

- Paleogene forms: 17%, amongst which *Isthmolithus recurvus* and *Braarudosphaera bigelowii*, pointing to the Latest Eocene - Earliest Oligocene.
- rest: *Coccolithus pelagicus*: <1%; some large specimen probably recent forms
- small *Prinsiaceae*: 8%, probably recent or sub-recent forms.

BC0322_230: Abundance nannoplankton: 10 ex/mm² glass-slide, very rich in diatoms, with following provenance:

- Cretaceous forms: 72%
- Paleogene forms: <1%, amongst which *Reticulofenestra umbilica*, *Coccolithus formosus*, *Braarudosphaera bigelowii* en *Pontosphaera zigzag*, pointing to biozone NP21
- rest: *Coccolithus pelagicus*: 2%; large specimen probably recent forms
- small *Prinsiaceae*: 26%, probably recent or sub-recent forms

SPM0322_330: Abundance nannoplankton: 11 ex/mm² glass-slide, may small coccoliths:

- Cretaceous forms: 31%
- Paleogene forms: 7%, amongst which *Reticulofenestra umbilica* and *Isthmolithus recurvus*, pointing to nannofossil zone NP21 or the Earliest Oligocene sequence Ba3 (Bassevelde) or PRI 3 (Vandenberghe et al.,2003)
- rest: *Coccolithus pelagicus*: <1%; some large specimen, probably recent forms.
- small *Prinsiaceae*: 62%, probably recent or sub-recent forms

4.5.2.1.4 Mouth of Westerschelde estuary

BC0322_250: some coccolith fragments, no interpretation possible.

SPM0322_250: Abundance nannoplankton: 6 ex/mm² glass-slide, very rich in diatoms, many small coccoliths:

- Cretaceous forms: 50%
- Paleogene forms: <1%, amongst which *Reticulofenestra umbilica*, *Dictyococcites bisectus* and *Dictyococcites daviesii*, pointing to nannofossil zone NP21 or Earliest Oligocene sequence Ba3 (Bassevelde) or PRI 3.
- rest: *Coccolithus pelagicus*: <1%; some large specimen, probably recent forms
- small *Prinsiaceae*: 49%, probably recent or sub-recent forms

4.5.2.2 Organic walled microfossils

Nannoplankton in chalk sediments is much more abundant than dinoflagellates, consequently reflecting the chances of finding these microfossils reworked. The dinoflagellate search was carried out on very limited sample volumes. Ratios between marine dinoflagellates and continental pollen and spores are variable.

BC0227_ZB1: *Chiropteridium spp.*, Membr. Aspinatum typical for Ruisbroek Formation (NP22) and possible younger, but not younger than S90 (mid NP23 Rupelian) because of the presence of *Enneadocysta*. This means an almost at location reworking.

RK0227_ZB3: Ba3 (Bassevelde) or marine Tongrian sequence, characteristic presence of *Areaosphaeridium dictyoplococus*

SPM0322_TT20-4: similar association as BC0227_ZB1

SPM0322_KW: *Dracodinium varielongitudum* point to Roubaix Member (Lower Ypresian). Possible from a local source as also suggested by the almost untransported microfossil properties

BC0322_KW7, SPM0322_330: one Cretaceous dinoflagellate

BC0227_OE13: no usefull information

BC0322_230, BC0322_250, SPM0322_115bis, SPM0322_130, SPM0322_250 do not contain useful information on dinoflagellates. The variable ratios between recent and reworked micro-fossils, and between pollen and spores on the one hand and dinoflagellates on the other hand, are remarkable and remain at the moment unexplained (table 4.15).

Table 4.15: Results of counting's of microfossils with organic wall: *1 = oval brown cyst, *2 = brown spherical with two 'leg', *3 = foram test lines, *4 = bissacate pollen (#=number, tot.=total, rec.=recent, fos.=fossils)

			Dinoflagellates (#)				(#)						
Sample	Mass (g)	Tot. (#)	Rec.	Fos.	*1	*2	*3	Spores	*4	Δ	□	⬠	⬡
BC0322_**115bis**	31	416	21	4	20	2	21	338	10	0	0	0	0
BC0322_**230**	15	153	8	4	30	2	31	22	44	6	3	0	3
BC0322_**250**	49	72	14	2	4	0	22	18	6	5	0	0	1
BC0322_**KW7**	30	247	16	8	43	9	84	25	56	4	0	1	1
BC0227_**OE13**	21	316	21	11	48	11	34	20	158	7	0	1	5
BC0227_**ZB1**	27	139	31	4	11	10	29	17	29	4	0	0	4
RK0227_**ZB3**	24	143	38	11	5	5	47	6	30	0	0	0	1
SPM0322_**130**	15	245	83	10	43	0	44	19	37	7	0	0	2
SPM0322_**250**	7	264	24	7	21	5	31	81	25	11	52	2	5
SPM0322_**330**	8	313	71	13	33	23	63	9	101	0	0	0	0
SPM0322_**KW**	36	337	29	9	38	25	66	13	155	0	0	0	2
SPM0322_**TT20-4**	9	404	72	14	29	21	81	27	155	1	0	0	4

BC=Box Core; RK=Reineck Core

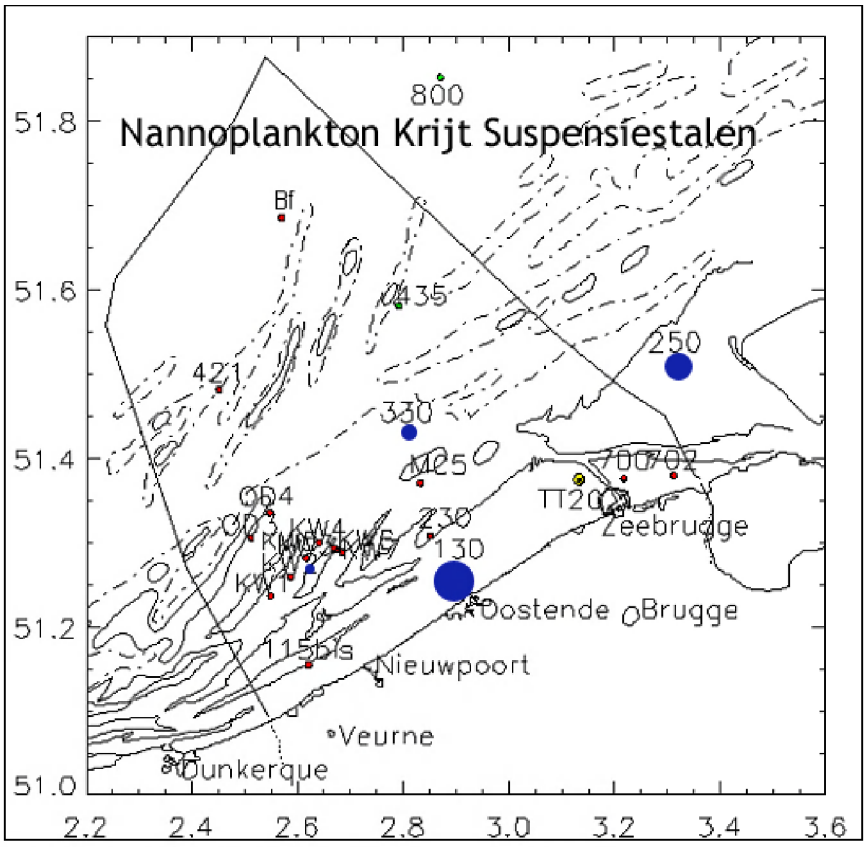

Figure 4.5: Content of nannoplankton of Cretaceous age in the suspension samples on the BCS.

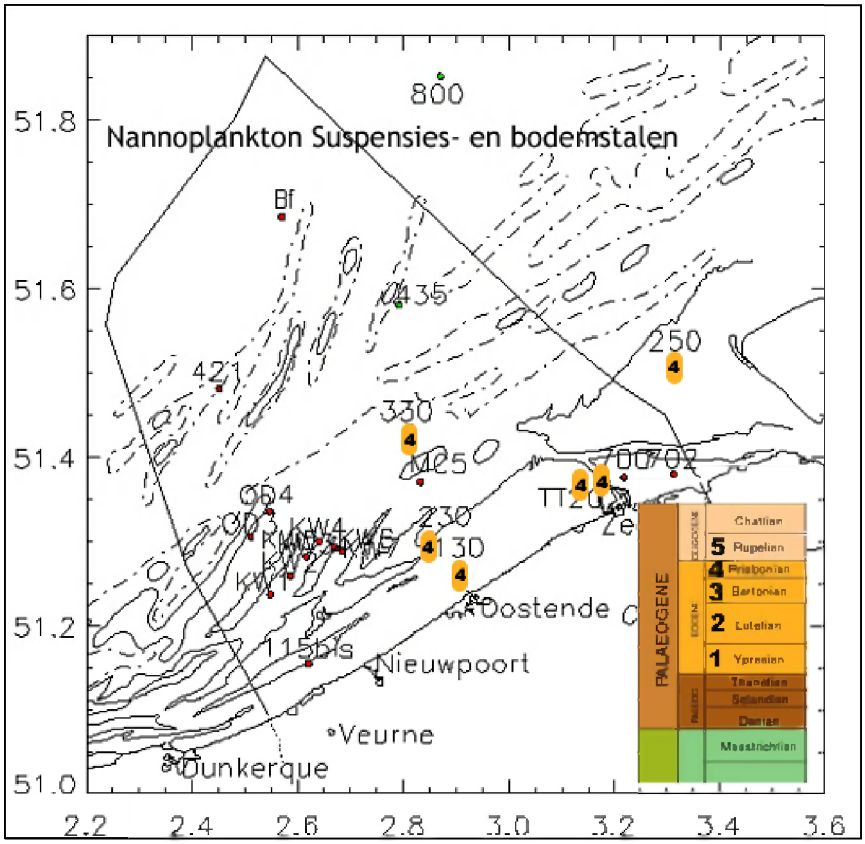

Figure 4.6: Graphical representation of the age of Paleogene reworked dinoflagellates.

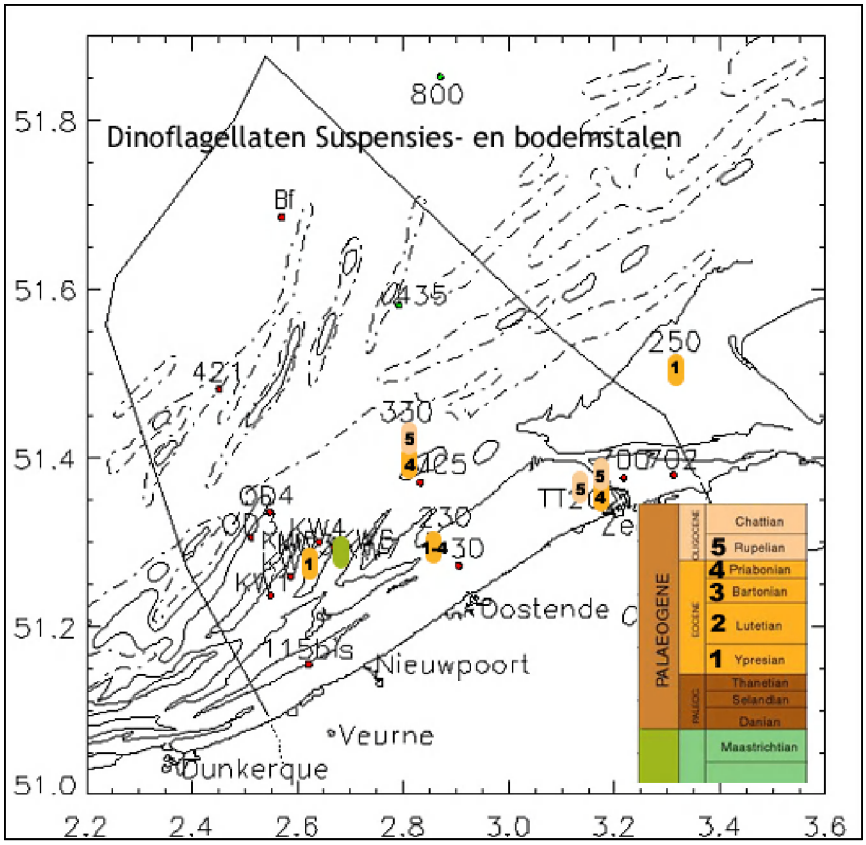

Figure 4.7: Graphical representation of the age of reworked dinoflagellates from suspension and bottom samples on the BCS.

4.5.2.3 Foraminifera

The study of the foraminifera shows that both suspension and bottom samples contain a substantial amount of reworked Upper Cretaceous specimen, probably of Campanian-Maastrichtian chalks. The samples however also contain Paleogene and Neogene-Pleistocene specimen. It is not impossible that some deep water specimen have been swept into the basin. The observed specimens are discussed according to age:

Cretaceous:

In the samples many biserial plankton and Hedbergella is found; seldom are double keeled forms observed.

Tappanina selmensis has the same white preservation as the Cretaceous plankton and hence is probably derived from the Campanian-Maastrichtian; in North Europe (North-Germany, Poland, Denmark) the species has only been described from the Maastrichtian (Frenzel, 2000).

Loxostomum subrostratum (= *Loxostomum eleyi*) is a species of Santonian-Maastrichtian age, occurring amongst others in North France, Germany, Poland, Sweden (Frenzel, 2000).

Paleogene:

Turrilina alsatica dates back from Late-Eocene till Early-Oligocene (Revets, 1987).

Pararotalia, also called *Rotalia*, are of Ypresian-Bartonian age (Kaasschieter, 1961).

Neogeen-sub-recent:

Uvigerina pergegrina groep, *Globbocassidulina* en *Cassidulina* are, surprisingly, deep water forms from older formations but their origin in the North Sea samples is unknown.

Recent species are a.o.: *Trifarina angulosa*, *Quinqueloculina spp.*, *Elphidium crispum* and many others (Dupeuble et al. 1972)

Ostracodes have been identified during the preparation for foraminifera. All observed species however are of recent age except for one Cretaceous form and one or two Pleistocene forms.

Large quantities of diatoms of recent origin are present in the samples.

Table 4.16: Results of counting's of carbonate microfossils

Sample	Mass (g)	Total Forams	Plankton	Benthos	Fossil	Recent	Miliolina	biserial &triserial	ostracodes
BC0322 **115bis**	16	286	262	200	43	243	11	89	0
BC0322 **230**	22	86	84	72	7	79	8	3	0
BC0322 **250**	18	219	208	111	54	165	17	8	1
BC0322_**KW3**	25	935	924	911	12	923	163	307	17
BC0322 **KW7**	22	349	341	325	12	337	89	59	18
BC0227 **ZB1**	17	278	262	210	34	244	35	27	60
RK0227 **ZB3**	14	108	105	86	11	97	9	2	16
RK0227 **ZB5**	27	739	703	647	46	693	56	115	30
SPM0322 **115bis**	15	151	135	83	34	117	1	40	1
SPM0322 **130**	13	614	584	570	22	592	49	47	61
SPM0322 **250**	8	111	103	91	10	101	1	23	4
SPM0322 **330**	6	112	101	88	12	100	6	19	9
SPM0322_**KW**	21	210	208	186	12	198	41	5	27
SPM0322 **TT20-4**	7	213	209	203	5	208	1	0	1

BC=Box Core, RK= Reineck Core

5. Classification of cohesive bottom and suspended sediments

5.1 Geology

On the Belgian continental shelf, the substratum is composed of solid layers of various ages. The Paleozoic basement is a relatively stable continental block called the London-Brabant Massif which was only flooded since Late Cretaceous times. The Cenozoic is confined to a series of Paleogene and Pleistocene/Holocene deposits. These layers were deposited during the Thanetian (started some 57 Ma) to Rupelian period (ended 30 Ma ago), outcropping locally on the seabed under a discontinuous cover of Pleistocene/Holocene sediments (Le Bot et al., 2003).

5.1.1 Paleogene (mostly Eocene)

De Batist (1989) recognized 8 seismo-stratigraphic units and a number of subunits within the Belgian offshore Paleogene succession using geometry and facies characteristics. Erosional truncation and valley incisions are common features at the top of the units and mark the base of the Pleistocene/Holocene deposits. The Paleogene units gently (0.5-1°) dip towards the NNE, which results in progressively younger strata subcropping below the sub-horizontal base of the Pleistocene/Holocene cover from SW to NE (figure 5.1; Le Bot et al., 2003).

Table 5.1 summarizes the nomenclature and characteristics of these deposits. The layers consist of either sandy or clayey deposits or a mixture. Y1, Y4b/Y4c, Y5 and P1 units and the Ursel, Zomergem and Onderdijke Members of B1 are clayey members. The Buisputten Member of unit B1 is made of sand. The majority of members are a mixture of sand and clay, often evolving laterally: clayey sands (Wemmel, Asse and Onderdale Members of unit B1 and Beernem Member of L1) and sandy clays (Asse Member of unit B1, Oedelem Member of unit L1, Y4, Y3 and Egem Member of Y2). The Oedelem Member is described as a clayey sand unit onland, but displays a vertical rapid alternation of clayey and sandy units towards the offshore. The sandy clay Pittem Member of Y3 contains numerous mud drapes and a rhythmic interlayered bedding. The Y4.a unit displays a fining of sand (medium coarse to fine) in the offshore direction, and the Y4.b unit displays an increasing amount of silt in this direction. The units displaying important lateral variability of the lithology (Oedelem member of unit L1, Y2 and Y5) concern sediments deposited in a very coastal environment where rapid changes of sedimentary sources and processes occurred.

The spatial distribution of the different Paleogene lithologies is presented in figure 5.2 whereby it is clear that clay is the dominant sediment. However to the east there is a band of sandy clay evolving in a small band of clayey sand and sand. The most eastern part again consists of clay. However it should be taken into account that there is relatively few offshore data and that the interpretations offshore are largely based on the better known equivalent onshore units

The thickness of the Paleogene deposits is highly variable from one unit to another, but quite constant within each unit (Table 5.1). The depth of the Paleogene shows more or less the morphology of the top erosion of the Paleogene subcrop surface. It marks the transition between Paleogene and Pleistocene/Holocene (figure 5.3). It consists of cuestas, scour hollows, slope breaks, scarps and paleovalleys (Liu et al., 1992). Important is that the more offshore the deeper this transition surface occurs. Another striking feature is the scour hollows offshore the harbour of Oostende causing the infill during Pleistocene/Holocene to be important and thicker than in the surrounding region.

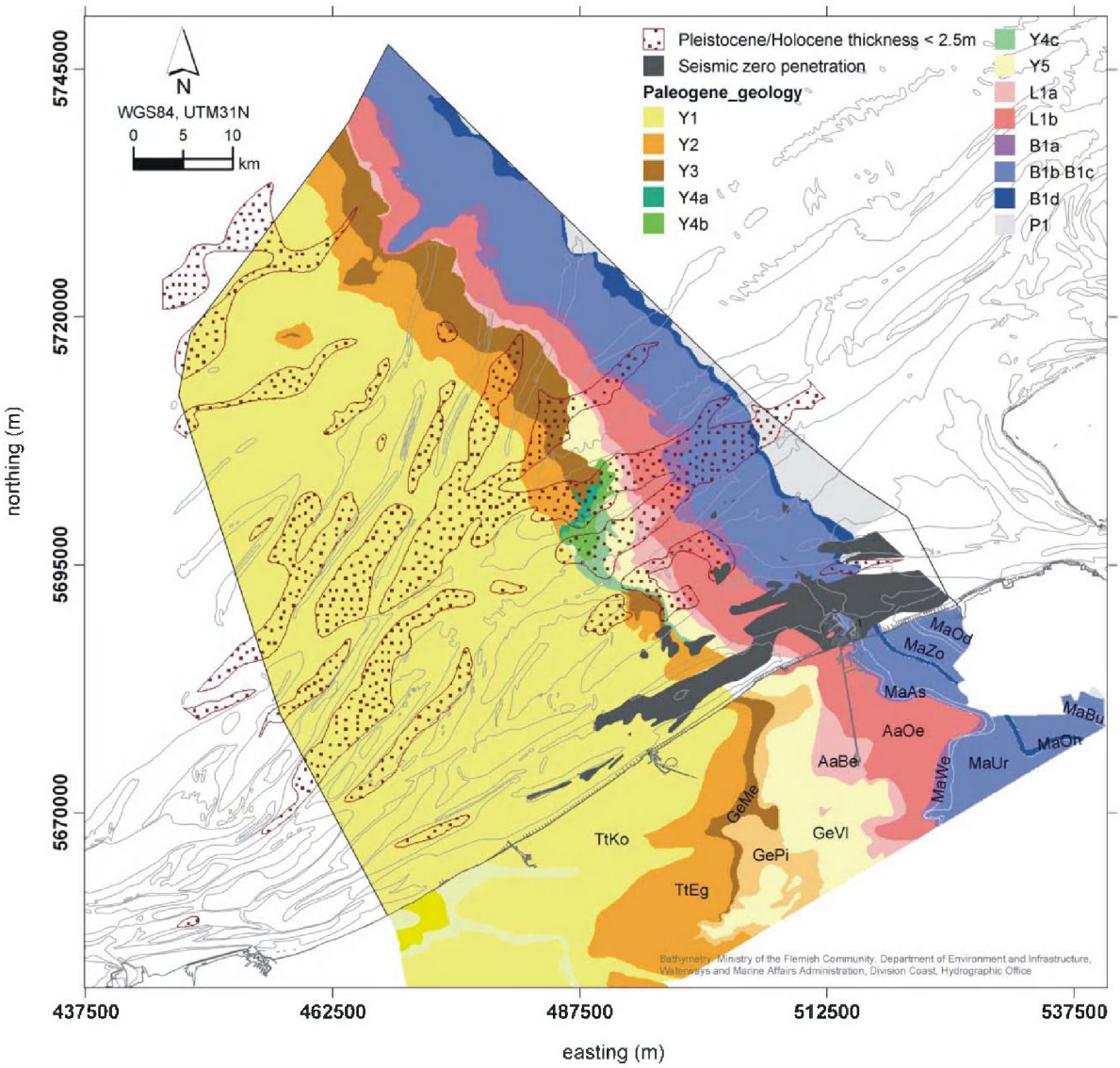

ONLAND MEMBERS

TtKo: Tielt Fm., Kortemark M.
TtEg: Tielt Fm., Egem M.
GeMe: Gentbrugge Fm., Merelbeke M.
GePi: Gentbrugge Fm., Pittem M.
GeVl: Gentbrugge Fm., Vlierzele M.
AaBe: Aalter Fm., Beernem M.
AaOe: Aalter Fm., Oedelem M.
MaWe: Maldegem Fm., Wemmel M.
MaAs: Maldegem Fm., Asse M.
MaUr: Maldegem Fm., Ursel M.
MaOn: Maldegem Fm., Onderdale M.
MaZo: Maldegem Fm., Zomergem M.
MaBu: Maldegem Fm., Buisputten M.
MaOd: Maldegem Fm., Onderdijke M.

Figure 5.1: Subcrops of solid deposits (Paleogene) under the non-consolidated deposits (Le Bot et al., 2003) (offshore data: compilation after Maréchal et al. (1986), De Batist (1989), De Batist & Henriet (1995) / onshore data: Jacobs et al. (2002)).

Table 5.1: Nomenclature and lithological properties of the BCP Paleogene units.

Seismic Unit	*Map*	*Formation*	*Member*	*Lithology*	*Thickness*
P1	Ze	Zelzate		Stiff and slightly sandy, green grey **clay**	40-90m
B1d	MaOd	Maldegem	Onderdijke	Stiff to very heavy **clay**, with various amounts sand	45-60m
B1c	MaBu	Maldegem	Buisputten	Sand	
B1b	MaZo	Maldegem	Zomergem	Strongly bioturbated blue-green **clay**	
	MaOn	Maldegem	Onderdale	Moderately clayey sands	
	MaUr	Maldegem	Ursel	Blue-grey bioturbated massive **clay** with pyrite concretions	
	MaAs	Maldegem	Asse	Bioturbated clayey sands and sandy **clays**	
B1a	MaWe	Maldegem	Wemmel	Grey glauconitic slightly clayey fine sands with sandstones	
L1b	AaOe	Aalter	Oedelem	Very stiff to hard silty to sandy **clay** with sandy parts	25-30m
L1a	AaBe	Aalter	Beernem	Grey-green bioturbated glauconitic clayey fine sands	
Y5	GeVl	Gent	Vlierzele (upper)	**Clay** with a low amount of very fine sand	0-17m
Y4c	GeVl	Gent	Vlierzele (basal)	Compact **clay** to **loam**	0-25m
Y4b	GeVl	Gent	Vlierzele (basal)	Brittle to compact **clay** to **loam**, low amount of shell debris	0-20m
Y4a	GeVl	Gent	Vlierzele (basal)	Compact **clay** with high amount of silt and sand	0-21m
Y3	GePi	Gent	Pittem	Bioturbated sandy **clay** with mud drapes	0-25m
	GeMe	Gent	Merelbeke	Strongly bioturbated silty **clay**	
Y2	TtEg	Tielt	Egem	Olive-grey, stiff, sandy **loam** to silty **clay**	+/- 30m
Y1	TtKo	Tielt	Kortemark	Silty sand laminae in a poor **clay** matrix	150-180m
	Ko	Kortrijk		Massive, very heavy and hard, green-grey **clay**	

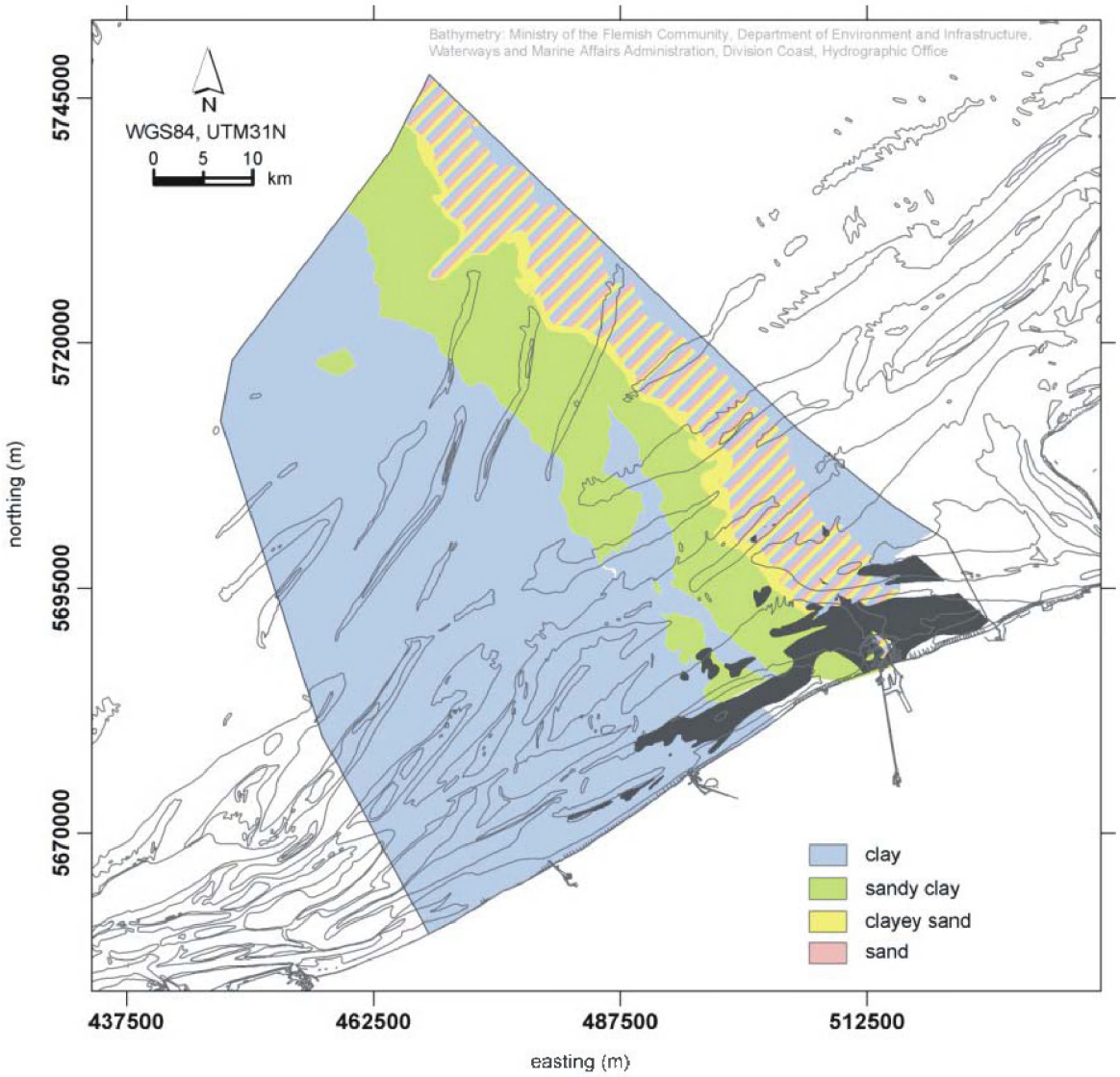

Figure 5.2: Distribution of clay and sand in the Paleogene deposits, largely based on sedimentology of the better known onshore equivalents (Cone Penetration Data and cores) and verified by a few offshore cores.

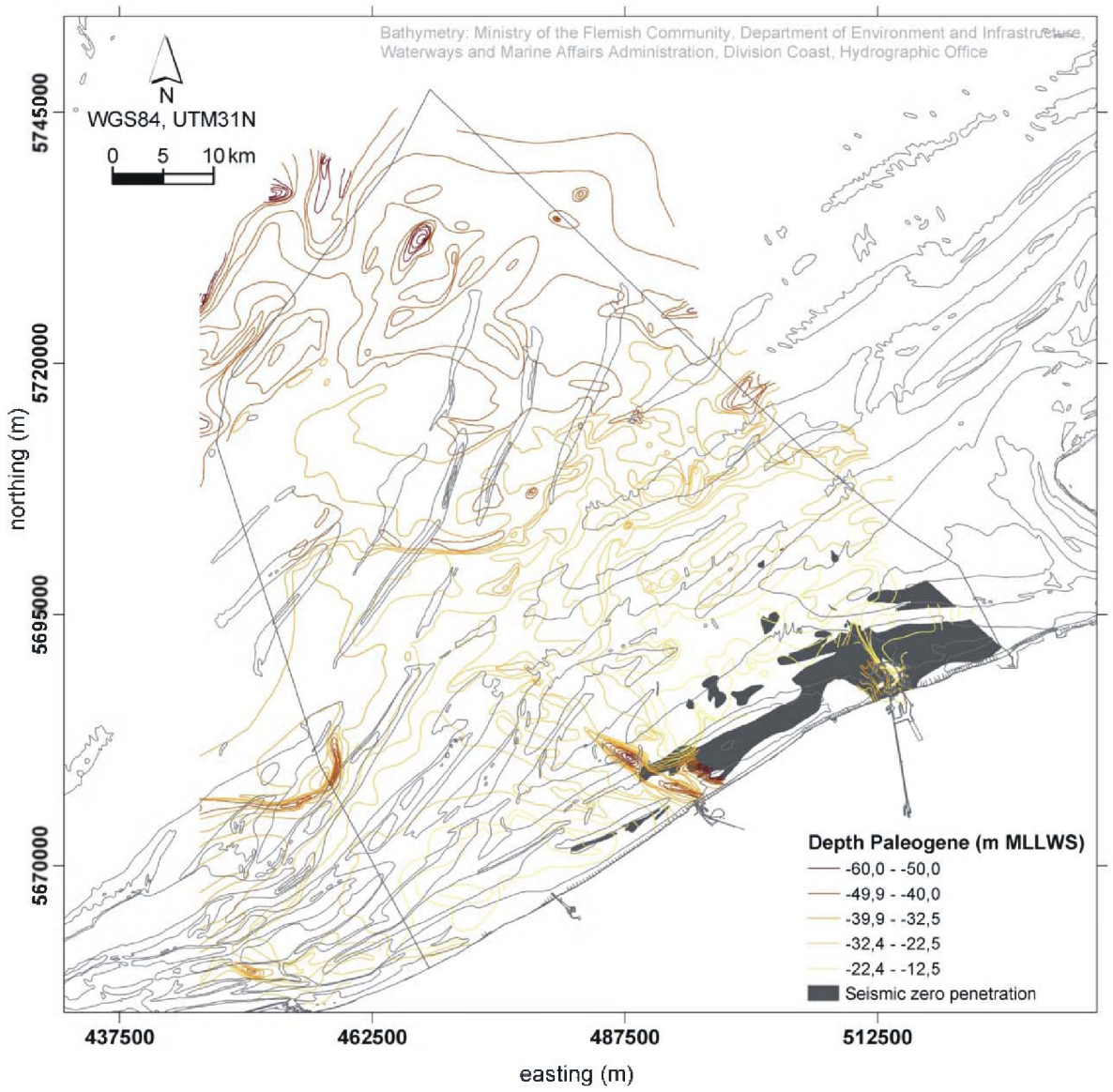

Figure 5.3: Depth contour lines of the Transition surface Paleogene and Pleistocene/Holocene (Liu, 1990).

5.1.2 Pleistocene/Holocene

The Pleistocene/Holocene deposits are regarded as non-cemented sediments and are characterized by a laterally as well as vertically complex and heterogeneous facies assemblage. These sediments consist essentially of sand with sporadic shelly layers (Le Bot et al., 2003). The main depositions consist of Pleistocene scour hollow infillings and Holocene tidal sandbanks (figure 5.4).

The geology of the BCS clearly allows erosion of clays only in areas where the present-day sea-floor reaches the Paleogene deposits. These are the swales in between the sandbanks created by current scouring. Navigation channels are not taken into account here although deepening of the navigation channels reaches the Paleogene deposits. In most of the swales on the Belgian continental shelf, the thickness of the Pleistocene/Holocene ranges between 0 and 10m, and is mostly less than 2.5m (Maréchal & Henriet, 1983, 1986) (figure 5.4). High-resolution reflection seismic mapping with a variety of different seismic tools over the whole Belgian continental shelf since 1978 by the RCMG resulted in a coverage of more than 16000 km. These data have been used to map the areal extent of the Paleogene units, the Paleogene deformation zones, the depth of the Paleogene/Pleistocene-Holocene border, the thickness of the Pleistocene/Holocene, the morphology of the Pleistocene/Holocene base surface, … (Liu, 1990; Le Bot et al., 2003).

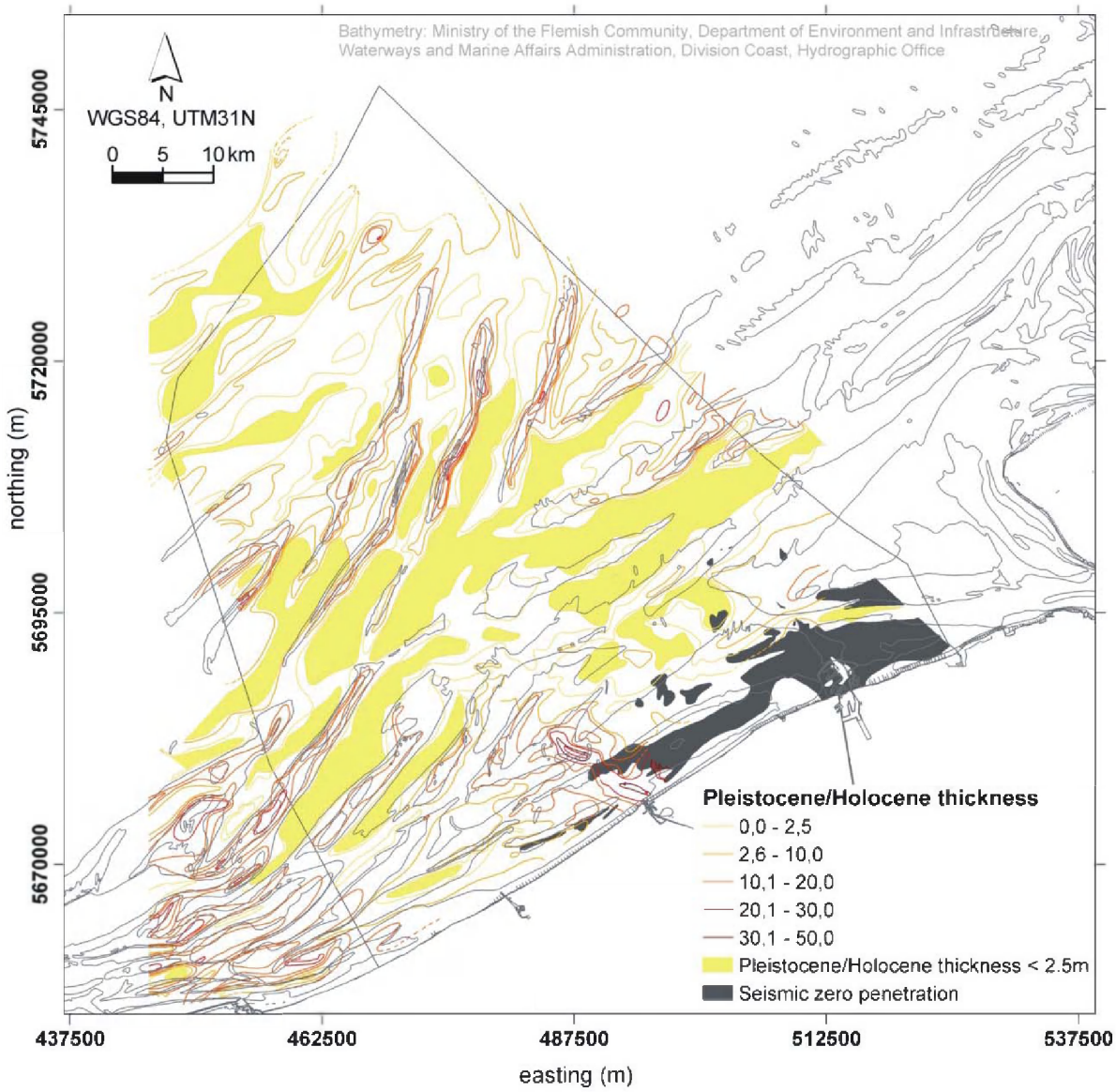

Figure 5.4: Thickness of the Pleistocene/Holocene sediments (Liu, 1990).

5.2 Dynamic classification of bottom sediments

5.2.1 Erosion capability of Paleogene sediments

The lithological descriptions of the Paleogene sediments clearly show a majority of clayey sediments over sandy sediments (Table 5.1). The large areal extent of the Y1 seismic unit, which covers more than half of the BCP (figure 5.1), shows the thickness and importance of this unit. Most of the Paleogene clays are however very hard, stiff clays which are not comparable with the lighter less compacted Pleistocene/Holocene mud which is abundantly present closer to the coast. Moreover the Paleogene sediments are buried under a Pleistocene/Holocene cover which mainly exists of sand (sandbank regions and scour hollow infillings) and of more fluid mud (confined to the areas around the Oostende and Zeebrugge harbour).

In this study, only the possible "natural" clay erosion will be estimated. Therefore, all the available geological data was introduced into a GIS environment. The used surfaces for estimating the erodible clay/mud quantity are the zones with less than 2.5 m of Pleistocene/Holocene cover (figures 5.1 & 5.4). It can be assumed that this cover is maximal at the sides of the polygons, while near their centre this cover is minimal and in some cases is even zero. This is e.g.

the case south and northeast of the Goote Bank, in the Westdiep swale and west of the Kwinte Bank (Le Bot et al., 2003). However, at this stage it is only possible to roughly estimate the erosion capabilities. No attention has been paid to the access channels towards the harbours or to the dredged areas. Only natural erosion sites have been considered (Table 5.2).

The total surface of the BCP is more or less 3485 km² from which 663 km² lies within the polygon edges representing the Pleistocene/Holocene cover less than 2.5 m. This means that theoretically 19.02 % of the BCP is the maximum possible area of natural erosion. The largest share comes from the Y1-unit which represents 63% of the possible erosion area and 12% of the total surface of the BCP. On the other hand, small units as the basal parts of the Vlierzele Member (Y4) seem to be located in a zone where 60 to 85 % of the unit surface can be eroded.

Table 5.2: This table firstly identifies the proportion of Paleogene units on the BCP, in area and percentage (Total BCP columns). Secondly, its share in possible erosion is expressed respectively in area and percentage with respect to the total possible erosion area, percentage possible erosion of the entire unit and percentage possible erosion with respect to the BCP (Possible erosion capability columns).

	Proportion of Paleogene units with respect to the BCP		Possible erosion capability			
			Share in erosion in relation to the total erosion area		*% erosion with respect to entire unit*	*% erosion with respect to BCP*
Seismic unit	Area (km²)	%	Area (km²)	%		
P1	90.04	2.58	7.86	1.19	8.73	0.23
B1d	45.49	1.31	1.87	0.28	4.12	0.05
B1b & B1c	*485.02*	*13.92*	*45.52*	6.87	9.39	1.31
B1a	71.91	2.06	12.93	1.95	17.99	0.37
L1b	267.72	7.68	*42.45*	6.40	15.85	1.22
L1a	63.41	1.82	17.80	2.69	28.07	0.51
Y5	65.42	1.88	23.14	3.49	35.37	0.66
Y4c	19.97	0.57	12.57	1.90	*62.94*	0.36
Y4b	14.64	0.42	10.94	1.65	*74.67*	0.31
Y4a	6.50	0.19	5.58	0.84	*85.89*	0.16
Y3	159.49	4.58	23.92	3.61	15.00	0.69
Y2	176.90	5.08	39.64	5.98	22.41	1.14
Y1	*1916.51*	*54.99*	*418.56*	*63.15*	21.84	*12.01*
No data	101.98	2.93				
Total	**3485.00**	100.00	**662.77**	100.00		**19.02**

Evidently, for this study, only the deposits containing clay can be taken into account for the origin of SPM. Here, we distinguish areas of pure clay-bearing sediments and areas containing clayey sediments mixed with silt and/or sand (figure 5.2). As the offshore distribution of the members of the B1b unit is not known, a raw division is made here on the basis of its onshore distribution.

The pure clay-bearing possible erosion areas (i.e. the areas falling in the polygons representing the Pleistocene/Holocene cover less than 2.5 m) represent 513.63 km² or 14.74 % of the BCP, while the clayey possible erosion area mixed with silt and/or sand is more or less 146.88 km² or 4.21 % of the BCP. The surficial cover of Paleogene sand (only the Buisputten member) inside the polygons representing the Pleistocene/Holocene cover less than 2.5 m is only 2.28 km² or 0.065% of the whole BCS. Nevertheless, one has to keep in mind that these are maximum values and probably only a smaller area is really undergoing erosion. Based on the size of the areas, the composition of the units and the areal distribution of the polygons representing the Pleistocene/Holocene cover less than 2.5 m, it is most likely that SPM will find its origin in Y1 or Y4 sediments.

5.2.2 Bulk density

The bulk density gives an indication of the consolidation of the mud and can be used to predict the erosion behaviour of the sediment. Williamson & Torfs (1996) did erosion tests with natural and in artificial deposited beds. They found an asymptotic function for the relation between the critical erosion shear stress and the density of the bed. The in-situ erosion shear stress measurements varied between 0.05 Pa for soft sand free beds to 1.9 Pa for sandy, consolidated beds. Lintern et al. (2002) wrote that the resistance to erosion is directly related to bed density. Houwing (1999) however found no straight relationship between the critical shear stress and the bulk density of the top layer on an intertidal mudflat. He proposed that contrary to what might be expected the beds become less resistant to erosion as they mature due to the development of biochemical surface layer and the feeding and reworking by marine worms. Zreik et al. (1998) argue that the increase in erosion strength of soft cohesive sediments between 1.8 and 5.7 days is mainly due to thixotropic hardening and only slightly to an increase in density due to consolidation.

The bulk density of the sediments on the BCS has been determined from box cores, which were sampled with PVC tubes of 8 cm diameter and closed by rubber stoppers. The method used to infer the density of the "non-disturbed" core sediments contained in a PVC tube is based on the transmission of gamma-ray photons through the core, it is a fast and non-destructive way of measuring bulk density, see Van Lancker et al. (2004) for a description of the method. Boc core samples have been taken near the old dumping place of Oostende, in the Zeebrugge area and in some of the monitorings points of MUMM. The distribution of the bulk density of the cohesive sediments is presented in figure 5.5. The bulk density of the bed sediments gives an indication of the consolidation and can be used to calculate the erosion behaviour (critical erosion shear stress) see figure 5.5.

The detailed results are presented in appendix V. The bulk density of the freshly deposited mud varies between 1200-1350 kg/m^3 (see near the old dumping site of Oostende: upper 1 cm in OE13; upper 30 cm in OE14, upper 10 cm in OE17 and on the BCS: whole the core 130 and upper 5 cm in 230). Soft to medium consolidated mud has a bulkdensity of 1500-1700 kg/m^3 (see Oostende area: OE13 and OE14; Zeebrugge area: ZB01, ZB02, ZB06 and 700). The thin sand (or muddy sand) layer covering the Holocene mud has a higher density (1800-2200 kg/m^3). Homogeneous sand beds have a density of 2000-2200 kg/m^3 (see OE01, OE03, bottom of OE14, KW01, KW05-KW07) or higher if shells or shell fragments (KW04) or gravels (KW03) are present.

5.2.3 Bottom shear stress

Cohesive beds are formed by settling and consolidation processes. The erodibility of the bed is influenced by the consolidation and composition and by the governing hydrodynamic conditions. The parameters for erosion and deposition are expressed as shear stresses, therefore the dynamic classification as presented below, will be based on the bottom shear stress exerted by the tidal currents and on the erosion resistance (expressed in Pa) of the surface sediments.

The currents, surface elevation and bottom shear stresses have been modelled with the 3D hydrodynamic model COHERENS. A full description of the numerical model, including the details on numerical discretisation as well as a user's guide is given by Luyten et al. (1999). The source code of the standard version is available publicly on CD-ROM. The 3D model solves the continuity and momentum equations on a staggered grid, sigma coordinate grid with an explicit mode-splitting treatment of the barotropic and baroclinic modes.

The 3D hydrodynamic model of the Belgian continental shelf (OPTOS-BCS) covers an area between 51°N and 51.92°N in latitude and between 2.08°E and 4.2°E. The model has a grid resolution of ±820×772 m^2 (coarse) or ±273×257 m^2 (fine) in the horizontal and 20 sigma levels in the vertical plane. Boundary conditions are water elevation and depth-averaged currents,

they are provided by the OPTOS-NOS model, which is also based on the COHERENS code, but covering whole the North Sea and part of the English Channel. Meteorological surface forcing is from the forecasts of the UK Meteorological Office at Bracknell. The current velocities of the OPTOS-BCS model have been validated using about 400 hours of ADCP current profiles collected during 12 campaigns from September 2002 on (see Van Lancker et al., 2004).

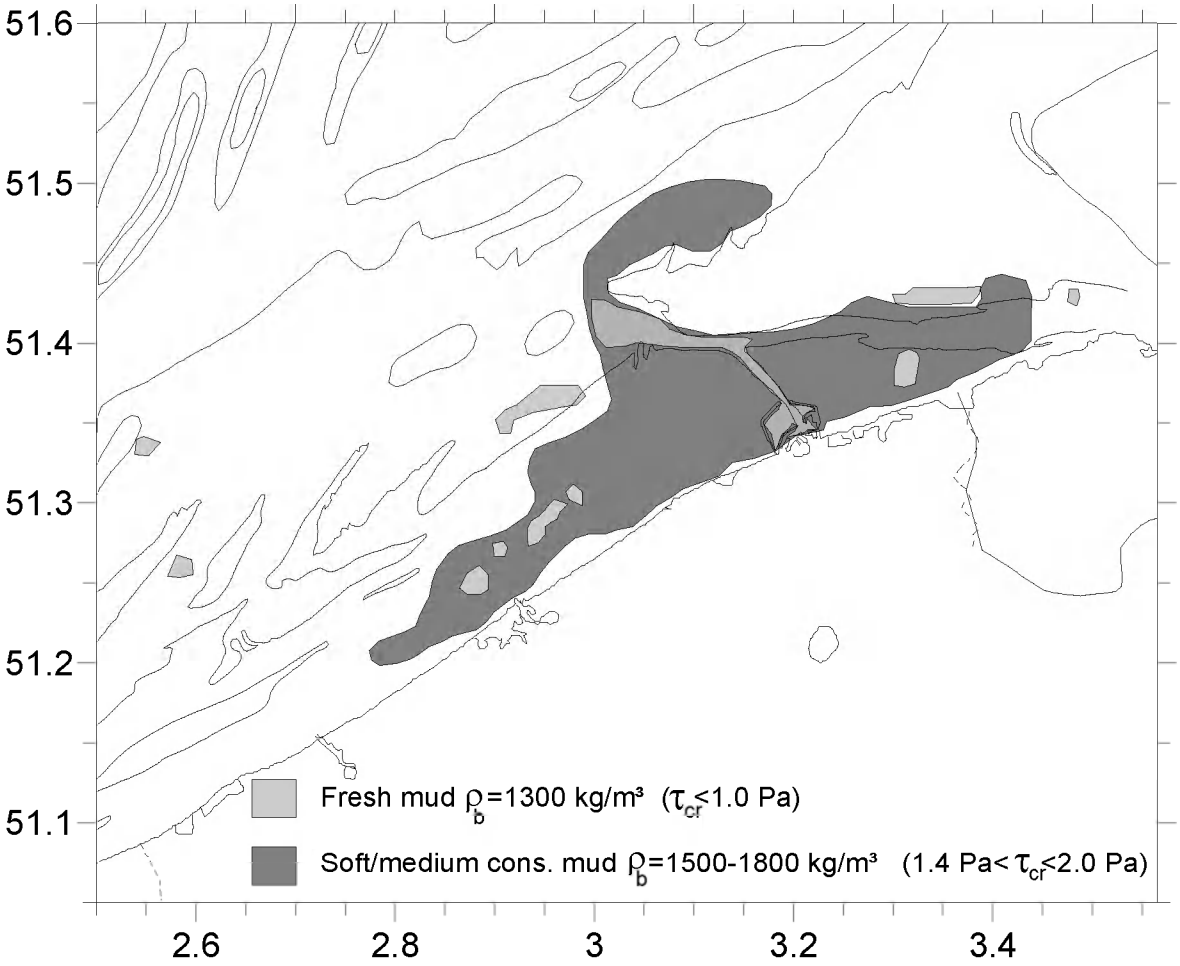

Figure 5.5: Bulk density and estimates of the critical shear stress for erosion of the cohesive sediments on the BCS,

The bottom shear stress during a typical neap and spring tide are shown in figures 5.6 and 5.7. Striking are the big differences in magnitude between neap and spring tide. The tidal averaged bottom shear stresses during a neap tide are below 0.5 Pa in almost whole the domain. The maximum bottom shear stresses are <0.5 Pa except in the navigation channel 'Scheur' and Pas van het Zand (<1 Pa). In the mud transport model of Fettweis & Van den Eynde (2003) the critical shear stress for erosion of fresh mud and deposition was set to 0.5 Pa. The current results affirm that during neap tide favourable conditions for mud deposition exist. During spring tide the bottom shear stresses are much higher and reach on average 0.7-1.5 Pa in the coastal zone with peak values up to 3 Pa and more. These values indicate that fresh mud layers are not stable and that - given the calculated critical shears stress values of the consolidated Holocene mud of 1.3-1.4 Pa (see above) – the hydrodynamics during extreme conditions are strong enough to erode the Holocene mud.

5.3 Dynamic classification of suspended sediments

5.3.1 Residual SPM transport

The SPM transport in the southern North Sea has been calculated by multiplying the residual discharge (calculated using the OPTOS modelling system) with the seasonal averaged SPM concentration, derived from corrected SeaWiFS images of 1997-2002 (Fettweis et al., 2004), see figure 5.8. SPM enters the southern North Sea through the Strait of Dover where it is partly deviated towards the English and partly towards the Belgian coast. The highest residual mud transports occur during winter and the lowest during summer. Winter and also autumn are seasons with a high SPM concentration while during winter and spring the highest residual discharges occur. Therefore the net mud transported are almost equal during spring and autumn and the highest mud transports are observed during winter. The residual mud transport has been calculated through the Strait of Dover (51°N, 1°E-2.0°E) and through a boundary between the UK and the Netherlands at 51.9°N. The residual transport through the Strait of Dover is situated between 1.45×10^6 t during summer and 11.59×10^6 t during winter. This results in a yearly SPM transport of 21.96×10^6 ton entering the southern North Sea, divided about equally between the English and French side of the Strait. These values correspond with values from literature (Lafite et al., 1993; McManus & Prandle, 1997; Velegrakis et al., 1999).

The residual transport of SPM entering the Belgian coastal zone (W-boundary: 51°-51.6°N, 2.08°E) is situated between 1.18×10^6 t during summer and 7.45×10^6 t during winter, corresponding thus to 14.38×10^6 t/yr. During spring and autumn more mud leaves the model domain through the N-boundary (51.6°N, 2.08-3.6°E) than is entering through the W-boundary. In winter the opposite occurs: more mud inflow via the Strait of Dover than outflow towards the Dutch continental shelf. The mud balance is more or less in equilibrium during summer.

On average thus 0.91×10^6 t/year of mud is more leaving the domain than is entering. This corresponds with an error of 7% on the sediment balance. The error could be due to inaccuracies in the SPM concentrations, which are derived from satellite images (see § 2.2.4) or due to erosion of cohesive sediment layers on the BCS. This would mean that we could expect a supplementary input of SPM of maximum 0.91×10^6 t/year originating from Holocene mud layers.

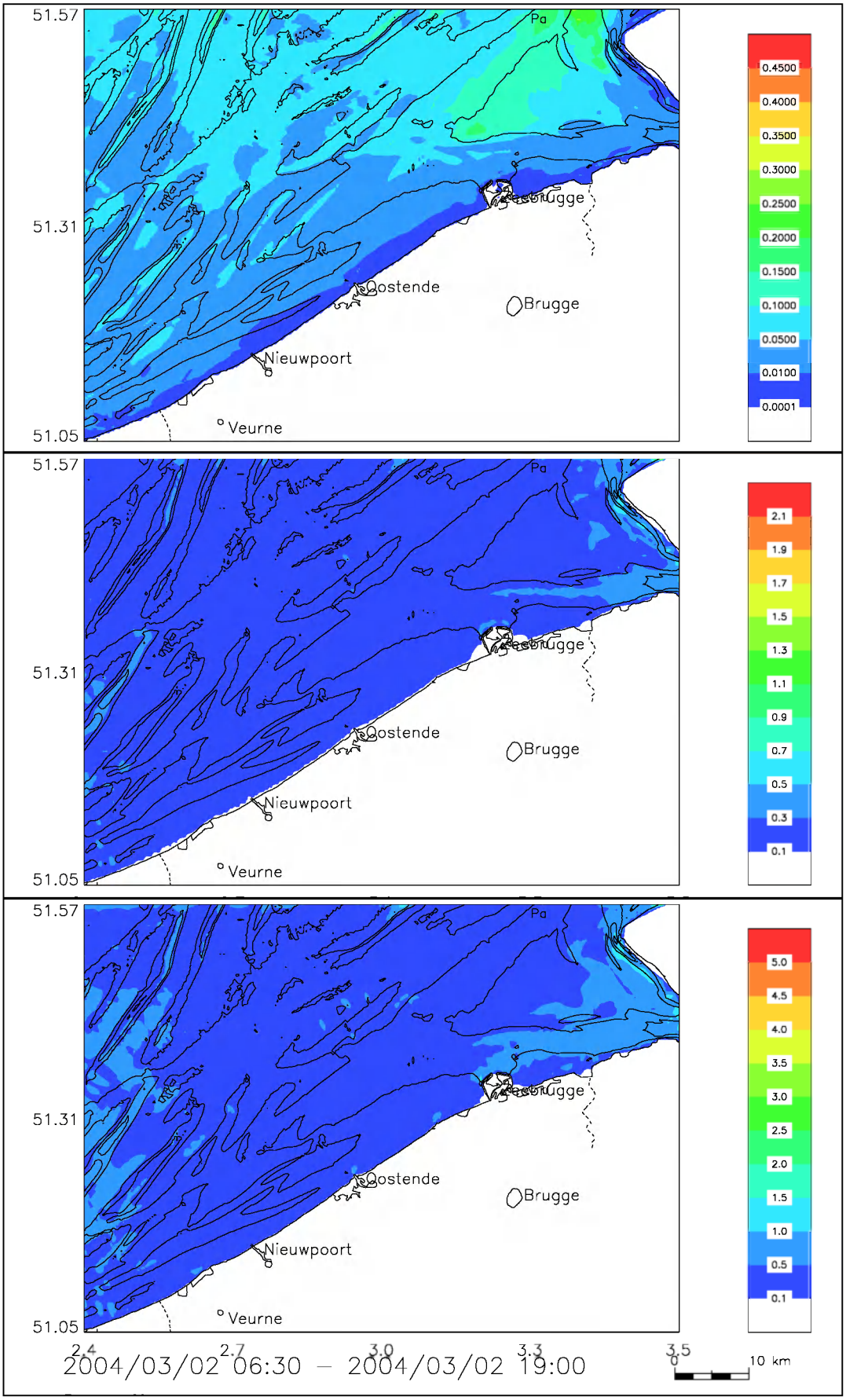

Figure 5.6: Bottom shear stress (Pa) calculated with the 3D OPTOS-BCS model (fine grid) during a neap tide. Above: minimum bottom shear stress. Middle: tidal averaged value. Below: maximum bottom shear stress. Also indicated are the 10 m, 20 m and 30 m bathymetrical lines (MSL).

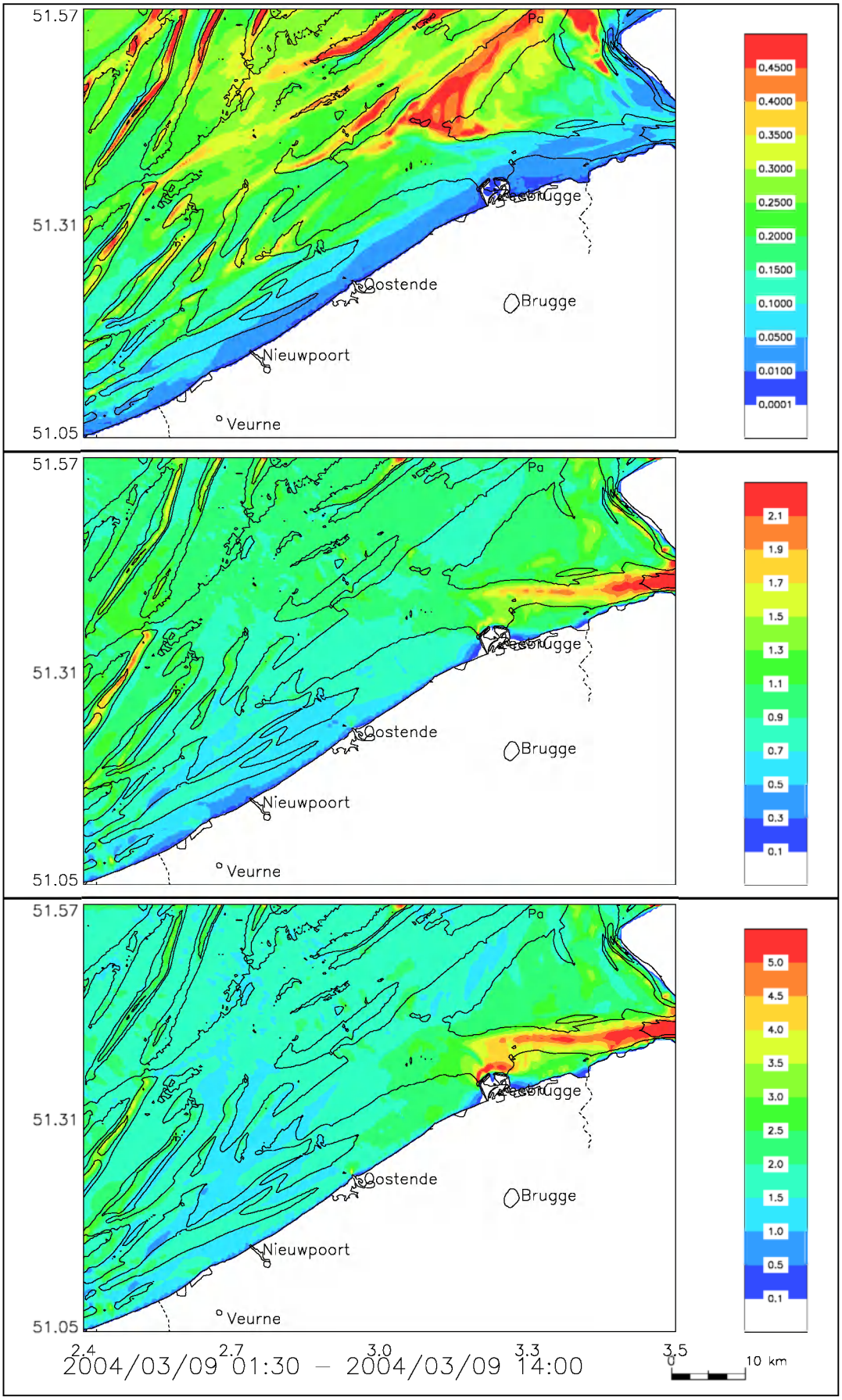

Figure 5.7: Bottom shear stress (Pa) calculated with the 3D OPTOS-BCS model (fine grid) during a spring tide. Above: minimum bottom shear stress. Middle: tidal averaged value. Below: maximum bottom shear stress. Also indicated are the 10 m, 20 m and 30 m bathymetrical lines (MSL).

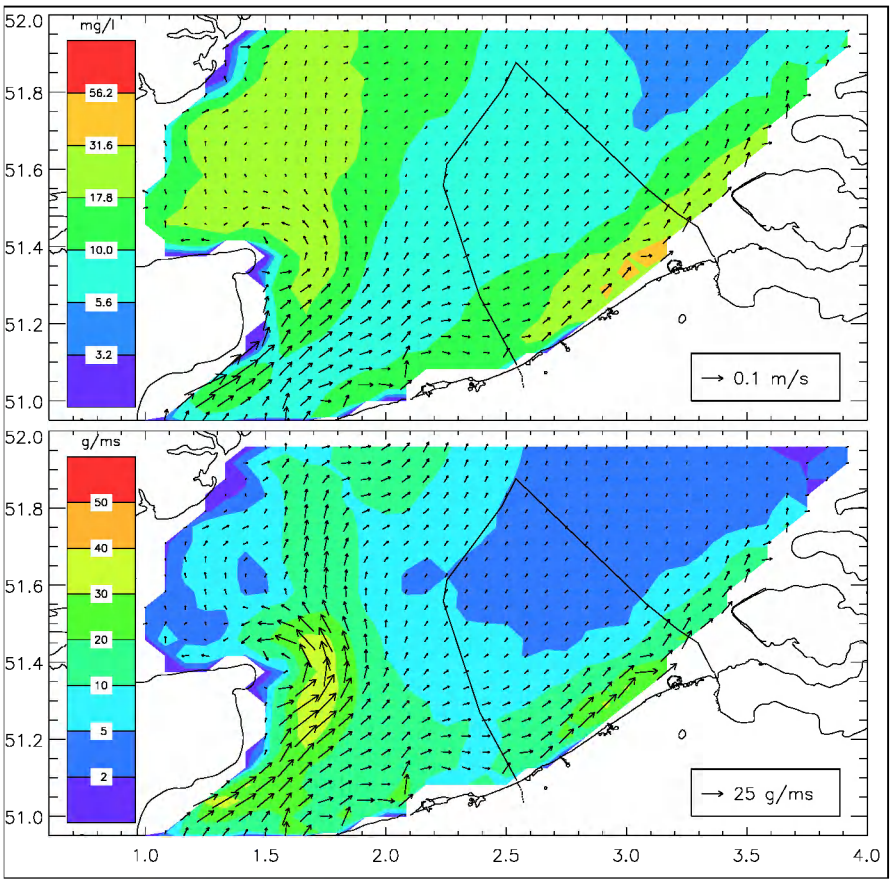

Figure 5.8: Above: yearly averaged residual water transport (vectors) and SPM concentration (colour shading). Below: SPM transport (vectors and shading). The SPM transport has been calculated by multiplying the residual H2O transport simulated by the OPTOS model (with meteorological forcing) with the seasonal averaged SPM concentration, derived from SeaWifs SPM maps.

5.3.2 SPM high correlation areas (HCA)

To further characterise the dynamics of SPM in the area of interest, the spatial correlation of the SPM concentration time-series was calculated to identify separate areas with similar SPM dynamics. The SeaWiFS images (see § 3.4.3) have been processed as explained below.

For each grid cell of the SeaWifs image, further called a reference grid cell, the following procedure was followed (Van den Eynde et al., 2005):

- all valid surface SPM concentrations for the reference grid cell, not disturbed due to clouds or to atmospheric correction failure, were selected.
- for another grid cell, the valid surface SPM concentrations are selected from the SeaWiFS images as well.
- if at least 100 corresponding valid SPM concentration pairs are found, the correlation between the SPM concentrations at these two grid cells is calculated. A value of 100 pairs is taken to insure that the results are based on a large number of SeaWiFS images.
- this selection of valid surface SPM concentrations and calculation of the correlation if 100 corresponding valid SPM concentration pairs are found is repeated for all grid cells.
- when all correlations between the SPM concentrations at the reference grid cell and the SPM concentrations at the other grid cells are calculated, a map can be prepared of the area with correlations higher then 70 %. This area is defined as the High Correlation Area (HCA) for that reference grid cell.

By doing so the BCS could be divided in three HCA (see figure 5.9). The first HCA has the largest surface (around 3500 km²) and is located offshore. A second high correlation area is located in the north east, near the mouth of the Westerschelde estuary. The area represents about

1100 km². The third HCA is situated in the 20 km band along the coast outside the HCA-1 and HCA-2. The SPM concentration in these three areas is characterised as follows:

- Offshore area, where SPM concentrations remain generally low (<10 mg/l).
- Zeebrugge area, which extends from about Zeebrugge to the mouth of the Westerschelde estuary. In 60 % of the images, the SPM concentration is lower than 50 mg/l, while 40 % of the images show a high SPM concentration in this area.
- Oostende area, which has high SPM concentrations more often than in the Zeebrugge area (70 % of the images show high SPM concentrations in this area).

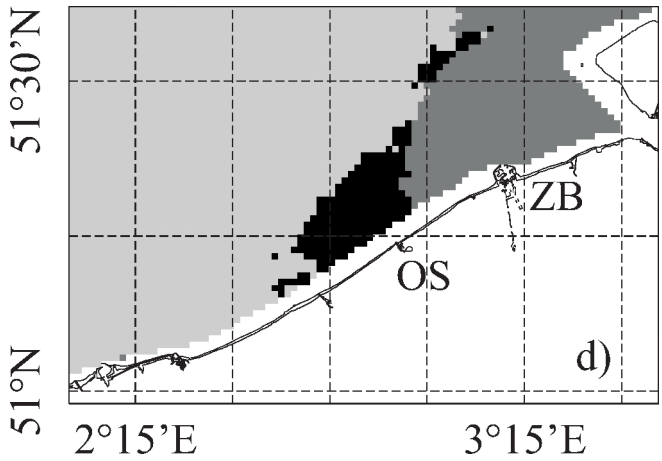

Figure 5.9: High Correlation Area (HCA) found in SeaWifs images: division of the BCS in the offshore area (light), Zeebrugge area (middle) and Oostende area (dark) (from Van den Eynde et al., 2005). (ZB=Zeebrugge, OS=Oostende)

The difference between the offshore area and the coastal areas is due to the fact that (1) the transport of SPM is mainly concentrated in the coastal area and (2) the differences in bathymetry. For the apparently different SPM dynamics in the two neighbouring Zeebrugge and Oostende areas on the other hand, a convincing explanation has not yet been established. Some striking differences between both areas can however offer explanations:

- 95 % of the dredging and dumping occurs in the Zeebrugge area. Comparison between the natural input of SPM and the quantities dredged and dumped at sea showed that an important part of the SPM is involved in the dredging/dumping cycle (Fettweis & Van den Eynde, 2003).
- The bottom in the Zeebrugge area consists of Holocene mud near the coast, which is difficult to erode, and shallow sand plates offshore, where the hydrodynamic conditions prevent mud from being permanently deposited. In the Oostende area, soft mud which has been deposited during slack water can be found (see above, §2.1.1.3). This could mean that in the Zeebrugge area the mud stays in suspension during most of the tidal cycle and that mud is only permanently deposited in the man-made environments of navigation channels and harbours. In the Oostende area on the other hand, the hydrodynamics allow SPM to be deposited and only severe storms will bring the fine material back into suspension.
- The Westerschelde estuary also has an influence, even if it is limited, on the SPM dynamics of the Zeebrugge area. Although the ratio of fluvial to marine SPM is almost constant at the mouth of the estuary (Verlaan et al., 1998), the SPM concentration varies significantly as a function of river discharge.

5.4 Clay minerals and microfossils in bottom and suspended sediments

5.4.1 Interpretation of the clay mineral data

A first important result from the analyses is that the observation that clay mineral proportions do vary on the Belgian continental platform and in the estuaries leading to the North Sea (see figures 5.10-13). The differences are important for illite varying between 15 and 83 % and smectite varying between 1 and 80 %. For kaolinite the differences are less varying between 1 and 36 %. Differences in chlorite content have not been quantified in detail.

A second certainly interesting observation is that the crystallinity of the smectites, measured as the v/p ratio, from suspended minerals and from bottom sediments is markedly different (figures. IV.7-IV.12); smectites from suspension are less well crystallized than from bottom sediments. More work on the influence of the sampling conditions on the v/p ration is necessary.

A third conclusion is that a trend can be observed, although certainly more data are needed for confirmation, in the bottom sediments of more smectite in the north and eastern sectors of the North Sea, and more illite in the south-western sector.

Remarkably this difference between sectors is not observed in the mineralogy of suspended matter which seems to have a more homogeneous composition.

A further observation concerns sample location 330, which is characterized by a high content of well crystallized smectite and a low illite content, especially in the bottom sediments and not in suspension. The reasons for this unusual composition need to be found. A possible explanation could be the influence of nearby dredging dump sites (B/1 and B/2) where eventually such smectite rich mud possibly from Eocene origin are dumped. The low concentration in suspension however is not supporting this hypothesis and also the mud sampled directly from the harbour access channel (ZB3 and ZB5) show low smectite contents (36% in ZB3 and 5% in ZB5), whereas it is usually assumes that the dumped mud flows partly back into the access channels.

Suspension samples in the Calais channel show very low smectite proportions (3 and 13%). This is somewhat unexpected as the erosion of the chalks exposed along the coast in this area would normally produce relatively high smectite proportions. This result suggests that the coastal erosion of chalk is not a major contributor to the suspended matter. The crystallinity of the smectites in suspension is low as is the case in all other suspension samples.

The sampling TT20-1 till 7 during a tidal cycle does not show any trend and the differences between the samples is limited. Sample TT20-2 shows a different composition which is probably due to some mishandling during sampling or analysis; unfortunately not enough suspended matter was available to do a repeat analysis. The good correspondence between the clay mineral compositions of the samples, except one, during one tidal cycle at the same spot indicates the repeatability of the results. Crystallinity values show no trend with the tide and v/p values vary between 0.2 and 0.5.

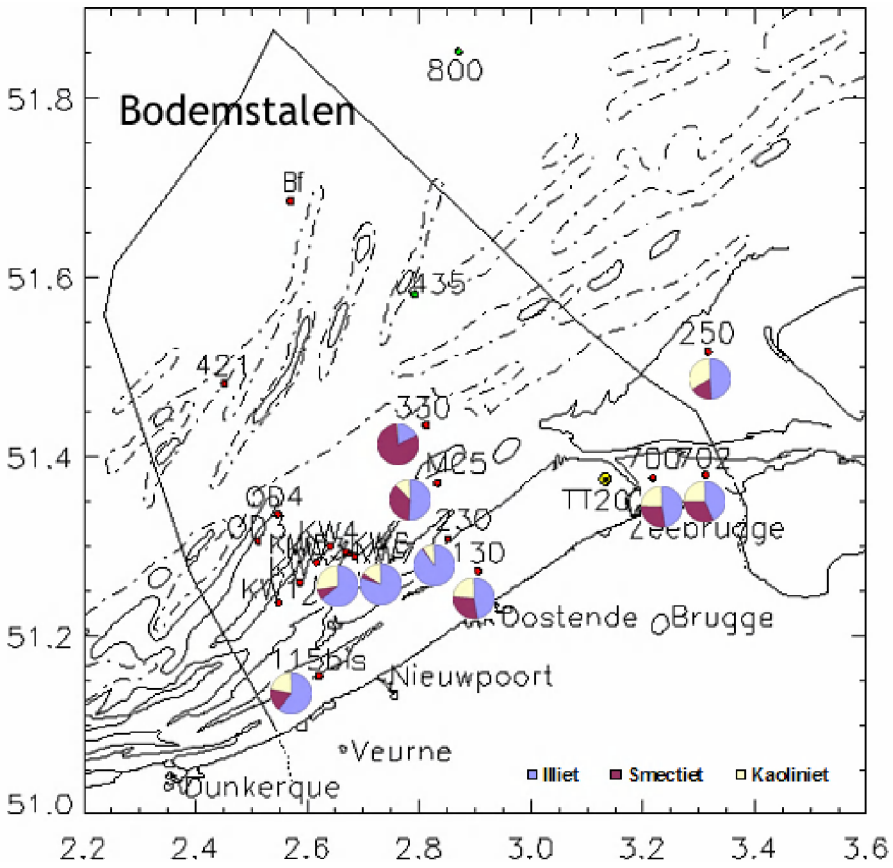

Figure 5.10: Illite, smectite and kaolinite content in the bottom samples from the BCS.

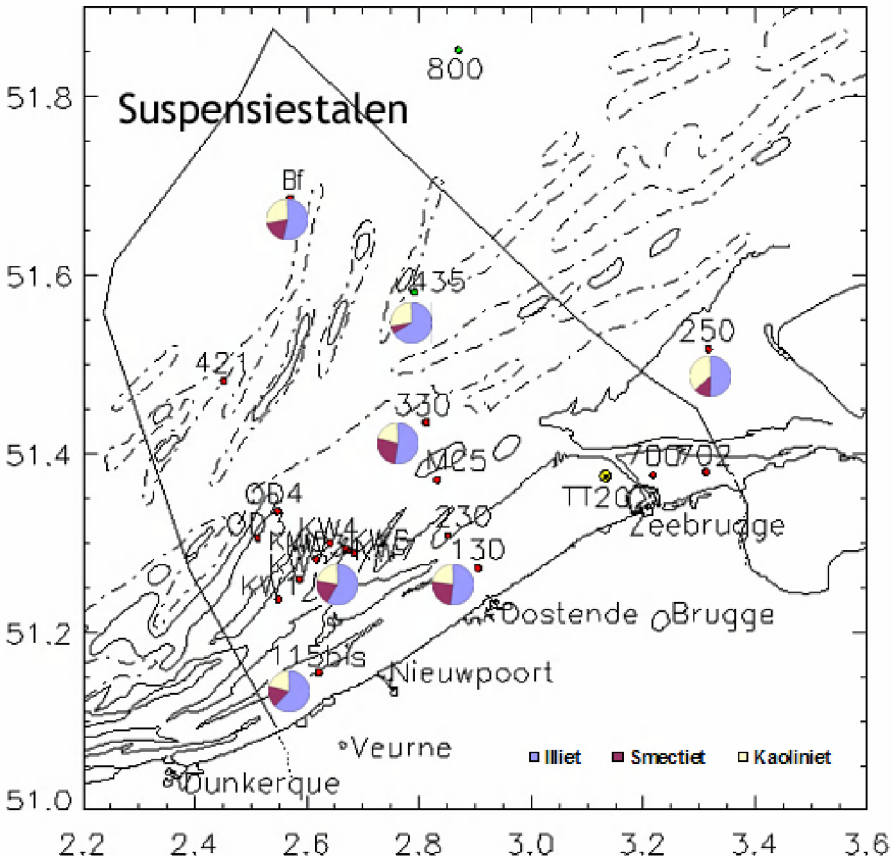

Figure 5.11: Illite, smectite and kaolinite content in the suspension samples from the BCS.

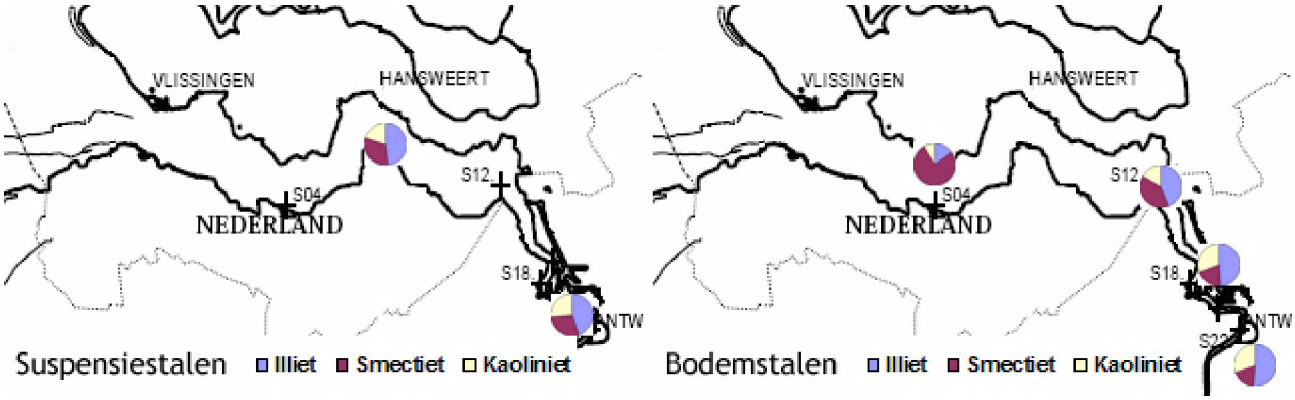

Figure 5.12: Illite, smectite and kaolinite content of suspension (left) and bottom (right) samples from the Schelde estuary.

The data for the Schelde estuary bottom samples show a clear trend, although it must be admitted that the sample locations are still limited. Downstream the smectite content increases, from 18% to 77% whilst the illite and kaolinite samples decrease respectively from 51 to 15% and from 31 to 8%. Accompanying the increase in smectite content also occur an increase in crystallinity of the mineral from 0 to 0.5. It should be remembered here that the North Sea mud in the sector at the mouth of the estuary is rich in smectite and could indicate that mud enters the estuary from the sea. However, in the suspension samples the smectite increase is much more limited.

In the Schelde estuary, by analysing core samples from the Paulina salt marsh, a clay mineral compositional trend with time can be demonstrated. Illite increase with depth from 46 to 71% whilst smectite and kaolinite decrease with depth, respectively from 18 to 2% and from 36 to 26%. With decreasing smectite also the crystallinity decreases with depth. Apparently one century ago there was more illite and less smectite and kaolinite in the Schelde mud. An explanation could be the dredging activity although also other anthropogenic changes in the Schelde river system might have contributed. More data are needed to study this phenomenon.

At two other locations a test was carried out to find out differences in composition with time by analysing two samples , one at the very top and one slightly deeper. Near Zeebrugge in sample ZB6 composition does not change. Near Oostende both the samples OE13 and OE14 show slight differences: the deeper sample in both locations shows higher illite and kaolinite, and lower smectite contents than the top sample. Higher smectite at the top also corresponds to higher crystallinity. These differences with depth are remarkably similar as in the case of the Paulina samples.

Finally, the Yser river canals discharging towards Nieuwpoort have lower illite and higher smectite contents than in the harbour mud of Nieuwpoort. The mud mineralogy of the harbour samples are similar in composition to the North Sea mud in front of Nieuwpoort. The exception is sample P1 from the tidal dock (tijdok) but earthworks during the construction of the dock have disturbed the natural soil composition. Also the smectite crystallinity in the harbour mud leads to generally negative v/p ratios unlike in the two samples of the canals. In conclusion it can be stated that the clay mineralogy strongly suggests that the Nieuwpoort harbour excessive mud sedimentation is derived from sea water suspended matter and not from river influx.

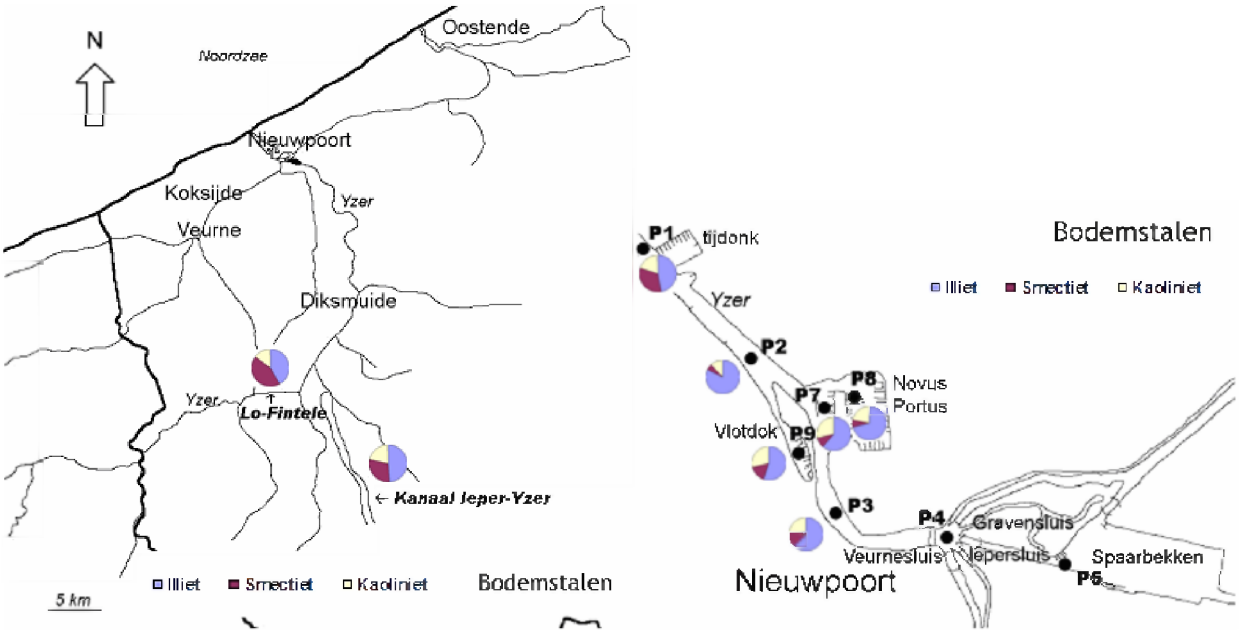

Figure 5.13: Illite, smectite and kaolinite content in the bottom samples from the river Yser and the harbour of Nieuwpoort.

5.4.2 Interpretation of the microfossils

For the 20O2/27 campaign in the vicinity of the harbour of Zeebrugge, including the dredging sludge dumping sites it can be stated that the:

- dominant majority of Cretaceous nannofossils, with a minority of recent forms and some percentages, are derived from the Bassevelde 3-Marine Tongrian and Ruisbroek sequence sensu Vandenberghe et al. (2003) described form the Doel 2b well. This earliest Oligocene is located definitely to the east of the samples but the chalks are located west.
- Dinoflagellates show associations from the Ruisbroek Sand, outcropping just to the east of the Bassevelde 3 sequence, and eventually the Boom Clay, younger than the S90 level.

This means that in the eastern coastal zone, suspensions must be transferred both from the west (Cretaceous nannoplankton) and from the east (nannoplankton and dinoflagellates) and possibly even from the Schelde estuary.

In the west coast-Nieuwpoort area, in present suspensions occur significant amounts of re-worked Cretaceous nannofossils and almost no Paleogene forms. Also in the bottom samples, the large majority of the nannofossils are Cretaceous specimen. In one sample, an untransported Lower Eocene dinoflagellate specimen was found. This means that only currents from the west are active, bringing Cretaceous and that also some at least local erosion of the Ieper Group Clay occurs.

At the middle coast in the Oostende area, mostly Cretaceous sediments occur in the bottom sediments pointing to currents coming from the west, but also some Earliest Oligocene specimens are present coming from the east. In the present suspension samples Cretaceous forms derived from the west dominate but also eastern derived Earliest Oligocene specimens are present.

A suspension sample just north of the Schelde estuary mouth shows half of the nannoplankton to be of Cretaceous origin and hence to be of western origin and not derived from the Schelde estuary. Some specimen are of Earliest Oligocene NP21 zone sediments and therefore either locally eroded, slightly to the west of the sample, or might be transported from the Schelde estuary. The latter is less likely as in that case also nannoplankton from other Eocene and Oligocene bio-zones would be expected to be mixed in the Schelde water.

In conclusion it can be said that on all sites the presence of currents bringing Cretaceous nannoplankton from the west are present and that in addition currents bringing material from the east, in particular from the Eocene-Oligocene transitional strata, are present in the east coastal area showing an influence till the area between Oostende and Nieuwpoort. Remarkably the zone of east- derived currents coincides with the mud bottom as mapped by Bastin (1974) and also the differences in clay mineral associations (smectite dominated versus illite dominated) are at first sight coinciding with these current influences as demonstrated by microfossil study. Could it be an indication that the mud in the mud bottom has an eastern origin?

6. References

Aberle, J., Nikora, V., Walters, R. 2004. Effects of bed material properties on cohesive sediment erosion. Marine Geology, 207 (1-4), 83-94.

Agrawal, Y. C., Pottsmith, H. C. 2000. Instruments for particle size and settling velocity observations in sediment transport. Marine Geology, 168, 89-114.

Ariathurai, C. R. 1974. A finite element model for sediment transport in estuaries. PhD thesis, University of California, Davis.

Baeteman, C. 1999. The Holocene depositional history of the IJzer palaeovalley (western Belgian coastal plain) with reference to the factors controlling the formation of intercalated peat beds. Geologica Belgica, 2/3-4, 39-72.

Bass, S.J., Aldridge, J.N., McCave, I.N., Vincent, C.E., 2002, Phase relationships between fine sediment suspensions and tidal currents in coastal seas. Journal of Geophysical Research, 107 (C10), 10:1-14.

Bastin, A. 1974. Regionale sedimentologie en morfologie van de zuidelijke Noordzee en het Schelde estuarium. PhD thesis, Katholieke Universiteit Leuven, 91pp.

Berlamont, J., Ockenden, M., Toorman, E., Winterwerp, J. 1993. The characterisation of cohesive sediment properties. Coastal Engineering, 21, 105-128.

Best, J. L., Leeder, M. R. 1993. Drag reduction in turbulent muddy seawater flows and some sedimentary consequences. Sedimentology 40, 1129-1137.

Bots, M. E. 1986. The effects of slaking on the engineering behaviour of clay shales. PhD thesis, Dep. of Civil, Environmental and Architectural Engineering University of Colorado, 262pp.

Brindley, G.W., Brown, G., 1984. Crystal structures of Clay Minerals and their X-ray identification. Mineral Society, London, 495p.

Chamley, H., 1989. Clay Sedimentology. Springer-Verlag, Berlin, 623p.

Chen, M., 2003. Suspended matter and flocculation in the estuarine environment. PhD thesis, V.U.Brussel, 184pp.

Coastal Engineering Manual. 2002. Erosion, transport and deposition of cohesive sediments. EM 1110-2-1100 (part III-chapter5).

Davidson-Arnott, R. G. D., Langham, D. R. J. 2000. The effects of softening on nearshore erosion of a cohesive shoreline. Marine Geology, 166 (1-4), 145-162.

De Batist, M. 1989. Seismo-stratigrafie en struktuur van het Paleogeen in de Zuidelijke Noordzee. Unpublished PhD Thesis, UGent, Ghent, 107pp.

De Batist, M. & Henriet, J.P. 1995. Seismic sequence stratigraphy of the Tertiary offshore of Belgium, Southern North Sea. Journal of the Geological Society of London, 152. pp.27-40.

Degraer, S., Volckaert, A., Vincx, M. 2002. Evaluatie en aanvullingen milieu effecten rapport windmolenpark "Wenduinebank". Rapport UGent i.o. BMM. 22pp.

Druyts, M. 2000. Veilig varen boven slib. In: Watergebonden veiligheid, een probleem met veel facetten, Colloquium at WLH Antwerpen.

Dupeuble, P., Mathieu, R., Momeni, I., Poignant, A., Rosset-Moulinier, M., Rouvillois, A., Ubaldo, M., 1972. Travaux récents sur les Foraminifères actuels des côtes françaises de la Manche. Mémoire du B.R.G.M., n°79.

Dyer, K. R. 1995. Sediment transport processes in estuaries. In: Geomorphology and Sedimentology of Estuaries. (Perillo, G. M. E., eds.), Elsevier Science BV. Developments in Sedimentology 53, 423-449.

Eisma, D., Kalf, J. 1979. Distribution and particle size of suspended matter in the Southern Bight of the North Sea and the Eastern Channel. Netherlands Journal of Sea Research. 13 (2), 298-324.

Fettweis, M., Nechad, B., Francken, F., Van den Eynde, D. 2002. Bepaling van de sedimentbalans voor de Belgische kustwateren, Dynamica van het gesuspendeerd particulair materiaal

op het Belgisch Continentale Plat. MUMM Report SEBAB/3/MF/200212/NL/AR/1, 30pp.

Fettweis, M., Van den Eynde, D. 2003. The mud deposits and the high turbidity in the Belgian-Dutch coastal zone, Southern bight of the North Sea. Continental Shelf Research, 23, 669-691.

Fettweis, M., Francken, F., Nechad, B., Van den Eynde, D. 2003. MOnitoring en MOdellering van het cohesieve sedimenttransport en evaluatie van de effecten op het mariene ecosysteem ten gevolge van bagger- en stortoperaties. MUMM report. MOMO/MF/200310/NL/AR/1, 34pp.

Fettweis, M., Francken, F., Nechad, B., Pison, V., Van den Eynde, D. 2004. MOnitoring en MOdellering van het cohesieve sedimenttransport en evaluatie van de effecten op het mariene ecosysteem ten gevolge van bagger- eb stortoperaties (MOMO). Activiteitsrapport 2 (oktober 2003 - maart 2004). BMM, Brussel. MOMO/MF/200404/NL/ER/1, 33pp.

Fettweis, M., Francken, F., Pison, V., Van den Eynde, D. 2005. Suspended particulate matter dynamics and aggregate sizes in a high turbidity area. Submitted to Marine Geology.

Francken, F., Fettweis, M. 2002. Bepaling van de sedimentbalans voor de Belgische kustwateren (SEBAB II). Technisch rapport 1: Sedimentologische analysen van bodemstalen. BMM, Brussel. SEBAB/2/FF/200204/NL/TR/1, 20pp.

Frenzel, P., 2000. Die benthischen Foramiferen der Rügener Schreibkreide (Unter-Maastricht, NE-Deutschland). Neue Paläont. Abhandl. 3, 361p.

Friederichs, H. M. 2004. Flow-induced effects of macrozoobenthic structures on the near-bed sediment transport. PhD thesis, Univesität Rostock, 80pp.

Fugate, D. C., Friederichs, C. T. 2003. Controls on suspended aggregate size in partially mixed estuaries. Estuarine Coastal and Shelf Science. 58 (2), 389-404.

Gartner, J. W., Cheng, R. T., Wang, P.-F., Richter, K. 2001. Laboratory and field evaluations of the LISST-100 instrument for suspended particle size detrminations. Marine Geology. 175, 199-219.

Gaskin, S.J., Pieterse, J., Al Shafie, A., Lepage, S. 2003. Erosion of undisturbed clay samples from the banks of the St. Lawrence River. Canadian Journal of Civil Engineering 30(3): 585-595.

Gerritsen, H., Vos, R. J., van der Kaaij, T., Lane, A., Boon, J. G. 2000. Suspended sediment modelling in a shelf sea (North Sea). Coastal Engineering 41, 317-352.

Gullentops, F., Moens, M., Ringelé, A., Sengier, R. 1976. Geologische kenmerken van de suspensie en de sedimenten. In: Project Zee/Projet Mer, Volume 4: Sedimentologie. (Nihoul, J. C. J., Gullentops, F., eds.) Brussels, Science Policy Office, 1-137.

Hamm, C. E. 2002. Interactive aggregation and sedimentation of diatoms and clay-sized lithogenic material. Limnology and Oceanography, 47(6), 1790-1795.

Hoitink, A.J.F., Hoekstra, P., van Maren, D.S., 2003. Flow asymmetry associated with astronomical tides: Implications for the residual transport of sediment. Journal of Geophysical Research, 108(C10), 13:1-8.

Holtzapffel, T., 1985. Les minéraux argileux. Annales de la Société Géologique du Nord 12, 74pp.

Houwing, E.-J. 1999. Determination of the critical erosion threshold of cohesive sediments on intertidal mudflats along the Dutch Wadden Sea coast. Estuarine, Coastal and Shelf Science, 49(4), 545-555.

Irion, G., Zölmer, V., 1999. Clay mineral associations in fine grained surface sediments of the North Sea. Journal of Sea Research, 41, 119-12.

Jacobs, P., De Ceukelaire, M., Moerkerke, G. & Polfliet, T. 2002. Toelichtingen bij de geologische kaart. 1:50.000. Kaartblad Blankenberge – Westkapelle – Oostduinkerke – Oostende (4-5-11-12). Ministerie van Economische Zaken – Belgische Geologische Dienst, Ministerie van de Vlaamse Gemeenschap – Afdeling Natuurlijke Rijkdommen en Energie, Brussel.

Kaasschieter, J., 1961. Foraminifera of the Eocene of Belgium. K.B.I.N. Verhandeling 147/3.

Kahle, M., Kleber, M., Jahn, R., 2002. Review of XRD-based quantitative analyses of clay minerals in soils: the suitability of mineral intensity factors. Geoderma, 109, 191-205.

Konert, M., Vandenberghe, J., 1997. Comparison of laser grain size analysis with pipette and sieve analysis: a solution for the underestimation of the clay fraction. Sedimentology, 44, 523-535.

Kornman, B., van Maldegem, D. C. 2002. Evaluatie van de effecten van het verspreiden van Boomse Klei in de Westerschelde. Eindrapportage monitoring boorspecie. RIKZ, Middelburg. rapport 2002.052, 36pp.

Kranenburg, C. 1994. On the fractal structure of cohesive sediment aggregates. Estuarine, Coastal and Shelf Science, 39, 451-460.

Krogel, F., Flemming, B. W. 1998. Evidence for temperature-adjusted sediment distribution in the back-barrier tidal flats of the east Frisian Wadden Sea (southern North Sea). In: Tidalites: Processes & Products, (Alexander, C. R., Davis, R. A., Henry, V. J., eds.). SEPM Special Publication No 61. Tulsa, Oklahoma, USA, Society for Sedimentary Geology.

Krone, R. B. 1962. Flume studies of the transport of sediment in estuarial shoaling processes. Hydraulic and Sanitary Engineering Research Laboratory, University of California, Berkeley, 118pp.

Lacroix, G., Ruddick, K., Ozer, J., Lancelot, C. 2004. Modelling the impact of the Scheldt and Rhine/Meuse plumes on the salinity distribution in Belgian waters (southern North Sea). Journal of Sea Research. 52 (3), 149-163.

Lafite, R., S.J. Shimwell, L.A. Nash, J.P. Dupont, M.F. Huault, N.T.L. Grochowski, JM. Lamboy & M.B. Collins, 1993. Sub-Task S1: Suspended material fluxes through the Strait of Dover. In: Hydrodynamics and Biogeochemical Fluxes in the Eastern Channel: Fluxes into the North Sea. FLUXMANCHE I Second annual rep., MAST 0053-C (EDB), 81-106.

Lanckneus, J., Van Lancker, V., Moerkerke, G., Van den Eynde, D., Fettweis, M., de Batist, M., Jacobs, P. 2001. Investigation of the natural sand transport on the Belgian continental shelf (BUDGET). PPS Science Policy, Belgium, Final report, 104 pp + annex.

Le Bot, S., Van Lancker, V., Deleu S., De Batist M. & Henriet J.P. 2003. Tertiary and Quaternary geology of the Belgian Continental Shelf. Scientific Support Plan for a Sustainable Development Policy. SPSD II North Sea. Brussels, PPS Science policy publication D/2003/1191/12, 75pp.

Li, M. Z., Gust, G. 2000. Boundary layer dynamics and drag reduction in flows of high cohesive sediment suspensions. Sedimentology, 47, 71-86.

Lintern, D. G., Sills, G. C., Roberts, W. 2002. Erosion properties of mud beds deposited in laboratory settling columns. In: Proceedings in Marine Science, Vol.5: Fine Sediment Dynamics in the Marine Environment (Winterwerp, J.C., Kranenburg, C., eds.), Elsevier Science, 343-358.

Liu, A.C. 1990. A seismic and geomorphological study of the erosion surface at the top of the Tertiary in the Southern North Sea (Belgian and Northern French sectors). Unpublished PhD Thesis, UGent, Ghent, vol.1: 119pp., vol.2: 97pp.

Liu, A.C., Missiaen, T. & Henriet, J.P. 1992. The morphology of the top-Tertiary erosion surface in the Belgian sector of the North Sea. Marine Geology, 105, 275-284.

Luyten, P. J., Jones, J. E., Proctor, R., Tabor, A., Tett, P., Wild-Allen, K. 1999. COHERENS, A Coupled Hydrodynamical-Ecological Model for Regional and Shelf Seas: User Documentation. MUMM report, Brussels, 911pp. [Available on CD-ROM at http://www.mumm.ac.be/coherens].

Maréchal, R. & Henriet, J.P. 1983. Seismisch onderzoek op het Belgisch Continentaal Plat. Eerste faze. Ontginninszone 2. Unpublished report, Ministry of Economic Affairs, 32pp.

Maréchal, R., Henriet, J.P., Mostaert, F., De Batist, M., Moons, A. & Verschuren M. 1986. Stu-

die oppervlaktelaag van het Belgisch Continentaal Plat. Seismisch prospectie sector B. Unpublished report, Ministry of Economic Affairs, 52pp.

McManus, J.P. & D. Prandle, 1997. Development of a model to reproduce observed suspended sediment distributions in the southern North Sea using Principal Component Analysis and Multiple Linear Regression. Cont. Shelf Res., 17, 761-778.

Mehta, A. J., Hayter, E. J., Parker, W. R., Krone, R. B., Teeter, A. M. 1989. Cohesive sediment transport. I Process description and II Application. Journal of Hydraulic Engineering, 115(8), 1076-1112.

Mikkelsen, O. A., Pejrup, M. 2001. The use of a LISST-100 laser particle sizer for in-situ estimates of floc size, density and settling velocity. Geo-Marine Letters, 20, 187-195.

Missiaen, T., Murphy, S., Loncke, L., Henriet, J.-P. 2002. Very high-resolution seismic mapping of shallow gas in the Belgian coastal zone. Continental Shelf Research, 22, 2291-2301.

Moore, D.M., Reynolds, R.C.Jr., 1997. X-ray Diffraction and the Identification and Analysis of Clay Minerals. Second Edition. Oxford University Press, Oxford, 378pp.

Nechad, B., De Cauwer, V., Park, Y., Ruddick, K., 2003. Suspended Particulate Matter (SPM) mapping from MERIS imagery, calibration of a regional algorithm for the Belgian coastal waters. Proceedings MERIS user workshop, 10-13th November 2003, Frascati. Special Publication of European Space Agency SP-549, CD-ROM, ESA Publication Division, Noordwijk, The Netherlands, 6pp.

Nihoul, J. C. J. 1975. Effect of tidal stress on residual circulation and mud deposition in the Southern Bight of the North Sea. Review of Pure and Applied Geophysics, 113, 577-591.

Proctor, R., Holt, J. T., Balson, P. S., 2001. Sediment deposition in Offshore Deeps of the Western North Sea: Questions for Models. Estuarine, Coastal and Shelf Science, 53, 553-567.

Ravens, T.M., Gschwend, P.M. 1999. Flume measurements of sediment erodibility in Boston Harbor. Journal of Hydraulic Engineering, 125(10), 998-1005.

Revets, S., 1987. A revision of the genus *Turrilina andreae*, 1884. Journal of Foraminiferal Research, 17(4), 321-332.

Ruddick, K.G., Ovidio, F., Rijkeboer, M., 2000. Atmospheric correction of SeaWiFS imagery for turbid coastal and inland waters. Applied Optics, 39(6), 897-912.

Sanford, L. P., Maa, J. P.-Y. 2001. A unified erosion formulation for fine sediments. Marine Geology, 179, 9-23.

Sels, O., 1997. Sedimentatie- en erosiekaarten en hun toepassing op het Schelde-estuarium. Licenciaatsthesis, Katholieke Universiteit Leuven.

Sills, G. C., Elder, D. M. 1986. The transition from sediment suspension to settling bed. In: Lecture Notes on Coastal and Estuarine Studies 14: Estuarine Cohesive Sediment Dynamics (Mehta, A. J., ed.), Springer Verlag, 192-205.

Strubbe, J. 1987. De Belgische Zeehavens, erfgoed voor morgen. Lannoo.

Temmerman, S. 2003. Sedimentation on tidal marshes in the Scheldt estuary. A field and numerical modelling study. PhD Thesis, Katholieke Universiteit Leuven, 222pp.

Thorez, J. 1976. Practical identification of clay minerals. G. Lelotte, Dison, 90pp.

Toorman, E. 1992. Modelling of fluid mud flow and consolidation. PhD thesis, Katholieke Universiteit Leuven, 219pp.

Toorman, E., Bruens, A. W., Kranenburg, C., Winterwerp, J. 2002. Interaction of suspended cohesive sediment and turbulence. In: Proceedings in Marine Science, Vol.5: Fine Sediment Dynamics in the Marine Environment (Winterwerp, J.C., Kranenburg, C., eds.), Elsevier Science, 7-23.

Traykovski, P., Latter, R. J., Irish, J. D. 1999. A laboratory evaluation of the laser in situ scattering and transmissometry instrument using natural sediments. Marine Geology, 159, 355-367.

Vandenberghe, N., Brinkhuis, H., & Steurbaut, E. (2003): The Eocene/Oligocene boundary in the North Sea area: A sequence stratigraphic approach. In: PROTHERO, D.R., IVANY, L.C. & NESBITT, E.A. (Eds): From Greenhouse to Icehouse. The marine Eocene-Oligocene transition. Columbia University Press, New York, 419-437.

Van den Eynde, D., Nechad, B., Fettweis, M., Francken, F. 2005. SPM dynamics in the southern North Sea derived from SeaWifs imagery, in situ measurements and numerical modelling. Proceedings in Marine Science, Elsevier. (in Press)

van der Lee, W. T. B. 2000. Temporal variation of floc size and settling velocity in the Dollard estuary. Continental Shelf Research, 20 (12-13), 1495-1511.

Van Lancker, V., Moerkerke, G., Fettweis, M., Van den Eynde, D., de Batist, M., Jacobs, P. 2002. Investigation of natural sand transport on the Belgian continental shelf (BUDGET). Final report. Federal Office for Scientific, Technical and Cultural Affairs (OSTC), 104+87pp.

Van Lancker, V., Deleu, S., Bellec, V., Le Bot, S., Verfaillie, E., Fettweis, M., Van den Eynde, D., Francken, F., Pison, V., Wartel, S., Monbaliu, J., Portilla, J., Lanckneus, J., Moerkerke, G., Degraer, S. 2004. Management, research and budgeting of aggregates in shelf seas related to end-users (Marebasse). Belgian Science Policy, Scientific Report Year 2, 144pp.

van Leussen, W. 1994. Estuarine macroflocs and their role in fine-grained sediment transport. PhD Thesis, Universiteit Utrecht, The Netherlands. 488pp.

van Loen , H., Houziaux, J-S., Van Goethem, J. 2002. The collection Gilson as a reference framework for the Belgian marine fauna: a feasibility study" Final Report OSTCMN/36/94.

Van Mierlo, C-J., 1897. Quelques mots sur le régime de la côte devant Heyst. Annales de l'association des ingénieurs sortis des écoles spéciales de Gand, tome XX, 4e livraison.

Van Mierlo, C.-J., 1899. La carte lithologique de la partie méridionale de la mer du Nord. Bulletin de la Société Belge de Géologie, Paléontologie et Hydrologie, XII, 2nde série (tome III), p. 219 – 265.

Van Mierlo, C-J, 1908. Le port de Heyst. Annales de l'association des ingénieurs sortis des écoles spéciales de Gand, 4e série, tome I, fasc. 3.

Van Parys, M., Pieters, M., 2001. Turbiditeit op de loswal B&W Zeebrugge Oost, stationaire metingen. Bijakte 14 Mobag 2000 - Ecologische impact. Rapport Tijdelijke Vereniging Noordzee en Kust, TVNK/Z/04/2001/MVP, 26pp.

Van Rijn, L.C., 1993. Principles of sediment transport in rivers, estuaries and coastal seas. Aqua Publications, Amsterdam, 686pp.

Velegrakis, A.F., Michel, D., Collins, M.B., Lafite, R., Oikonomou, E.K., Dupont, J.P., Huault, M.F., Lecouturier, M., Salomon, J.C., Bishop, C., 1999. Sources, sinks and resuspension of suspended particulate matter in the eastern English Channel. Continental Shelf Research 19, 1933-1957.

Verlaan, P. A. J., Donze, M. & Kuik, P. 1998. Marine vs fluvial suspended matter in the Scheldt estuary. Estuarine, Coastal and Shelf Science, 46 (6), 873-883.

Verreet, G., Berlamont, J. 1989. Rheology and non-Newtonian behaviour of sea and estuarine mud. Encyclopedia of Fluid Mechanics, Vol. VII: Rheology and non-Newtonian flows (Chereminisoff, ed.), Gulf Publishing Co.

Wartel, S., Parker, R., Francken, F. 2000. Bepaling van de sedimenttypes en de opstelling van een lithologische kaart van de Beneden-Zeeschelde. Rapport K.B.I.N., Brussel.

Williamson, H., Torfs, H. 1996. Erosion of mud/sand mixtures. Coastal Engineering, 29, 1-25.

Wang, Y. H. 2003. The intertidal erosion rate of cohesive sediment: a case study from Long Island Sound. Estuarine, Coastal and Shelf Science, 56, 891-896.

Winterwerp, J., Bale, A. J., Christie, M. C., Dyer, K. R., Jones, J. E., Lintern, D. G., Manning, A. J., Roberts, W. 2002a. Flocculation and settling velocity of fine sediments. In: Proceedings in Marine Science, Vol.5: Fine Sediment Dynamics in the Marine Environment (Winterwerp, J.C., Kranenburg, C., eds.), Elsevier Science, 25-40.

Winterwerp, J.C., Bruens, A.W., Gratiot, N., Kranenburg, C., Mory, M., Toorman, E.A. 2002b. Dynamics of concentrated benthic suspension layers. In: Proceedings in Marine Science, Vol.5: Fine Sediment Dynamics in the Marine Environment (Winterwerp, J.C., Kranenburg, C., eds.), Elsevier Science, 41-55.

Winterwerp, J. 2002. On the flocculation and settling velocity of estuarine mud. Continental Shelf Research, 22, 1339-1360.

Ziervogel, K. 2003. Aggregation and transport behaviour of sediment surface particles in Mecklenburg Bight, south-western Baltic Sea, affected by biogenic stickiness. PhD thesis, Univ. Rostock, Germany. 94pp.

Zreik, D. A., Krishnappan, B.G., Germaine, J.T., Madsen, O.S., Ladd, C.C. 1998. Erosional and mechanical strengths of deposited cohesive sediments. Journal of Hydraulic Engineering, 124(11), 1076-1085.

Appendix I

Through tide measurements – SPM concentration

The measurements, which are presented below, have been carried out with a Sea-Bird SBE19 'SeaCat' CTD profiler and a Sea-Bird SBE09 CTD system with Sea-Bird carrousel water sampling system 'SBE32'. Optical Backscatter Sensors (OBS) were used to measure backscattering. The OBS signal was calibrated with SPM concentrations determined from water samples and filtration. The 'SeaCat' has been installed at about 3 m from the water surface, whereas the Sea-Bird SBE09 was kept at about 3 m above the bottom.

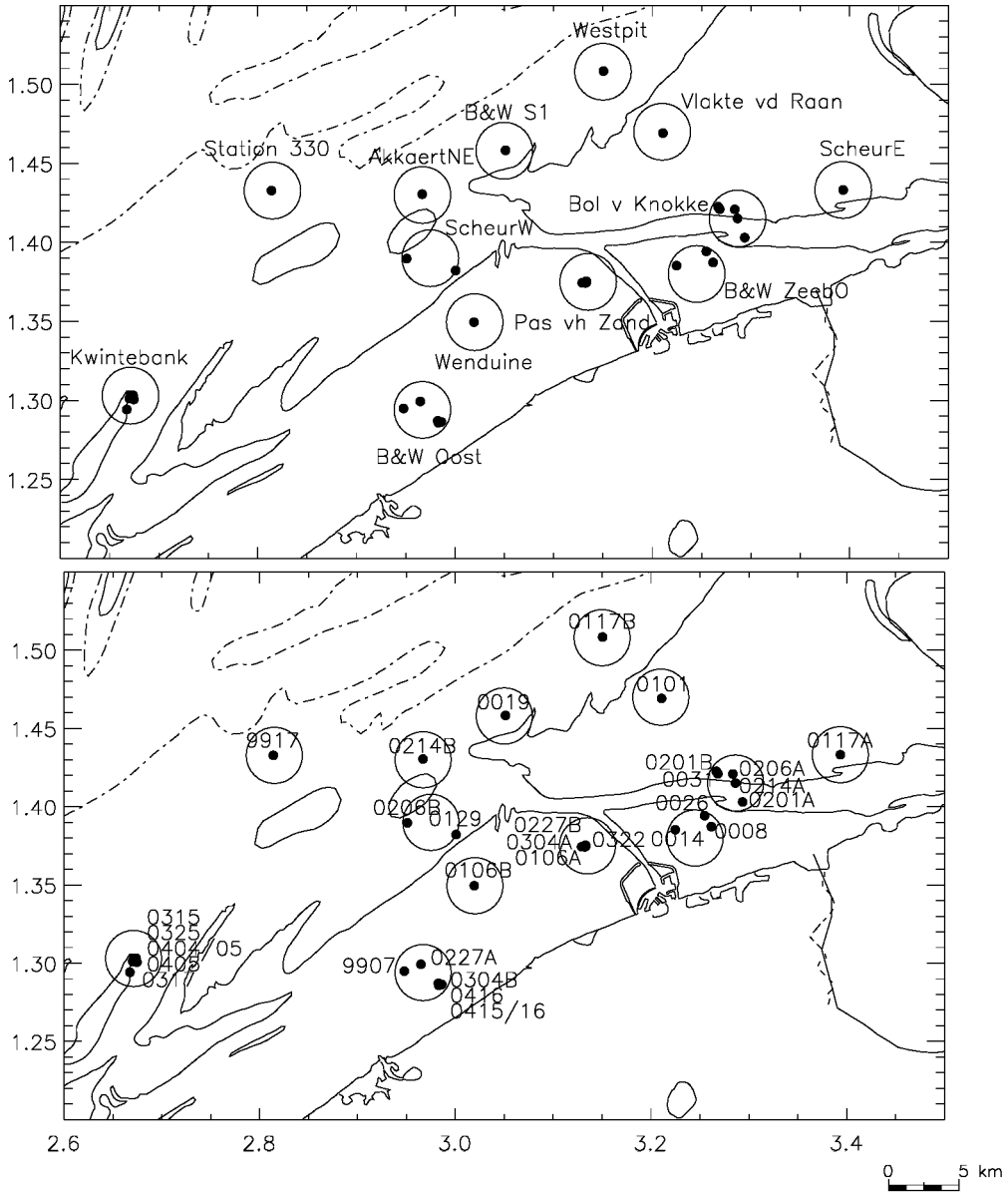

Figure1-1: Location of through tide and tripode measurements, period 1999-2004. (a) location names, (b) R/V Belgica campaign numbers..

Through tide measurements locations. The measurements are classified according to location (see fig I-1).

Cmp. yy/nr	Start timed (GMT)	End time (GMT)	Latitude (N)	Longitude (E)	Season
B&W Oostende					
99/07	08/03/1999 15h47	09/03/1999 05h03	51° 17.69'	2° 56.87'	winter
02/27-a	25/11/2002 18h12	26/11/2002 7h09	51° 17.958'	2° 57.888'	autumn
03/04-b	20/02/2003 18h53	21/02/2003 08h10	51° 17.224	2° 58.953'	winter
Wenduine					
01/06-b	08/03/2001 10h37	09/03/2001 06h00	51° 20.97'	3° 01.23'	winter
Pas van het Zand					
01/06-a	07/03/2001 16h12	08/03/2001 09h38	51° 22.51'	3° 07.960'	winter
02/27-b	26/11/200218h32	27/11/2002 7h31	51° 22.525'	3° 07.987'	atumn
03/04-a	19/02/2003 18h22	20/02/2003 07h09	51° 22.464'	3° 07.738'	winter
03/22	08/09/2003 18h02	09/09/2003 07h09	51° 22.477'	3° 07.986'	summer
B&W Zeebrugge Oost					
00/08	21/03/2000 10h15	21/03/2000 23h00	51° 23.238'	3° 15.697	spring
00/14	29/05/2000 08h53	29/05/2000 22h01	51° 23.12'	3° 13.48'	spring
00/26	23/10/2000 20h10	24/10/2000 08h52	51° 23.66'	3° 15.28'	autumn
Bol van Knokke					
00/31	07/12/2000 10h01	08/12/2000 06h44	51° 25.26'	3° 16.10'	autumn
02/01-a	30/01/2002 10h40	31/01/2002 00h09	51° 25.38	3° 15.96'	winter
02/01-b	31/01/2002 01h16	31/01/2002 04h19	51° 24.19'	3° 17.49'	winter
02/06-a	11/03/2002 16h04	12/03/2002 06h40	51° 24.88'	3° 16.95'	winter
02/14-a	26/06/2002 12h30	27/06/2002 04h12	51° 24.905'	3° 17.181'	summer
Scheur E					
01/17-a	18/06/2001 18h34	19/06/2001 07h11	51° 25.99'	3° 23.66'	summer
Kwintebank					
03/15	11/06/2003 18h23	13/06/2003 07h07	51° 18,071'	2° 40,206'	spring
03/17	26/06/2003 16h33	27/06/2003 05h25	51° 17.65'	2° 40.280'	summer
03/25	09/10/2003 15h41	10/10/2003 04h21	51°18.035'	2°40.470'	autumn
04/04-05	02/03/2004 12h45		51°18.151'	2°40.245'	winter
B&W S1					
00/19	10/07/2000 09h18	10/07/2000 22h22	51° 27.5'	3° 03.07'	summer
Akkaert NE					
02/14-b	27/06/2002 17h25	28/06/2002 6h08	51° 25.832'	2°58.007'	summer
Station330					
99/17	13/07/1999 06h17	13/07/1999 19h20	51° 25.97'	2° 48.14'	summer
Scheur W					
01/29	12/11/2001 17h17	13/11/2001 06h56	51° 22.93'	3° 00.42	autumn
02/06-b	12/03/2002 15h15	13/03/2002 4h31	51° 23.38'	2°57.06'	winter
Vlakte van de Raan					
01/01	25/01/2001 11h45	26/01/2001 00h27	51° 28.12'	3° 12.57'	winter
Westpit					
01/17-b	19/06/2001 19h41	20/06/2001 8h29	51° 30.51'	3°09.03'	summer

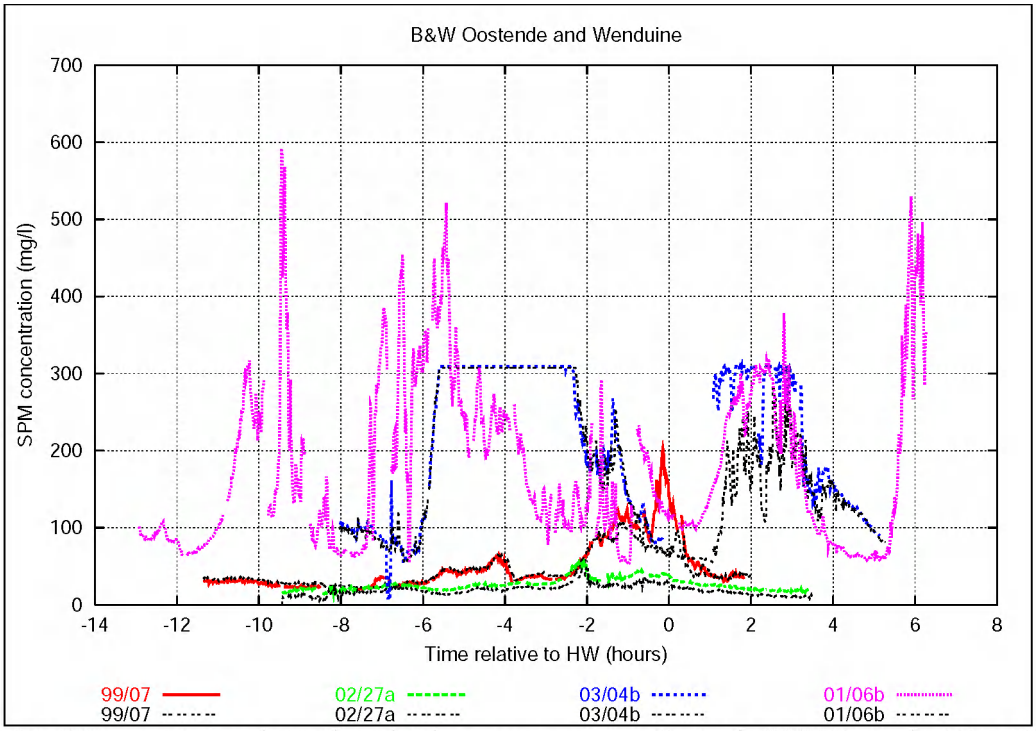

Figure I-2: SPM concentration during through tide measurements near **Oostende** (B&W Oostende: 99/07, 02/27a, 0304b and Wenduine: 01/06b). Time is related to HW at Oostende. Coloured lines represents data of the SBE09 CTD system (about 3 m above the bottom), black lines of the SBE19 system (about 3 m from surface). The OBS's during TT 03/04b were saturated from -6h to -2h and 1h to 3h.

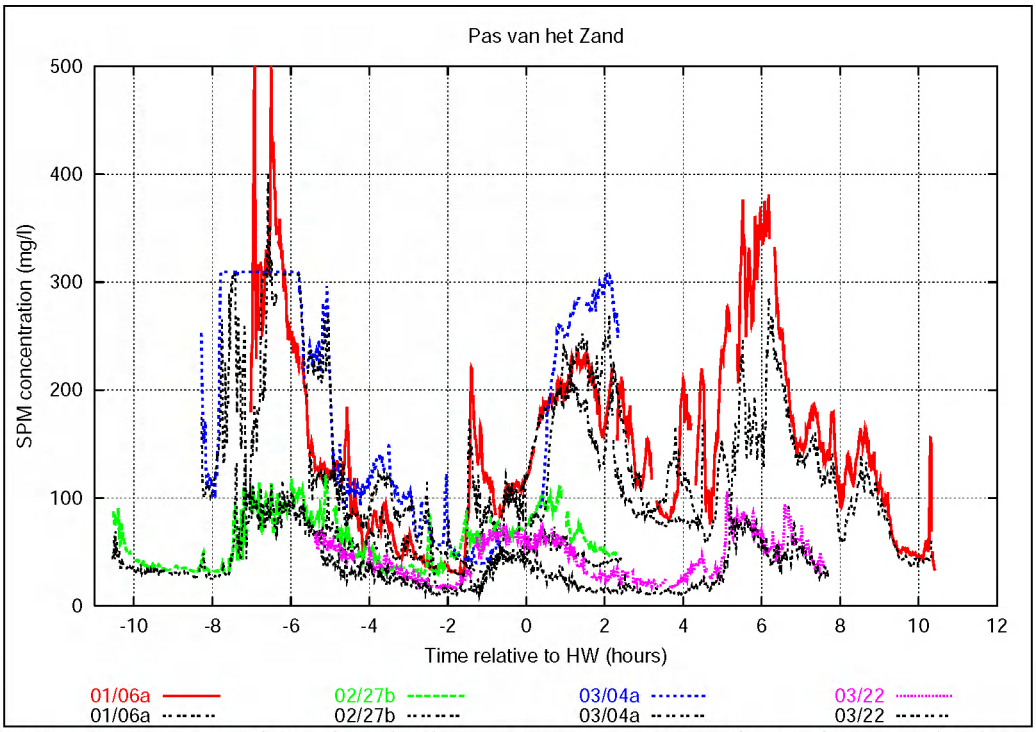

Figure I-3: SPM concentration during through tide measurements near **Pas van het Zand.** Time is related to HW at Zeebrugge. Coloured lines represents data measured by the Sea-Bird SBE09 CTD system (about 3 m above the bottom), black ones of the SBE19 system (about 3 m from surface). The OBS's during TT 03/04a were saturated from -8h to -6h and around 2h.

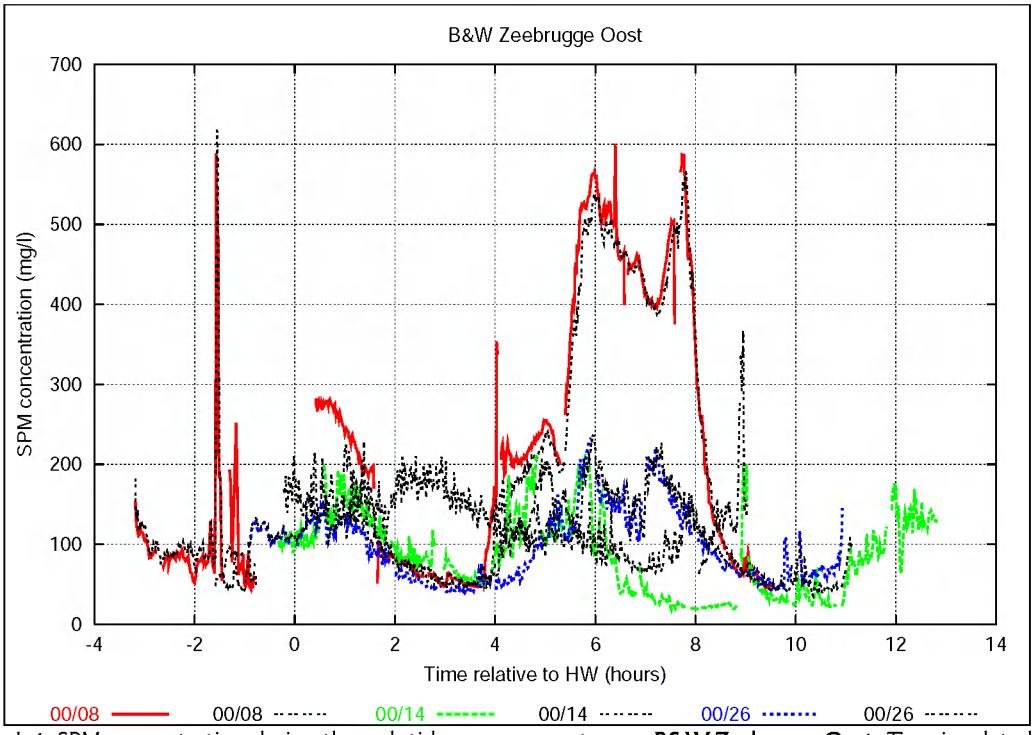

Figure I-4: SPM concentration during through tide measurements near **B&W Zeebrugge Oost**. Time is related to HW at Zeebrugge. Coloured lines represents data measured by the Sea-Bird SBE09 CTD system (about 3 m above the bottom), black ones of the SBE19 system (about 3 m from surface).

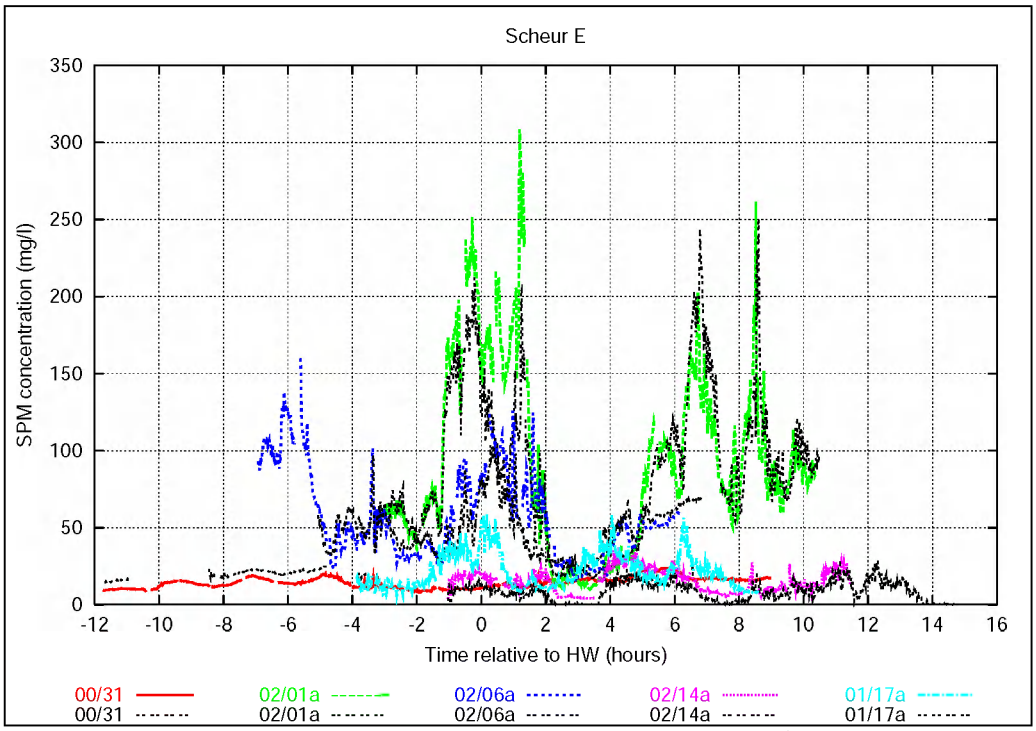

Figure I-5: SPM concentration during through tide measurements near **eastern Scheur** (Bol van Knokke: 00/31, 02/01a, 02/06a, 02/14a and ScheurE: 01/17a). Time is related to HW at Zeebrugge. Coloured lines represents data measured by the Sea-Bird SBE09 CTD system (about 3 m above the bottom), black ones of the SBE19 system (about 3 m from surface).

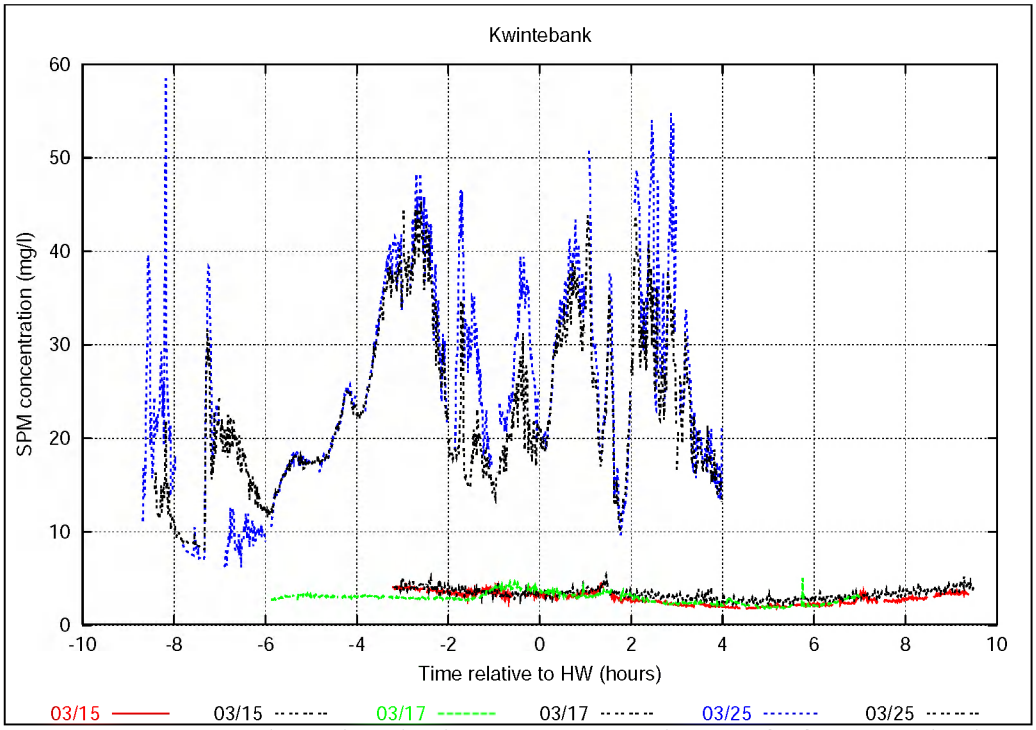

Figure I-6: SPM concentration during through tide measurements on the **Kwintebank.** Time is related to HW at Oostende. Coloured lines represents data measured by the Sea-Bird SBE09 CTD system (about 3 m above the bottom), black ones of the SBE19 system (about 3 m from surface).

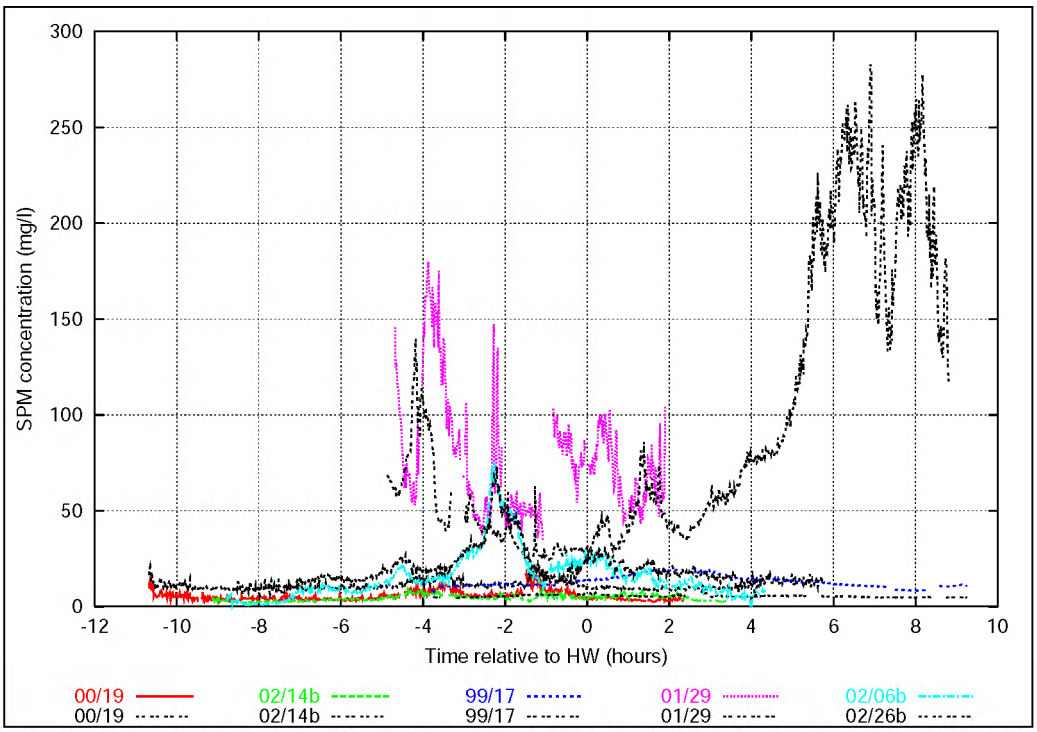

Figure I-7: SPM concentration during through tide measurements **off shore** (B&W S1: 00/19; Akkaert: 02/14b; Station 330: 99/17 and ScheurW: 01/29, 02/06a). Time is related to HW at Zeebrugge/Oostende. Coloured lines represents data measured by the Sea-Bird SBE09 CTD system (about 3 m above the bottom), black ones of the SBE19 system (about 3 m from surface).

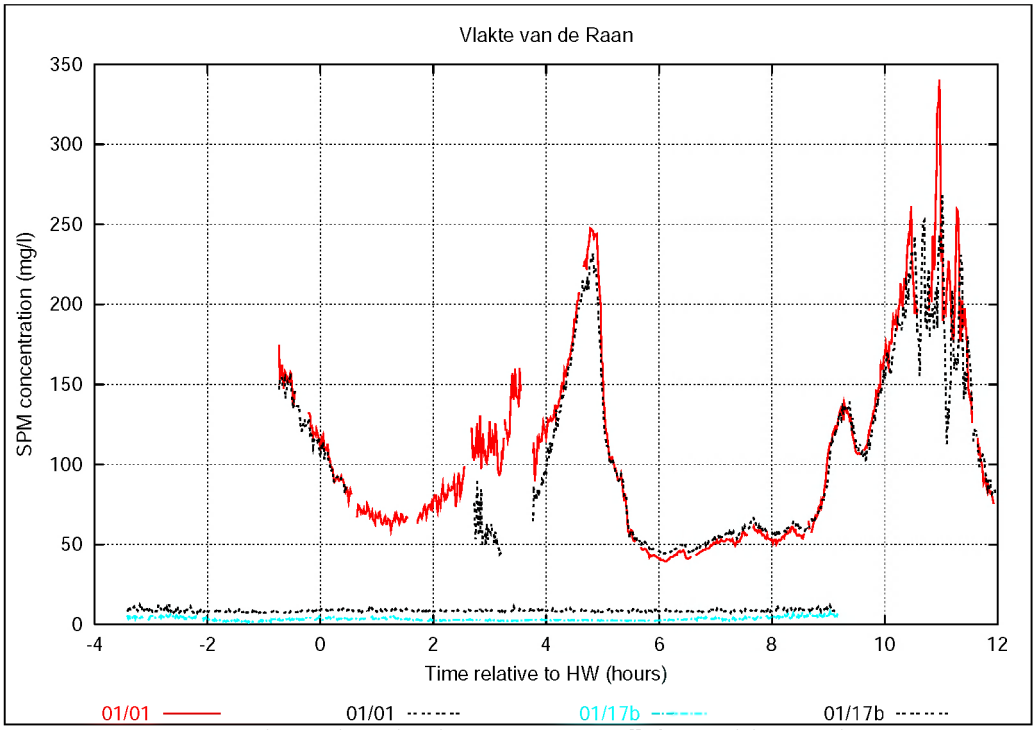

Figure I-8: SPM concentration during through tide measurements **off shore** (Vlakte van de Raan: 01/01; Westpit: 01/17b). Time is related to HW at Zeebrugge/Oostende. Coloured lines represents data measured by the Sea-Bird SBE09 CTD system (about 3 m above the bottom), black ones of the SBE19 system (about 3 m from surface).

Appendix II

Clay mineralogy of North Sea mud

Quantitative XRD clay mineral analysis

II.1 Basics of the XRD method

Although other techniques, such as thermal analysis, electron microscopy and infrared spectroscopy, can significantly contribute to a quantitative analysis of clay mineral compositions of mud sediments, the main technique used is X ray diffraction.

A Philips PW 1050/37 X-ray diffractometer is used with a PW2236/20 cobalt-anode. The cobalt-anode is hit by electrons moving in a high tension field, producing Co-Kα (α_1 and α_2 have very close wavelengths but the intensity of the first is double the intensity of the second) radiation (the Kβ radiation is filtered using Fe filter), is commonly used to avoid fluorescence excitation in the samples which would be particularly the case if more than about 5% iron is present (Brindley & Brown, 1984). The operation conditions for the generator are 40 kV and 30 mA. Divergence- and receiving-slits are respectively 1° and 0.2°.

The measuring time per step is a balance between peak to noise ratio and the duration time required for an analysis; our analyses have been carried out counting 1 sec per step of 0.030°2ϑ. Smaller step length could produce patterns with higher resolution.

For the analysis of clay minerals the recording interval chosen is 2°2ϑ to 35°2ϑ. The relevant d(001) en d(002) values of the clay minerals do occur in this interval and allow their identification. The digital records are produced as graphs using the Philips software PW1877 version 3.6.

The diffraction phenomena of the radiation on the sample are made possible by the fact that a similar distance exists between dispersion centres (atom centres) and the X ray wave length. The diffraction conditions are then governed by Bragg's law (eq.1), which specifies the condition for constructive interference of the individual X rays:

$$n.\lambda = 2.d.\sin\vartheta \qquad (1)$$

with n a whole number, λ the X-ray wavelength, d the distance between two successive atomic layers and ϑ the angle of incidence of the X-rays on the atomic layers.

The diffracted radiation is passing through a series of slits and counted in a photo-multiplying counter. Peak intensities, expressed in counts per second, are recorded versus the 2ϑ angle of incidence of the X rays on the sample. The intensities are determined by the Bragg law, by the Lorenz-Polarization factor which expresses the dependence on the angle ϑ, and by the precise chemical-structural properties of the minerals in the sample. In addition to the coherently diffracted X- rays also background noise is also recorded.

Minerals can be identified based on the recorded X-ray peaks for which Bragg's law is valid and a d value can be calculated. Clay mineral identification poses a particular problem because of the similarity of the different minerals which will require particular treatments of the samples and because of the poor regularity in the crystal lattices requiring particular sample mounting techniques to increase the reflection intensities (Moore & Reynolds, 1997).

II.2 Sample preparation and mounting for clay mineral investigation

Chemical treatment

Preliminary analyses of the North Sea mud clay minerals have shown that following the classical procedure (Thorez, 1976) of applying no chemical treatment of the samples and working only in demineralised water, did produce low peak to noise ratio diffraction records. To improve this peak to noise ratio the samples in this research project have been systematically treated for removal of carbonates and organic matter.

Carbonates hinder the orientation of the platy clay minerals in the sample mounts and have been removed by adding 1.5N HCl till no further effervescence could be observed. The remaining acid is evaporated.

Organic matter agglomerates the mud particles hindering the full dispersion of the samples and a good orientation of the platy minerals in the sample mounts. Organic matter is removed by oxidation in 15% H_2O_2 on a 60°C hot plate. This treatment is carried out after carbonate removal as the peroxide treatment is not efficient in alkalic environment.

The separation of the clay minerals from the mud samples

The clay minerals have almost exclusively sizes smaller than 2 μm (defined by settling velocity). Therefore a size separation is carried out, concentrating the clay minerals and avoiding coarser spherical particles to hinder the orientation of the minerals in the sample mounts. The separation procedure used is as follows:

- 5 gram of clay rich sediments and 20 g of sandy samples, already treated for carbonates and organic matter, are sub-sampled, soaked in demineralised water, and shaken for 24 hours to improve dispersion.
- Subsequently the sample is centrifuged and a neat separation between the coarser grainy sediment population and the fine clay population is produced in the centrifuge tube.
- The clay population is carefully scraped off and brought in a small flask with demineralised water and put back in the shaking table.
- The suspension is then put to rest and the upper 2 cm are pipetted after 1 hour 36 minutes, containing only <2 μm sized particles according to Stokes law.
- The pipette drops part of the suspension on two small horizontal glass plates which fit the diffractometer sample chamber. The suspension is left evaporating on a 60°C hot plate. The slow evaporation and the almost pure platy clay mineral composition produce a highly oriented sample.

With respect to this pre-treatment procedure, the exact chemical treatment and the sample mount procedure (evaporation versus smear or suction mounts) can be debated. The followed procedure however follows from experience and testing over the years in the laboratory.

XRD-records of the sample mount

In order to differentiate between the different clay mineral lattices, the oriented sample mount is scanned by X-rays after different treatments.

A first record is made without any treatment (N record), a second record is scanned after vapour saturation with ethylene glycol molecules (EG record) and a third and fourth record after heating the sample mount during 24 hours respectively at 300°C and 500°C (H). The lower temperature leaves chlorites unaffected but has already degraded smectites; the higher temperature degrades in addition kaolinite and poorly crystalline chlorite. Illites and well crystalline chlorite remain unaffected at 500°C.

More advanced treatments are possible, such as cation treatments followed by saturation with different organic molecules and/or different heat regimes; such treatments can confirm difficult identification of species or give more detailed information on the nature of the minerals.

II.3 Identification and qualification criteria of clay minerals relevant for North Sea mud

The table below, after Thorez (1976), gives a summary of the main d-values of (00l) reflections of clay minerals relevant for the North Sea cohesive sediments, on N, EG and H 550° records. The selection of succession of (00l) lattice spacing is justified because of the orientation of the clay minerals on the glass plate.

Table II.1: Main d-values of clay mineral reflections relevant for North Sea mud's on N, EG and H 500°C records..

	Treatment	d(001)	d(002)	d(003)	d(004)
Chlorite	N	14	7	4.7	3.5
	EG	14	7	4.7	3.5
	500° C	14	7	4.7	3.5
Kaolinite	N	7.1	3.58	2.33	-
	EG	7.1	3.58	2.33	-
	500° C	-	-	-	-
Illite	N	10	5	3.3	2.5
	EG	10	5	3.3	2.5
	500° C	10	5	3.3	2.5
Smectite	N	15.4	-	5.1	-
	EG	17	8.5	5.7	4.2
	500° C	10	-	5	-

Illite

Illite reflections are not influenced by the different treatments. The reflections are rather symmetrical. The d(001) and d(003) reflections have similar intensities and the d(002) reflection has only one third of the intensity of both others. The ratio of (001) and (002) intensities can be used to estimate the octahedral iron content (Esquevin parameter). The exact d-(001) value is influenced by the nature of the exchangeable cations at the interlayer position (Holtzapffel, 1985).

The exact shape of the (001) reflection on the XRD record, from very narrow and sharp to broad and asymmetrical or open illite, can be interpreted in terms of the progressive loss of interlayer potassium .The behaviour of the broad asymmetrical shoulder after the different treatments, can be interpreted in terms of the nature of the intercalated lattice patterns (smectitic I_M, chloritic I_C or vermiculitic I_V) appearing upon altering the pure illite structure (see figure II.1).

Smectite

Smectites have a large range of compositional variations. Their main characteristic is a complete swelling after EG treatment shifting the d(001)-reflection at 12-14.5 Å to 17-18 Å, accompanied by a collapse of the structure after heating, due to the evacuation of the interlayer water molecules hydrating the exchangeable cations, shifting the d-(001) reflection to 10 Å. The d(001)-reflection of smectite under N condition can show a broad tail till even 10Å. It is probably related to hydration conditions and to the admixture of illite-smectite random layers in the mineral.

The shape of the 17Å-reflection on EG records is generally broad and takes variable profiles. The geometrical description of this 17 Å-reflection in terms of the ratio between V and P (see figure II.2)- respectively the peak height above background of the valley (V) at the high 2ϑ side and the height above background at the 17 Å peak (P) is interpreted as a measure for the crystallinity of the mineral. This ratio can become negative if no true peak

is observed. Although the exact mineralogical interpretation of this ratio is debatable, it helps to describe the mineralogical content and establish variations between samples.

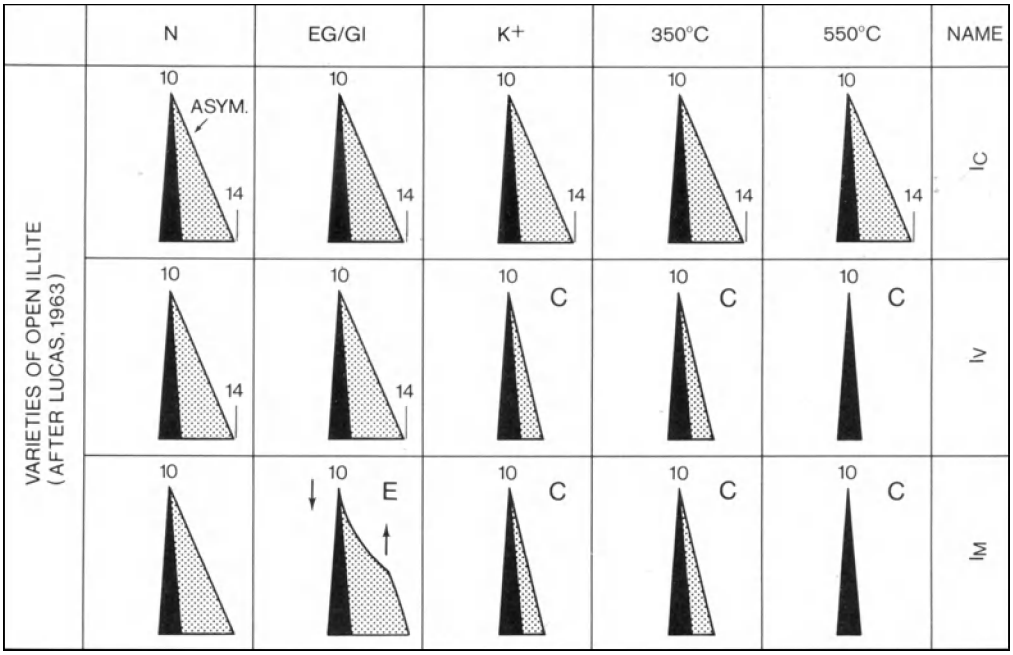

Figure II.1: Shapes of d(001) reflection in open illite, their interpretation and nomenclature (Thorez, 1976) .

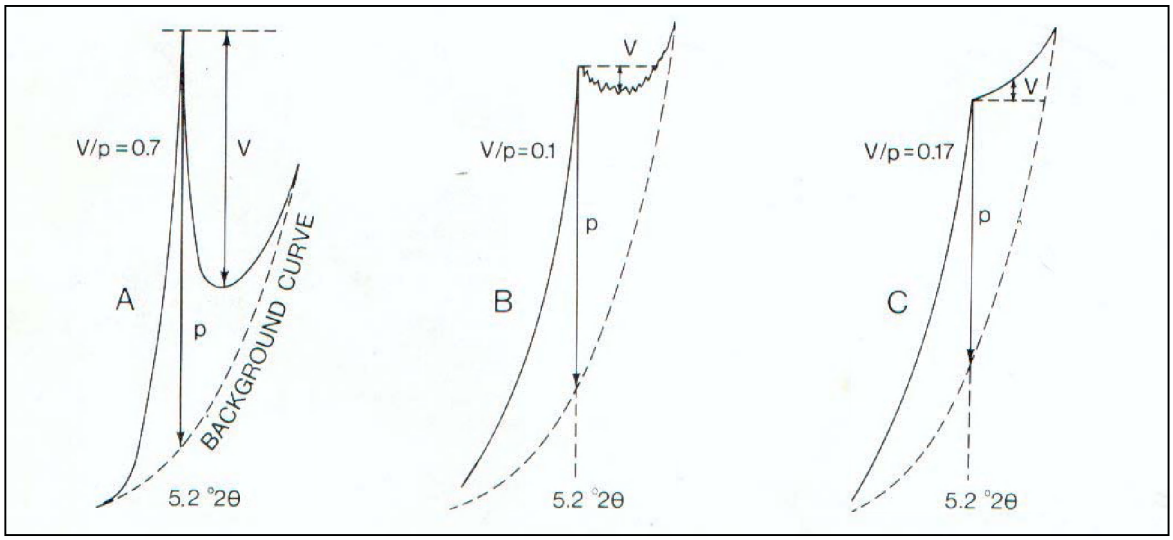

Figure II.2: V/P ratio for characterizing the crystallinity of smectite A: well crystallized and B & C: poorly crystallized smectites (Thorez, 1976).

Kaolinite

Kaolinite is characterized by the d(001)-reflection at 7.1 Å and the d(002)-reflection at 3.58 Å (distinguishing it from the 3,54 Å peak of chlorite), which remain unchanged after EG treatment but disappear after H treatment. The identification of kaolinite in the presence of chlorite is hindered by the fact that (00l) reflections of chlorite where l is even overlap with the kaolinite reflections and show the same behaviour as kaolinite after EG and H treatments. The variable crystallinity of the chlorite influences its stability at higher temperatures which makes heat treatments an unreliable criterion.

In the North Sea mud samples the presence of chlorite was checked at H 300 °C; only a

very poorly expressed chlorite d(001)-reflection could be observed. Therefore chlorite can not have much influence on the kaolinite peak and no further attempts were made to confirm the presence of kaolinite. Positive identification of kaolinite can be done by saturating it with DMSO which shifts the 7 Å peak to about 11 Å.

Chlorite

Chlorites have a very variable chemical composition. Most chlorites are rich in Mg but Fe-, Mn-, Co-, Cr- and Ni-rich varieties exist, with the iron variety as the most commonly occurring one. Reflections at 14 Å, 7 Å, 4.7 Å, 3.54 Å are present under N conditions and remain unchanged after EG treatment. On heating at 500 °C the 14 Å d(001) the peak position shifts to 13,6-13,8 Å whilst the intensity increases as a function of the iron content and the crystallinity of the chlorite present. Characteristically, the even 00l diffraction peaks disappear upon heating at 500-550°C.

Poorly crystallized chlorites however, as found in recent sediments, soils and altered rocks can decompose already at lower temperatures (see table II.2). The replacement of the brucite layer in the chlorite atomic pattern by hydrated cations leads to random interlayering patterns, sometimes described as 'degraded chlorite'.

Table II.2: Influence of crystallinity on the d(001)-peak of chlorites due to heating (Holtzapffel, 1985).

Chlorite (d001) in Å	N	EG	550°C
well crystallised chlorite	14	14	13.8-14 Å
bottom chlorite of degraded chlorite with instable interlayers	14	14	decomposed or between 10-13 Å
bottom chlorite	14	14	decomposed

Random mixed layer clay minerals

The can form mixed stacks in irregular proportions. These random individual clay minerals have similar crystallographic pattern and consequently, the mixed layer minerals have properties analogous to the individual composing minerals and proportional to their relative quantities in the mixed mineral.

Appendix III

Clay mineralogy of North Sea mud

Sample location and description

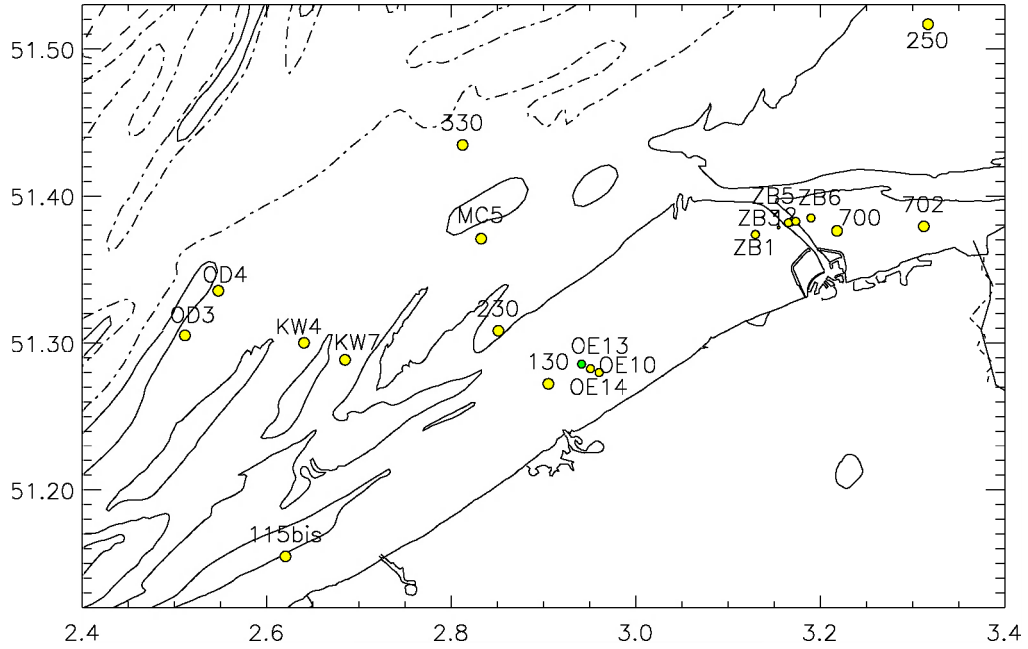

Figure III-1: Bottom samples on the BCS

Id	Description
BC0322_**115bis**	3 cm of very fine sand; underneath is black muddy sand Bc=Box core, Rk=Reineck corer; KW=Kwintebank, OD=Oostdyck, OE=Oostende)
BC0322_**130**	1 cm muddy sand on top with shells, 10 cm of black rather soft mud, 1 cm of muddy sand, black more consolidated mud beneath with layer of 'tubes' (2-3 mm diameter, 3-4 cm long) inside (box core full)
BC0322_**230**	Surface: 3 cm mud to sandy mud, living snail on top; 10 cm of fine sand with shell fragments and shells; 10 cm black muddy sand with shell fragments and shells, living Ensys
BC0322_**250**	Top: 3 cm fine sand; underneath: about 7 cm sand with shell fragments, lowest 10-15 cm black reduced sand with shell fragments and shells. Lot of living Ensys
BC0322_**330**	Top: 30 cm of medium sand with lot of shell fragments and some shells, a thin mud layer inside; underneath is gravel with pebbles of 1-10 cm
BC0322_**700**	Top: thin layer of grey silt, underneath black compact and consolidated mud from probably Holocene age with thin sandy mud layers inside
BC0322_**702**	5 cm soft silty mud above fine sand and at the bottom of the bucket black sand
BC0322_**MC5**	Fine sand with lot of shell fragments. On the surface are rather soft grey clay-pebbles of 1-5 cm. In the sand matrix some black clay lenses were found (separately sampled)
BC0322_**KW4**	Top: medium sand with lots of shell fragments and shells, clay pebbles are in and on top of the sand; at the bottom: fine sand within a layer of shell fragments
BC0322_**KW7**	Top: 30 cm of fine brown sand; underneath: black muddy sand with lots of shells
BC0322_**OD3**	Top: gravel with pebbles of 1-10 cm. no core sample
BC0322_**OD4**	on top is a thin layer of mud; 5 cm of medium sand underneath gravel with pebbles of 2-15 cm; no core sample
BC0227_**ZB1**	Surface: grey sand with shell fragments (1 cm); underneath: consolidated black mud
Rk0227_**ZB3**	soft mud
Rk0227_**ZB5**	surface: fine oxidated mud; underneath: gray consolidated fine silt
BC0227_**ZB6**	20 cm brown mud; underneath: black consolidated mud (full box core)
BC0304_**OE10**	Top: 5cm fluid mud, underneath 2cm medium sand; under black consolidated mud
BC0227_**OE13**	surface: 20cm green mud; underneath: consolidated black mud (box core full)
BC0304_**OE14**	Core full (50cm); Top: fluid mud (2-3cm); under 30 cm little bit compacted mud; 4-5 cm shell fragments+sand+mud; underneath black little compacted mud

BC=Box Core, RK=Reineck core

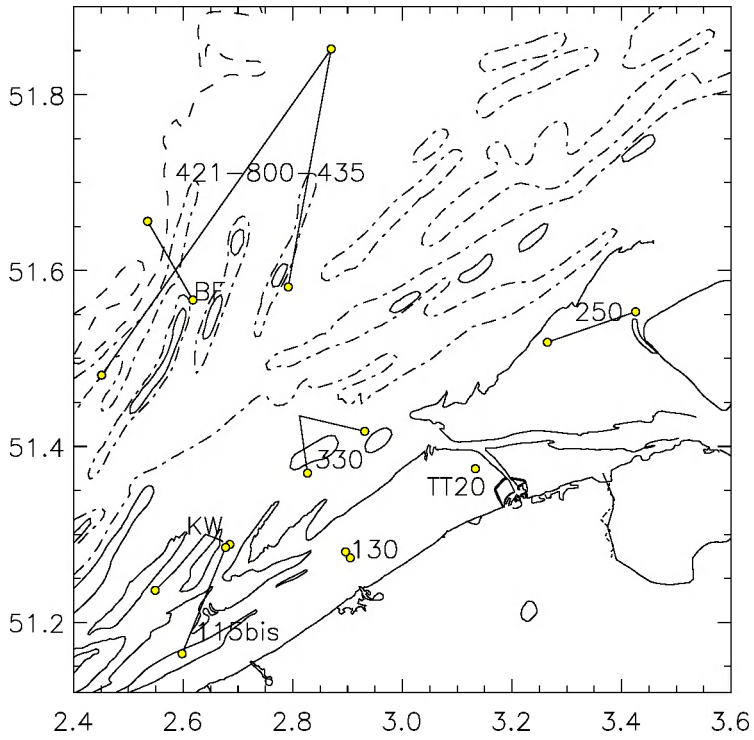

Figure III-2: Suspension samples from the BCS, which have been used for clay mineral analysis

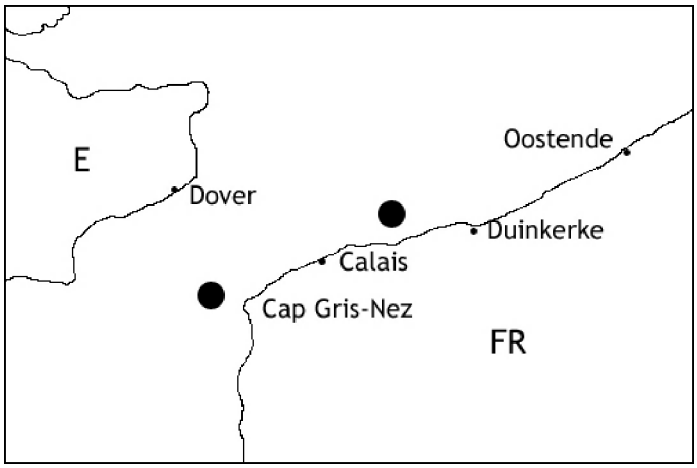

Figure III-3: Suspension samples from the Strait of Dover (R/V Belgica campaign 2004/03).

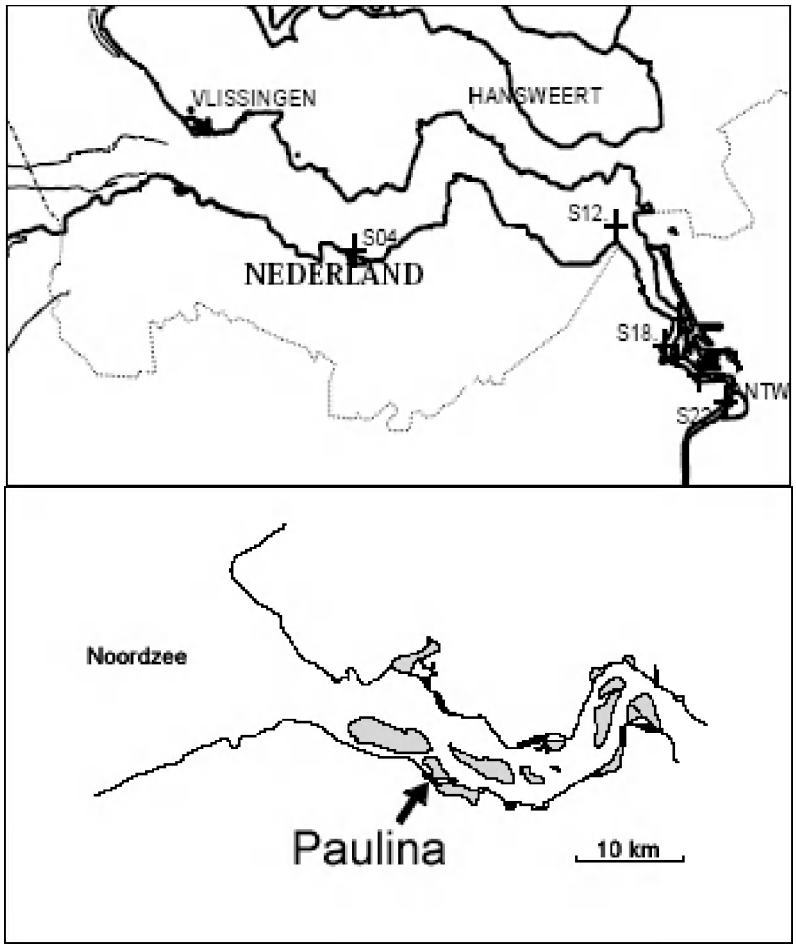

Figure III-4: Samples taken in the Schelde estuary.

Id	Description
VV0409_S4	Muddy sand, lot of shell fragments
VV0409_S12	Muddy sand
VV0409_S18	Muddy sand
VV0409_S22	Muddy sand

VV=Van Veen grab

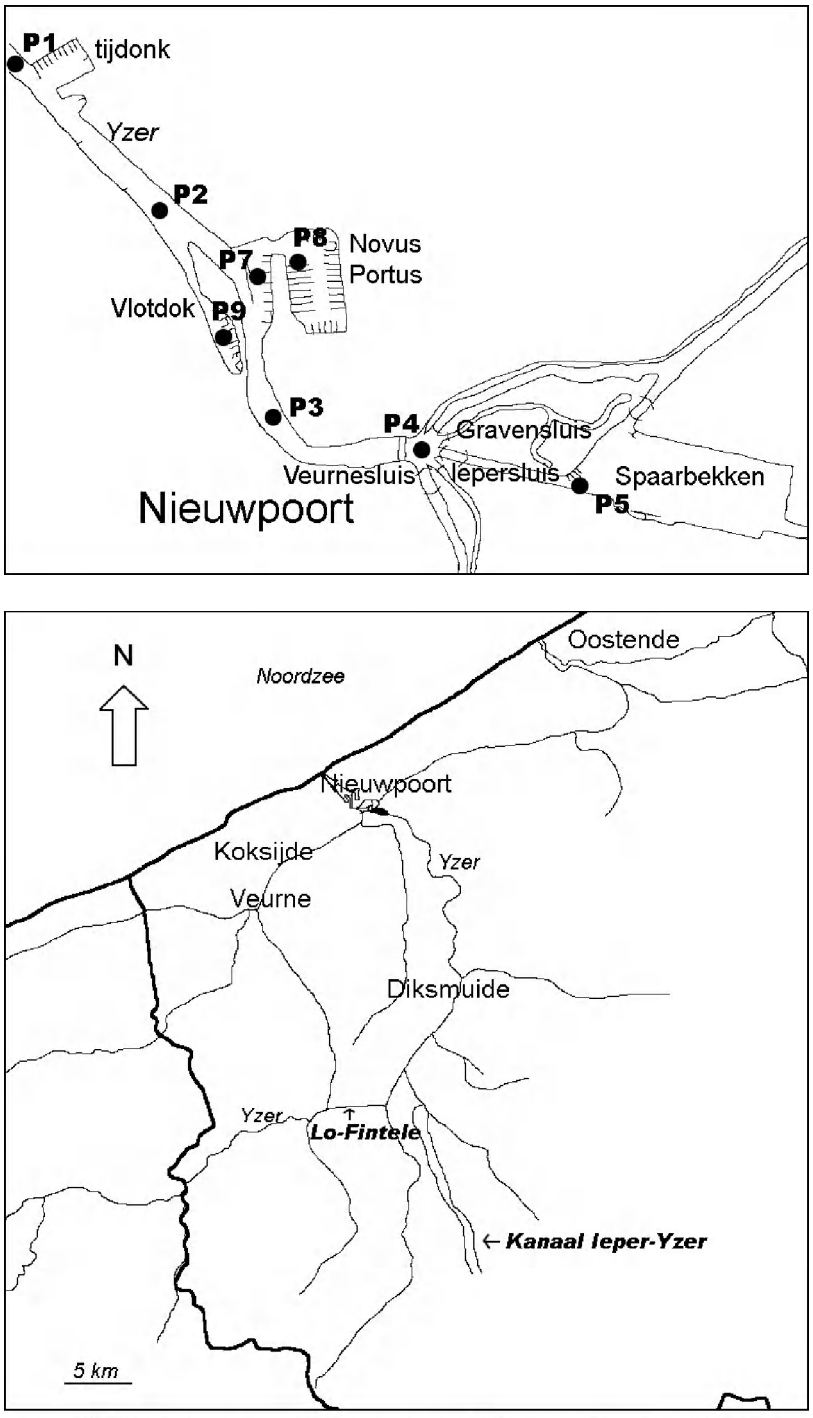

Figure III-5: Sample locations in the harbour of Nieuwpoort and the Yzer basin.

Appendix IV

Clay mineralogy of North Sea mud:

Identification and quantification of the clay minerals

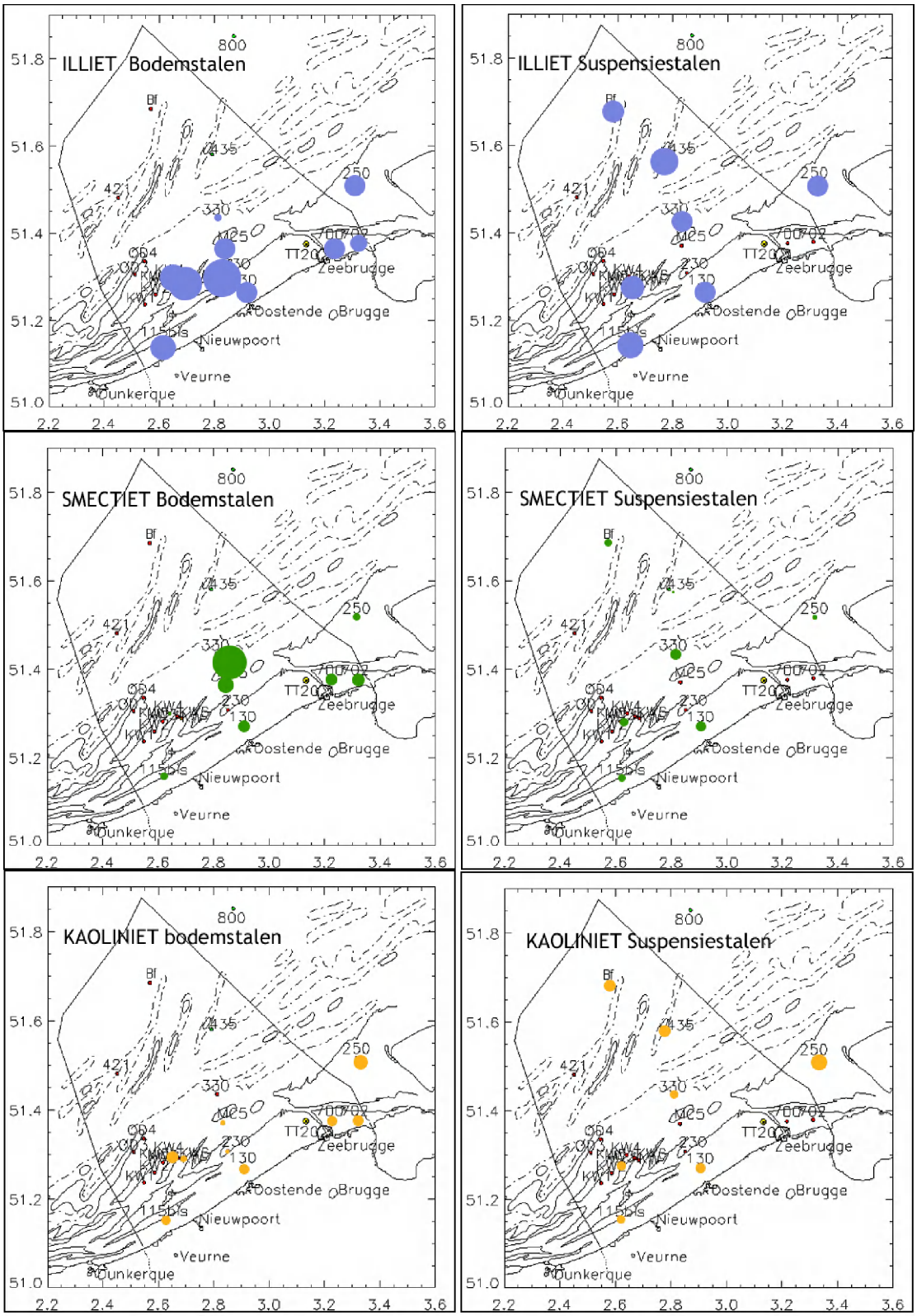

Figure IV-1: Clay mineralogy of the bottom (l) and suspension (r) samples on the BCS. The diameter of the circles is proportional to the content and the positioned on the map with their centre at the sample location.

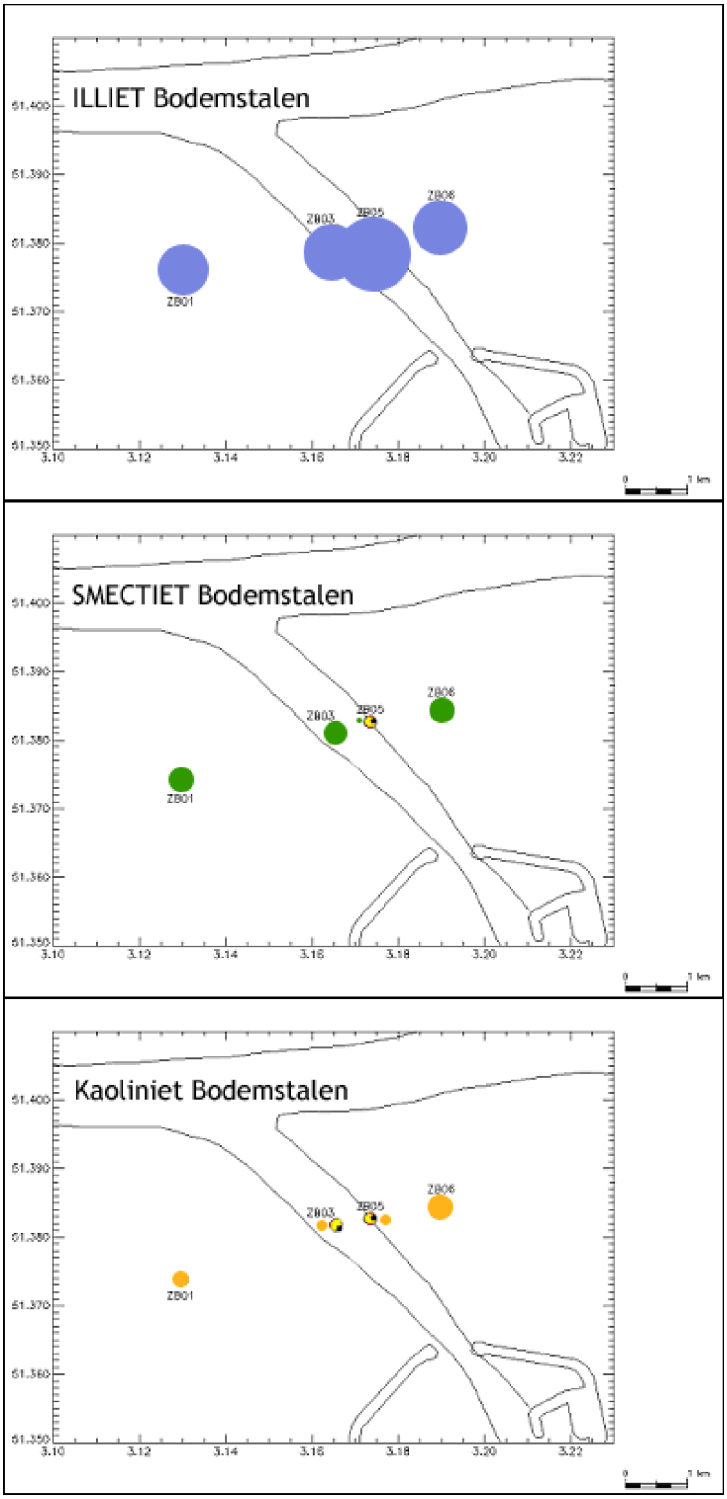

Figure IV-2: Clay mineralogy of the bottom samples in the vicinity of Zeebrugge. The diameter of the circles is proportional to the content and the positioned on the map with their centre at the sample location.

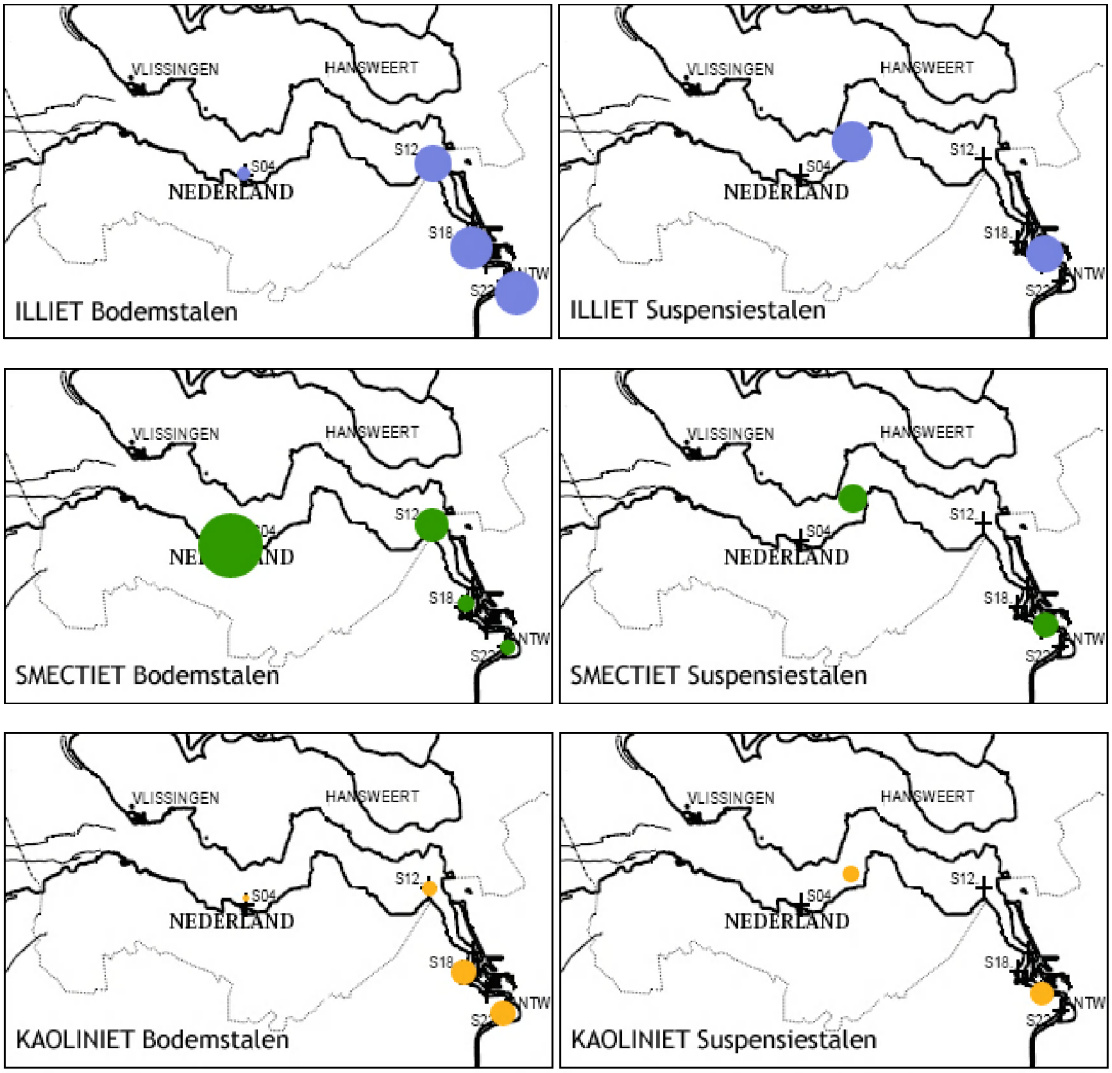

Figure IV-3: Clay mineralogy of the bottom (left) and suspension (right) samples in the Scheldt estuary. The diameter of the circles is proportional to the content and the positioned on the map with their centre at the sample location.

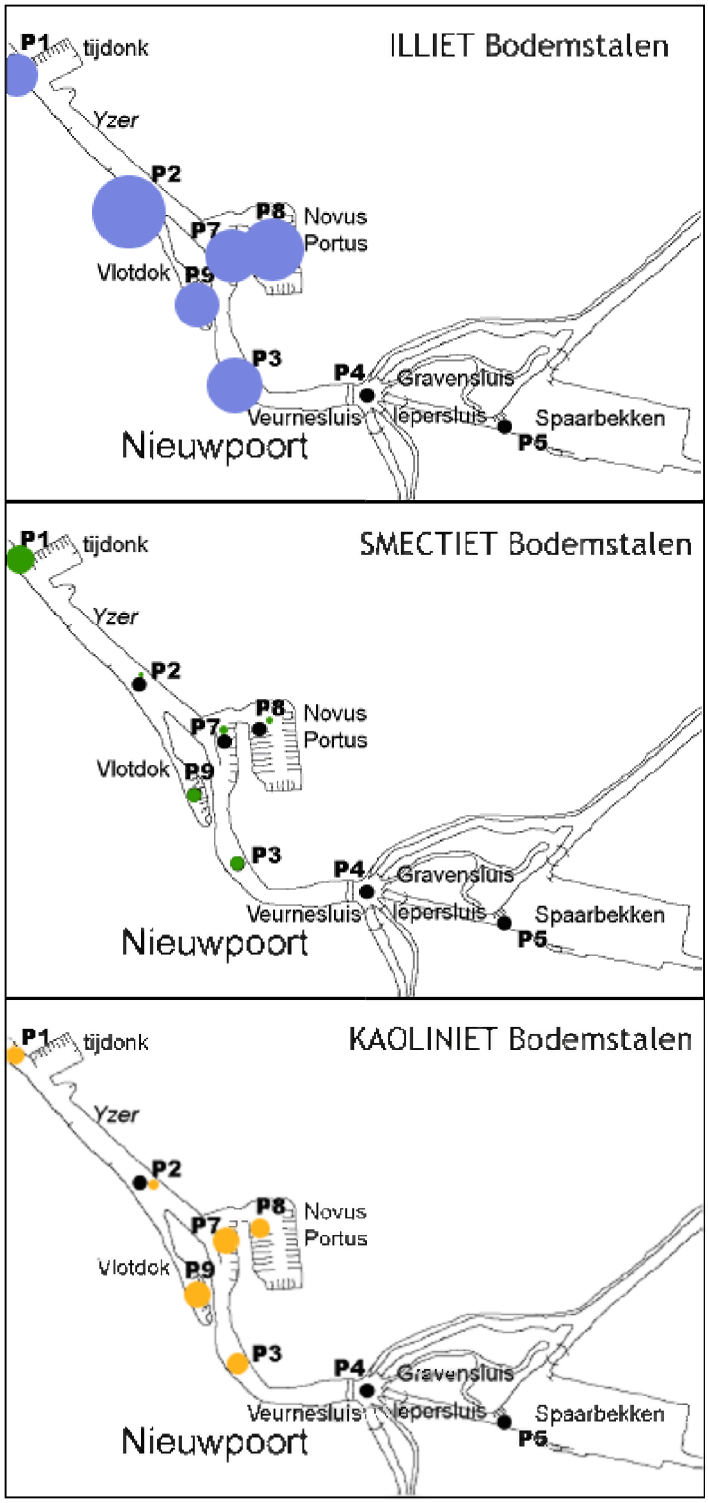

Figure IV-4: Clay mineralogy of the bottom samples from the harbour of Nieuwpoort. The diameter of the circles is proportional to the content and the positioned on the map with their centre at the sample location.

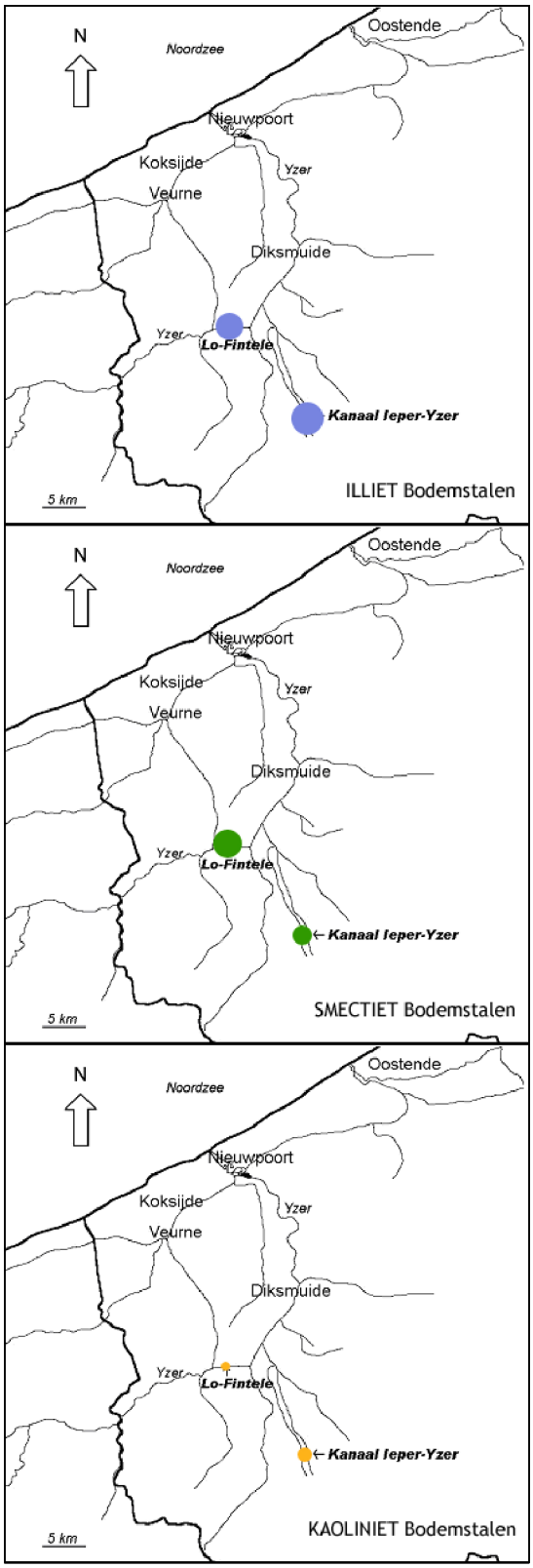

Figure IV-5: Clay mineralogy of the bottom samples from the river Yzer (Lo-Fintele and Kanaal Ieper-Yzer). The diameter of the circles is proportional to the content and the positioned on the map with their centre at the sample location.

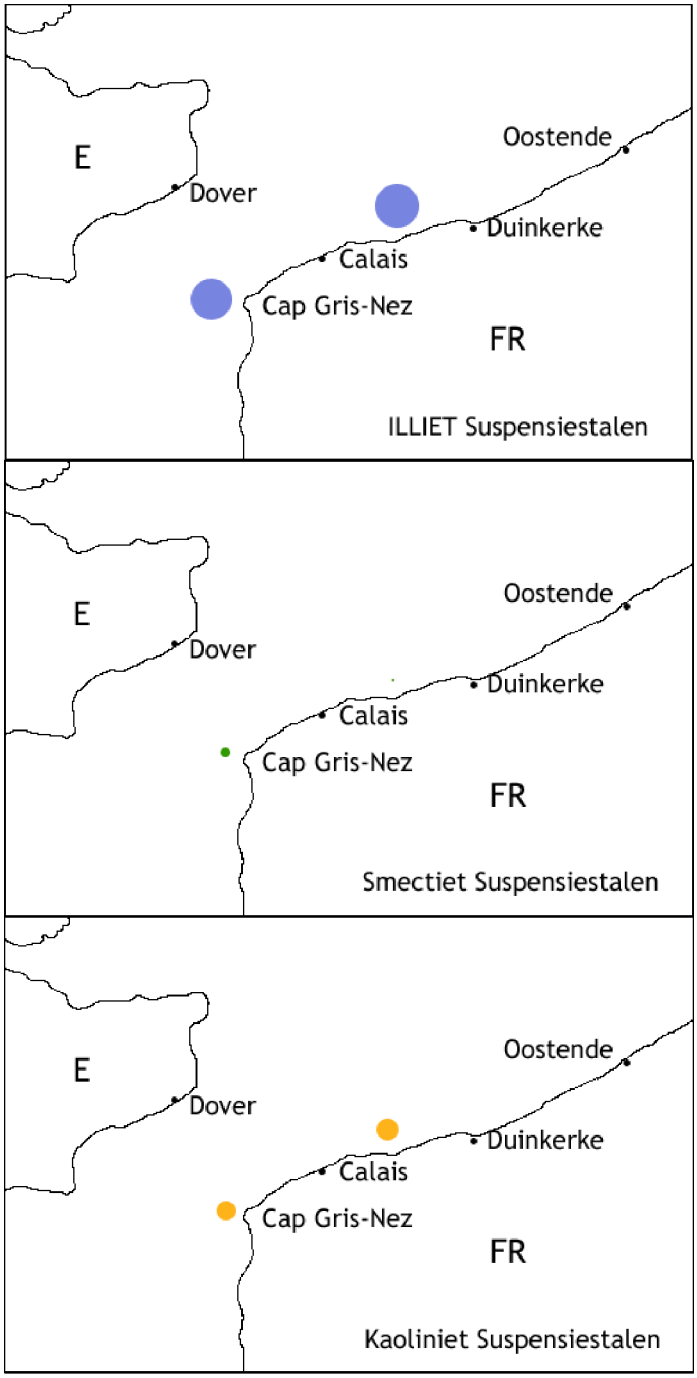

Figure IV-6: Clay mineralogy of the suspension samples from the Strait of Dover. The diameter of the circles is proportional to the content and the positioned on the map with their centre at the sample location.

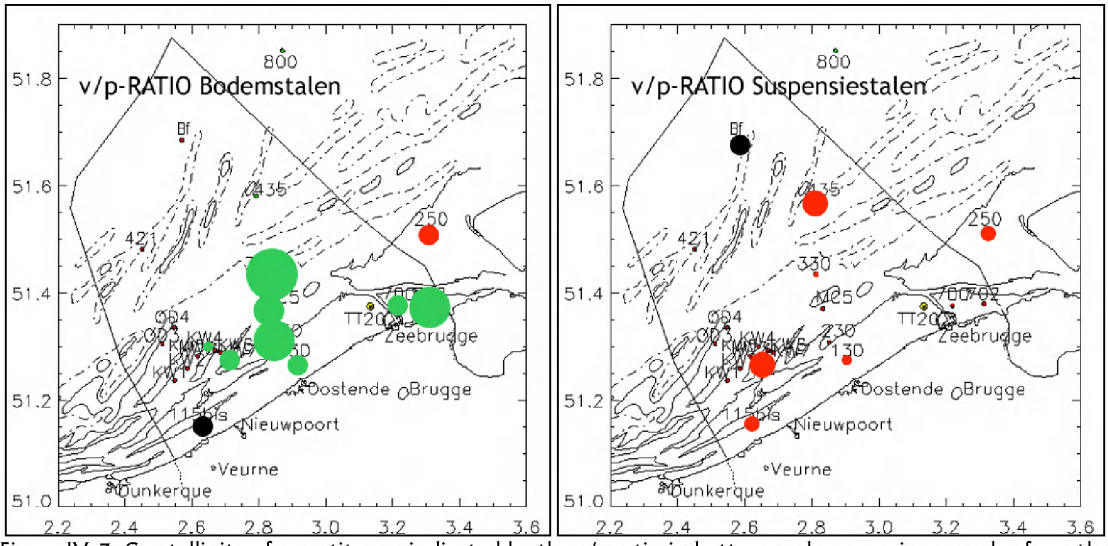

Figure IV-7: Crystallinity of smectites as indicated by the v/p ratio in bottom and suspension samples from the BCS. The v/p ratio is represented as a sphere with radius proportional to the absolute value of the ratio and a colour code for negative (red) and positive (green) values; zero values are represented by a black colour and with a radius without quantitative meaning.

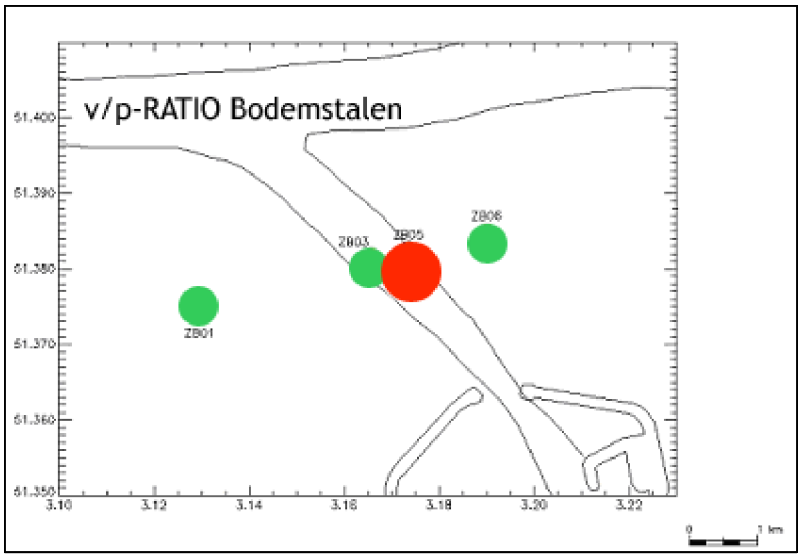

Figure IV-8: Crystallinity of the smectites as indicated by the v/p ratio in bottom samples near Zeebrugge. The v/p ratio is represented as a sphere with radius proportional to the absolute value of the ratio and a colour code for negative (red) and positive (green) values; zero values are represented by a black colour and with a radius without quantitative meaning.

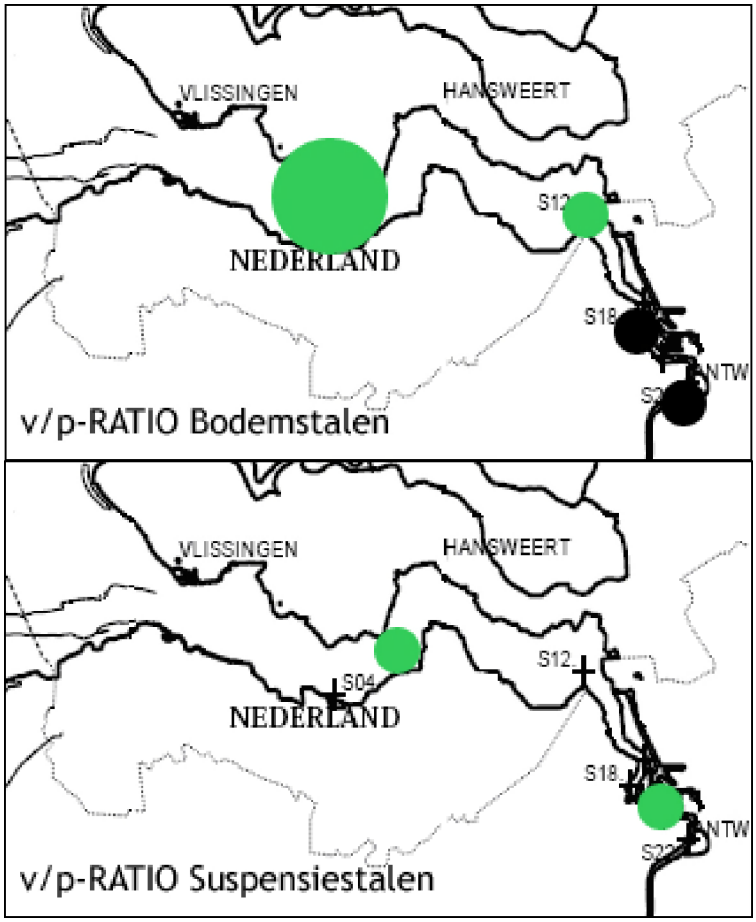

Figure IV-9: Crystallinity of the smectites as indicated by the v/p ratio in bottom and suspension samples of the Scheldt estuary. The v/p ratio is represented as a sphere with radius proportional to the absolute value of the ratio and a colour code for negative (red) and positive (green) values; zero values are represented by a black colour and with a radius without quantitative meaning.

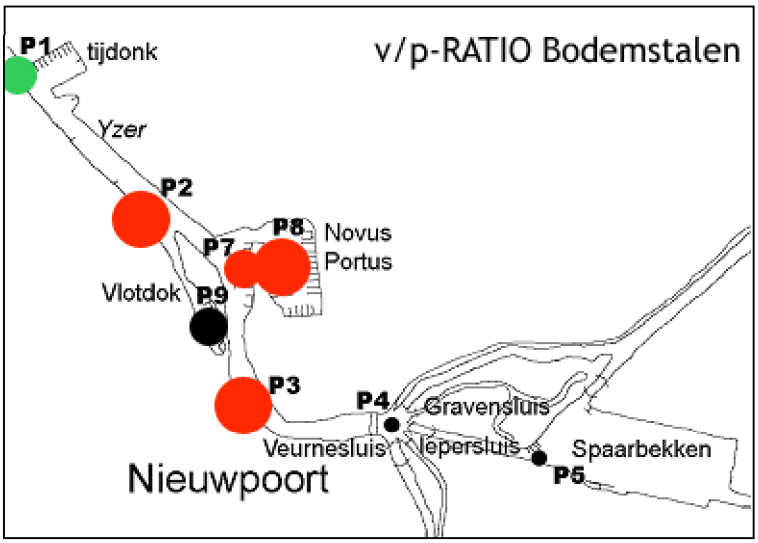

Figure IV-10: Crystallinity of the smectites as indicated by the v/p ratio in bottom samples from the harbour of Nieuwpoort. The v/p ratio is represented as a sphere with radius proportional to the absolute value of the ratio and a colour code for negative (red) and positive (green) values; zero values are represented by a black colour and with a radius without quantitative meaning.

Figure IV-11: Crystallinity of the smectites as indicated by the v/p ratio in bottom samples from the Yzer. The v/p ratio is represented as a sphere with radius proportional to the absolute value of the ratio and a colour code for negative (red) and positive (green) values; zero values are represented by a black colour and with a radius without quantitative meaning.

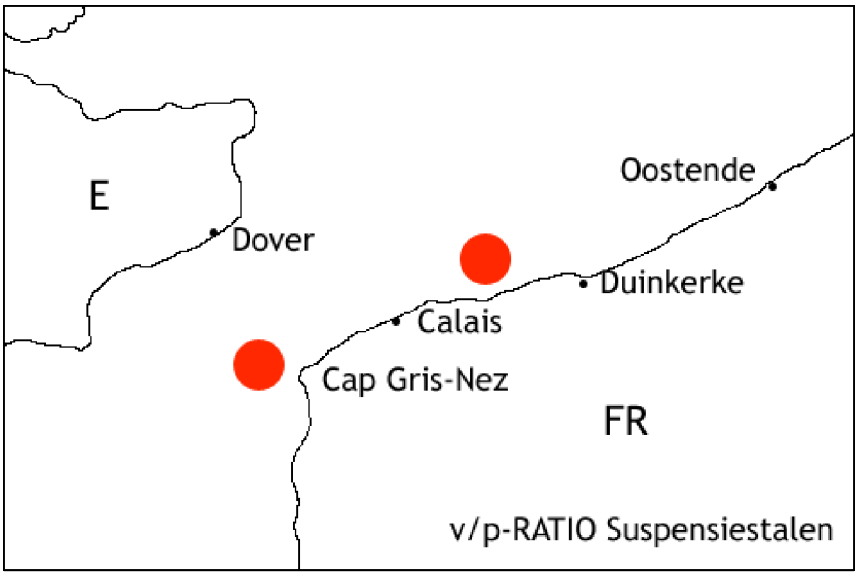

Figure IV-12: Crystallinity of the smectites as indicated by the v/p ratio in suspension samples from the Dover Strait. The v/p ratio is represented as a sphere with radius proportional to the absolute value of the ratio and a colour code for negative (red) and positive (green) values; zero values are represented by a black colour and with a radius without quantitative meaning.

Appendix V

Bulk density measurements of box core samples

Oostende area (old dumping site)

Box core Nr	Description
BC0405_OE1	Homogeneous fine sand
BC0405_OE3	Fine to medium sand, layer with shells and shell fragments at the bottom
BC0405_OE7	Fine to medium sand, layer with shells and shell fragments at the bottom
BC0405_OE11	Top: 1 cm of beige and non compacted (recent) mud, then 30-35 cm of dark mud then ~5 cm of dark fine sand then consolidated dark mud
BC0405_OE13	30/35 cm of grey mud
BC0405_OE14	Top: a few cm of beige non compacted (recent) mud then 30-35 cm of dark mud then ~5 cm of dark fine sand; at the bottom: dark and more compact mud
BC0405_OE17	Top: non compacted (recent) mud, then beige sandy mud then more compact mud
BC0405_OE22	Top: ~5cm of beige muddy sand then dark grey muddy sand

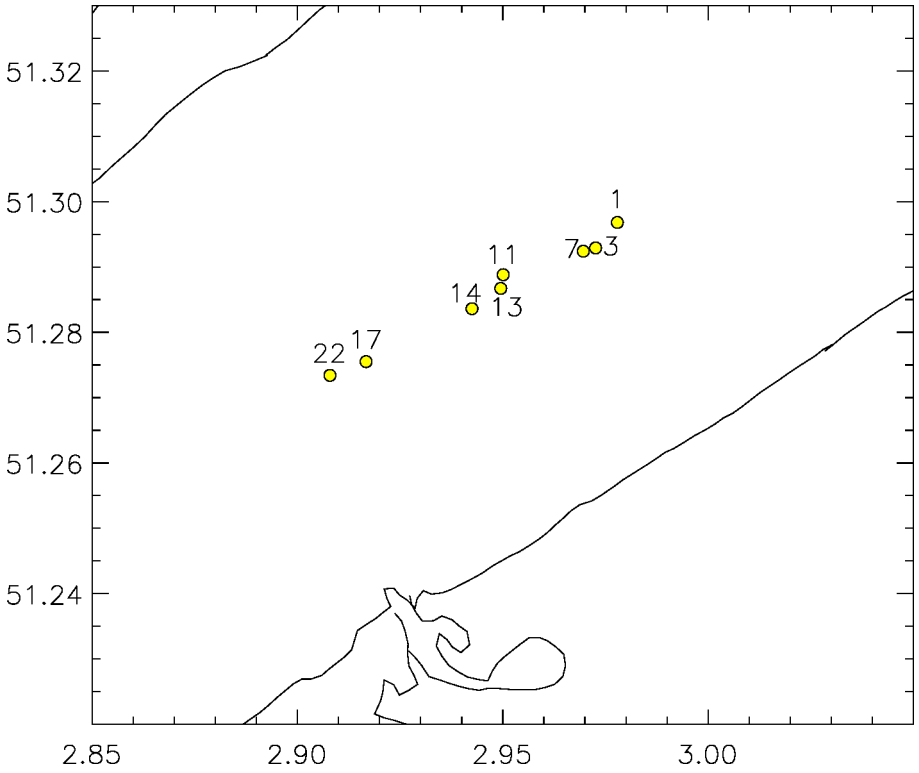

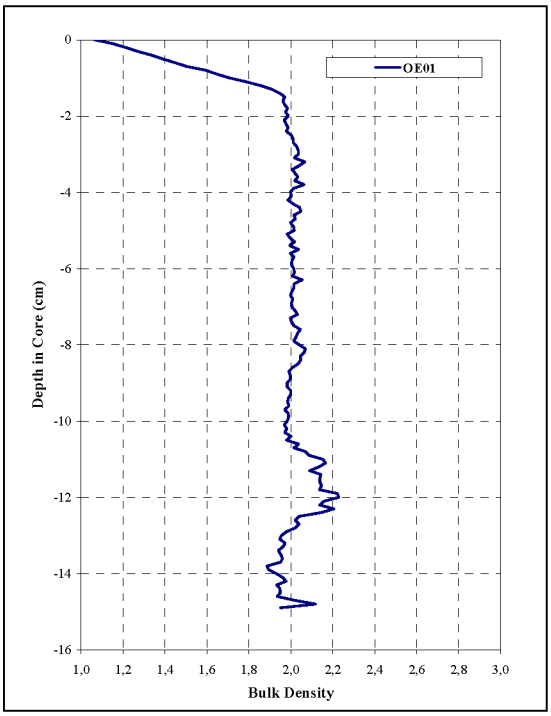
OE01
Depth in Core (cm)
0
-2
-4
-6
-8
-10
-12
-14
-16
1,0 1,2 1,4 1,6 1,8 2,0 2,2 2,4 2,6 2,8 3,0
Bulk Density

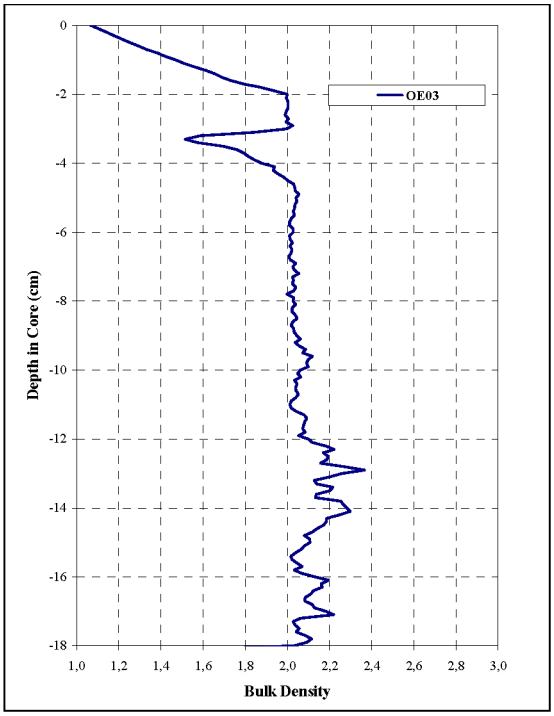
OE03
Depth in Core (cm)
0
-2
-4
-6
-8
-10
-12
-14
-16
-18
1,0 1,2 1,4 1,6 1,8 2,0 2,2 2,4 2,6 2,8 3,0
Bulk Density

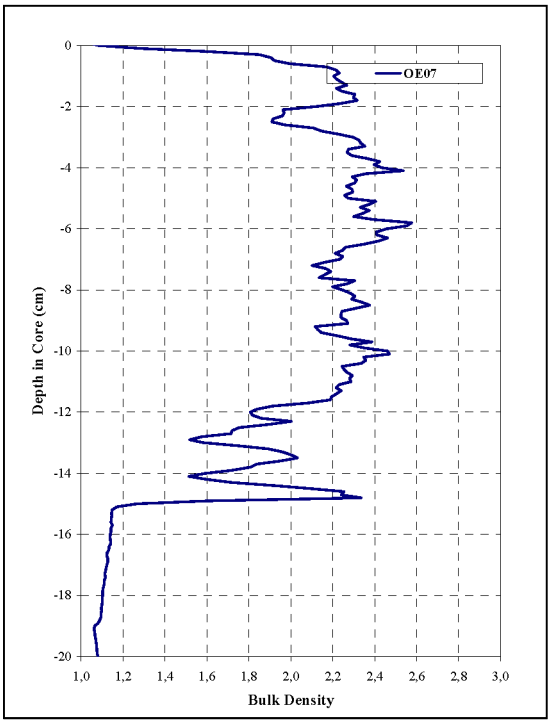
OE07
Depth in Core (cm)
0
-2
-4
-6
-8
-10
-12
-14
-16
-18
-20
1,0 1,2 1,4 1,6 1,8 2,0 2,2 2,4 2,6 2,8 3,0
Bulk Density

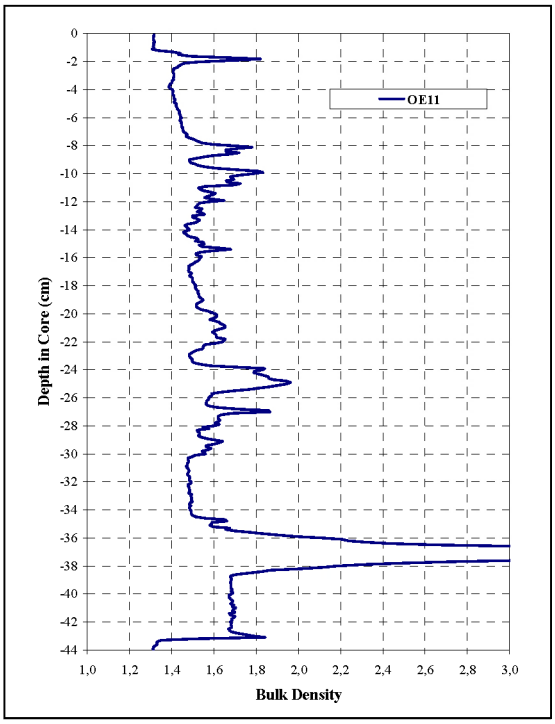
OE11
Depth in Core (cm)
0
-2
-4
-6
-8
-10
-12
-14
-16
-18
-20
-22
-24
-26
-28
-30
-32
-34
-36
-38
-40
-42
-44
1,0 1,2 1,4 1,6 1,8 2,0 2,2 2,4 2,6 2,8 3,0
Bulk Density

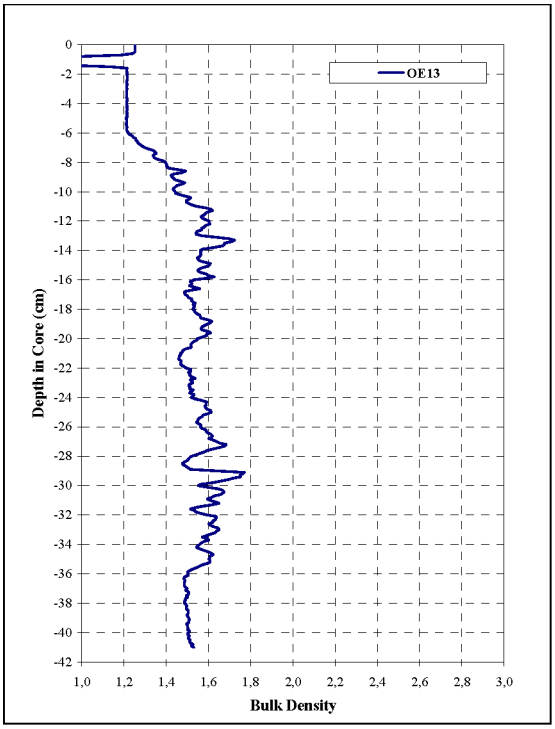
OE13
Depth in Core (cm)
Bulk Density

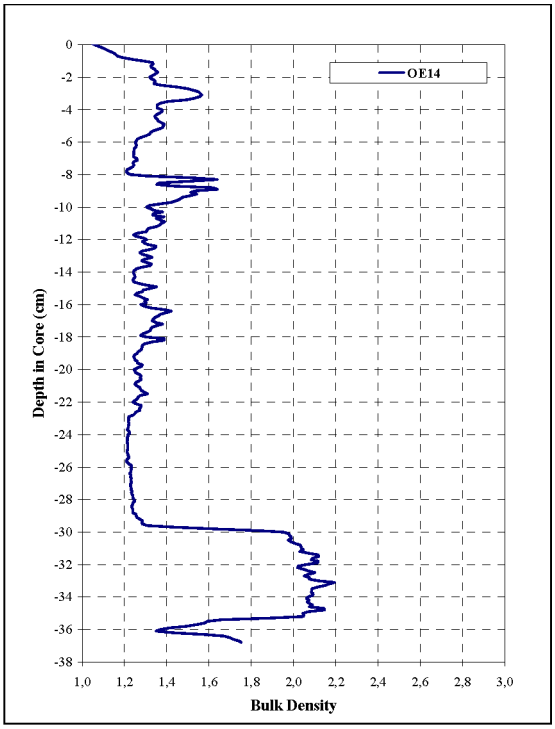
OE14
Depth in Core (cm)
Bulk Density

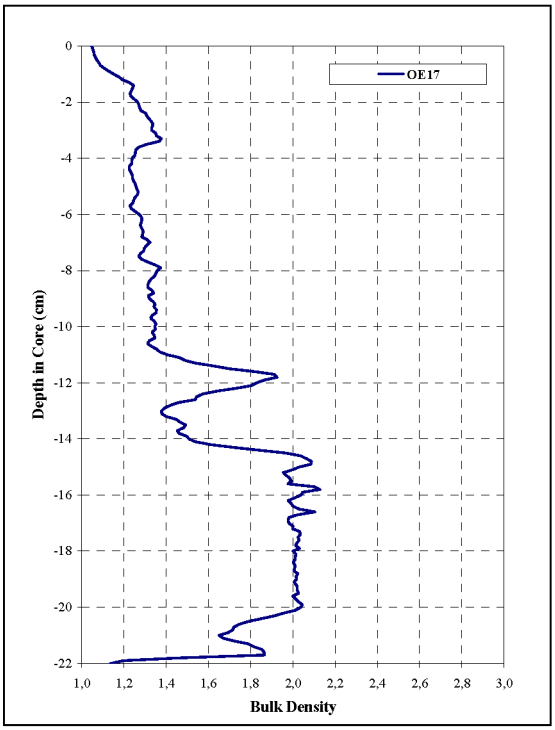
OE17
Depth in Core (cm)
Bulk Density

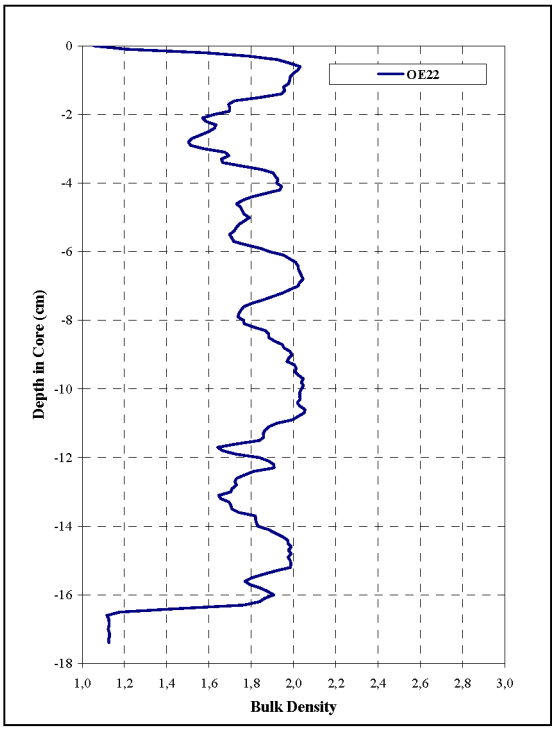
OE22
Depth in Core (cm)
Bulk Density

Zeebrugge area

Box core Nr	Description
BC0304_ZB1	Surface: 2mm of fresh mud; 4 cm muddy sand; beneath: consolidated mud
BC0304_ZB2	Surface: recent mud (several mm); underneath consolidated mud with shell fragment (<1 cm); then consolidated mud
BC0227_ZB6	Surface 20 cm brown mud; under: black consolidated mud (full box core)
BC0227_ZB7	Surface: green-grey sand with shells and broken shells; then: 0.5 cm sand with few shells; 1 cm mud; coarse sand with intercalation of mud; bottom: alternation of mud and coarse sand
BC0227_ZB08	Surface: sand with shells and shell fragments; then 15 cm sand; bottom black consolidated mud.

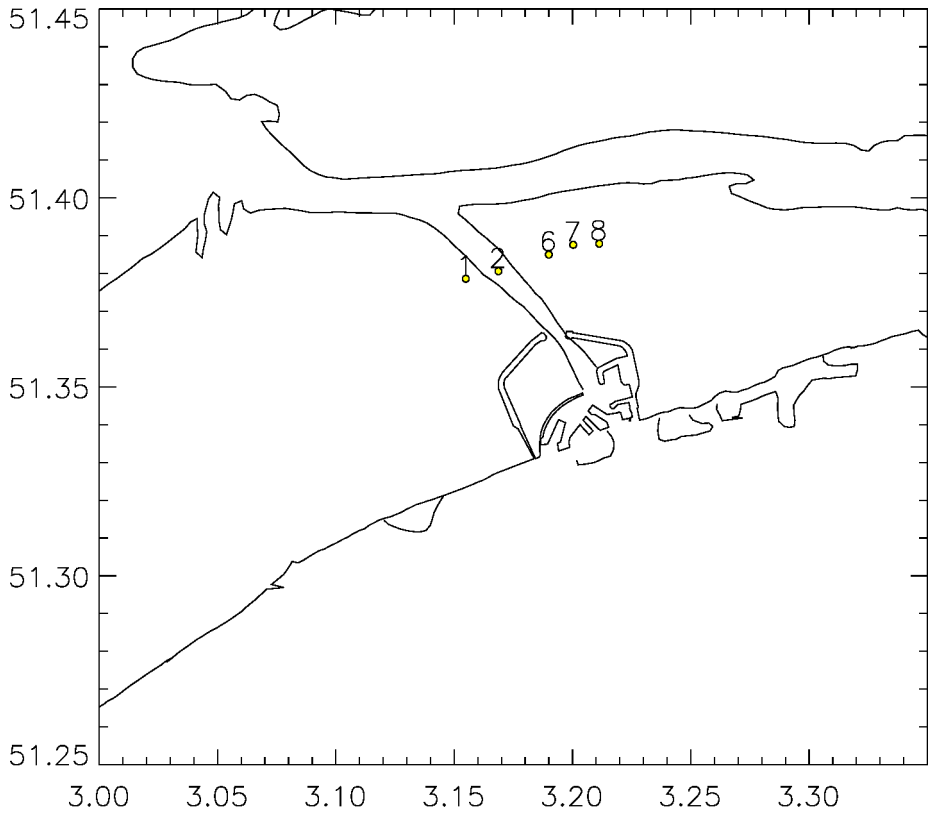

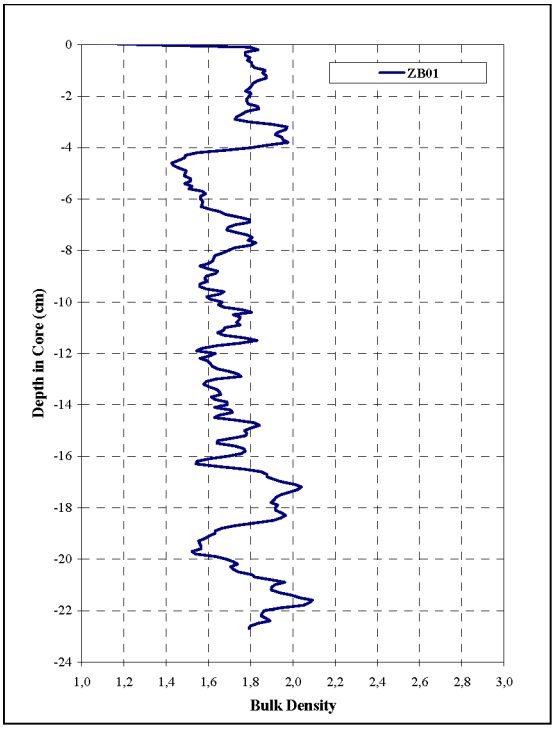
ZB01
Depth in Core (cm)
0
-2
-4
-6
-8
-10
-12
-14
-16
-18
-20
-22
-24
1,0 1,2 1,4 1,6 1,8 2,0 2,2 2,4 2,6 2,8 3,0
Bulk Density

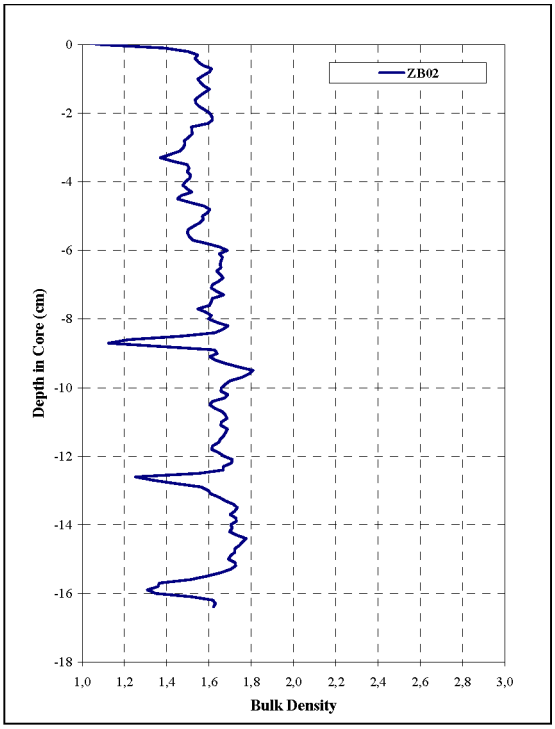
ZB02
Depth in Core (cm)
0
-2
-4
-6
-8
-10
-12
-14
-16
-18
1,0 1,2 1,4 1,6 1,8 2,0 2,2 2,4 2,6 2,8 3,0
Bulk Density

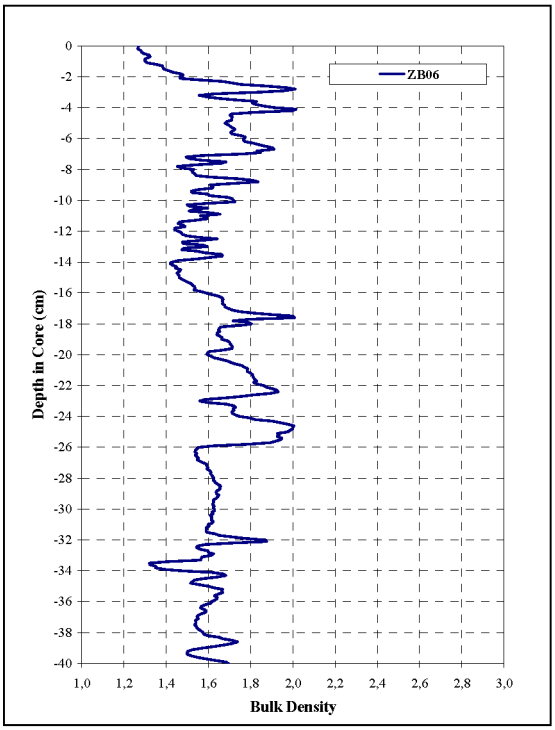
ZB06
Depth in Core (cm)
0
-2
-4
-6
-8
-10
-12
-14
-16
-18
-20
-22
-24
-26
-28
-30
-32
-34
-36
-38
-40
1,0 1,2 1,4 1,6 1,8 2,0 2,2 2,4 2,6 2,8 3,0
Bulk Density

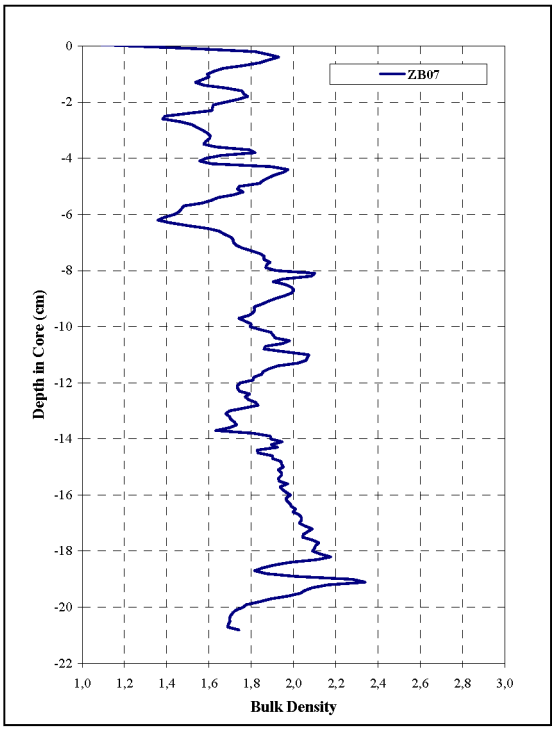
ZB07
Depth in Core (cm)
0
-2
-4
-6
-8
-10
-12
-14
-16
-18
-20
-22
1,0 1,2 1,4 1,6 1,8 2,0 2,2 2,4 2,6 2,8 3,0
Bulk Density

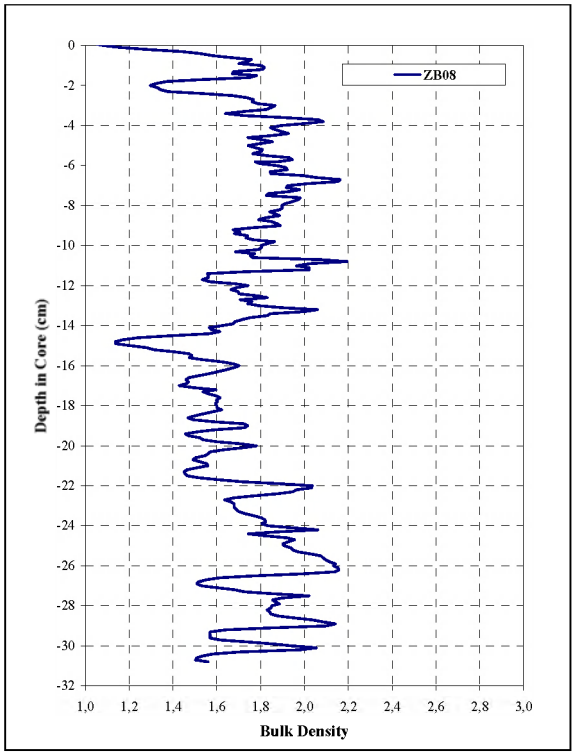
ZB08
Depth in Core (cm)
0
-2
-4
-6
-8
-10
-12
-14
-16
-18
-20
-22
-24
-26
-28
-30
-32
1,0
1,2
1,4
1,6
1,8
2,0
2,2
2,4
2,6
2,8
3,0
Bulk Density

Kwinte Bank

Box core Nr	Description
BC0322_KW1	fine homogeneous sand with shell fragments
BC0322_KW3	on top 2 mm mud; beneath: a few cm of sand with a lot of gravel and shells beneath: gravel layer with pebbles of 2 to 5 cm total thickness: 10cm
BC0322_KW4	medium sand with lots of shell fragments and shells, clay pebbles are in and on top of the sand, at the bottom: fine sand within a layer of shell fragments
BC0322_KW5	clean sand muddy black spots at a depth from 15 cm on
BC0322_KW6	25 cm fine to medium clean sand without shells
BC0322_KW7	30 cm of fine brown sand, underneath: black muddy sand with lots of shells

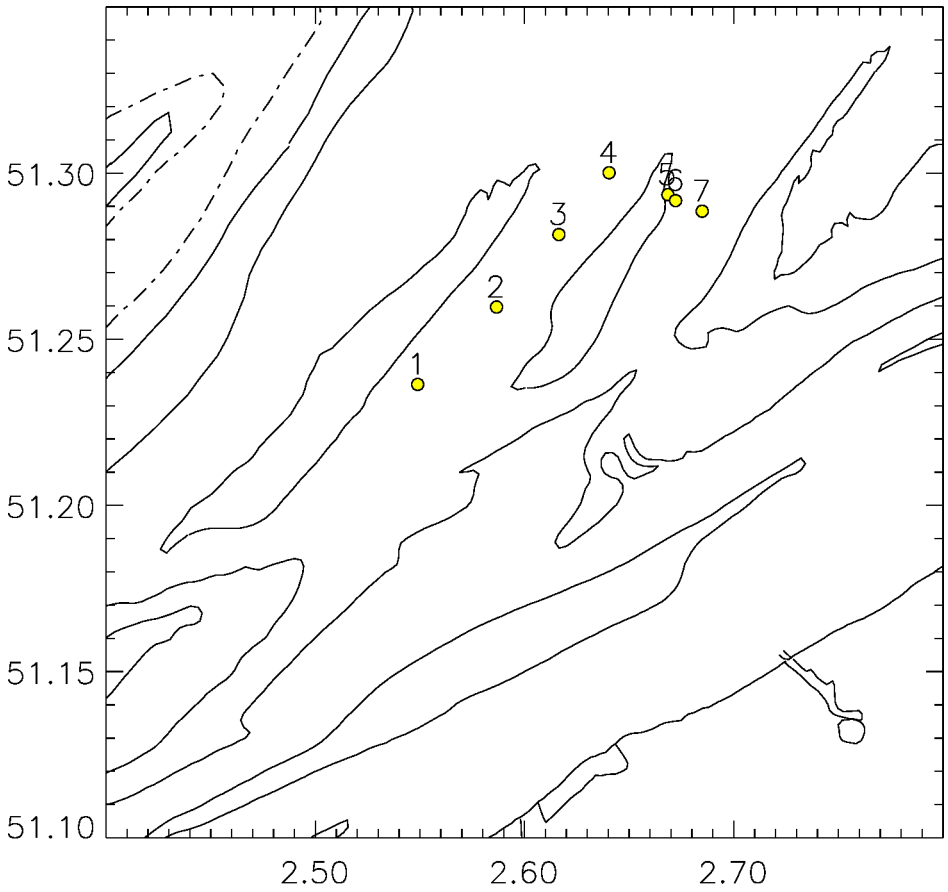

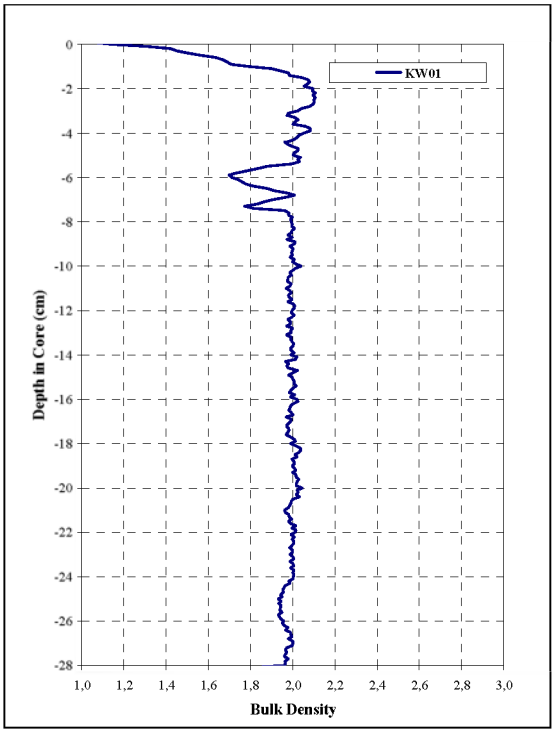
KW01
Depth in Core (cm)
Bulk Density

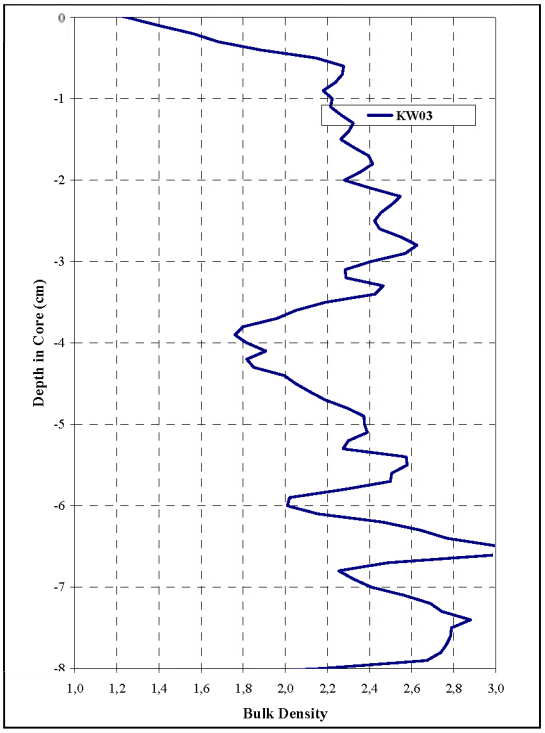
KW03
Depth in Core (cm)
Bulk Density

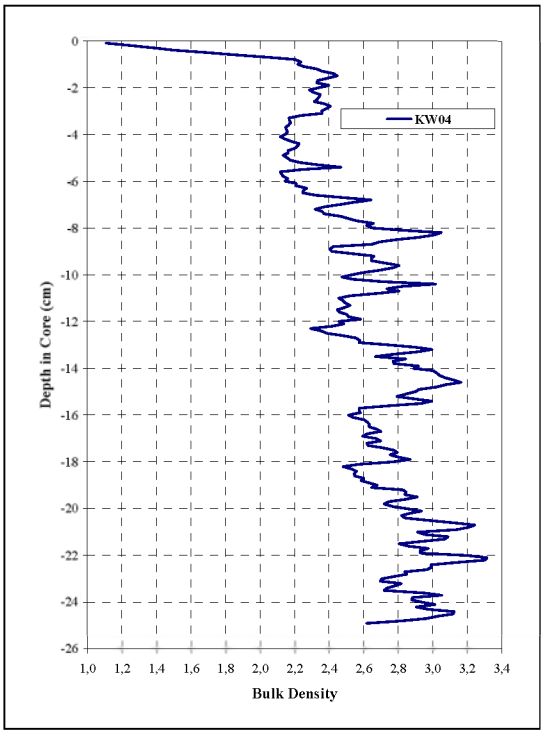
KW04
Depth in Core (cm)
Bulk Density

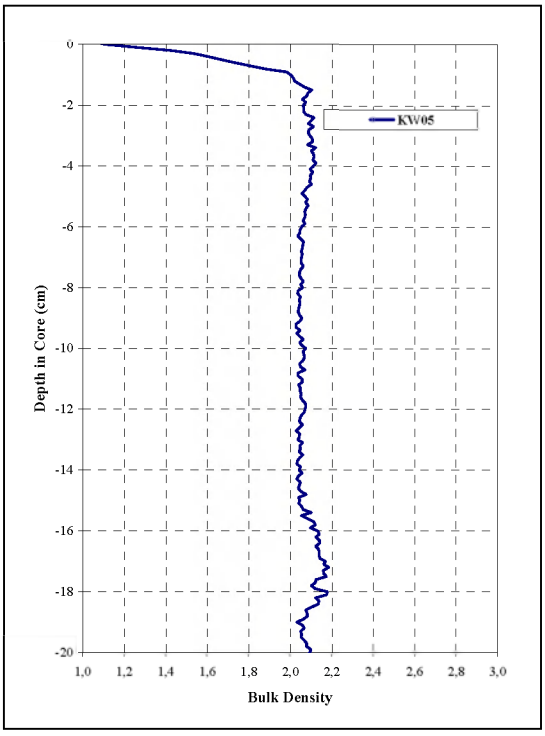
KW05
Depth in Core (cm)
Bulk Density

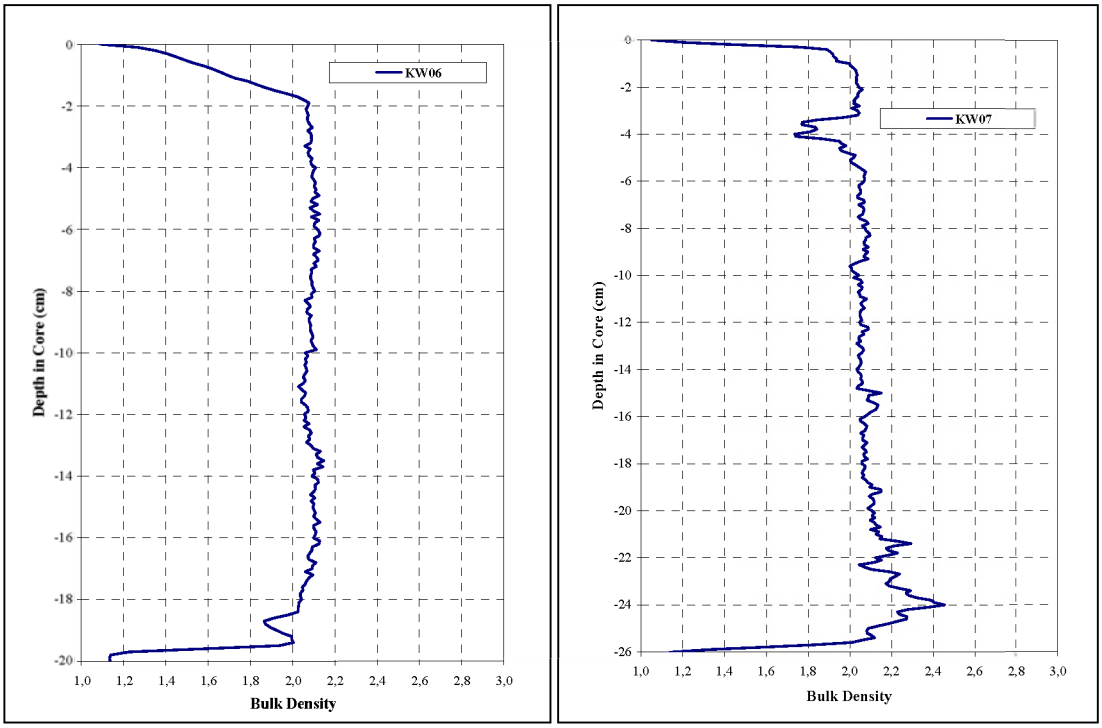
KW06
Depth in Core (cm)
0
-2
-4
-6
-8
-10
-12
-14
-16
-18
-20
1,0
1,2
1,4
1,6
1,8
2,0
2,2
2,4
2,6
2,8
3,0
Bulk Density
KW07
Depth in Core (cm)
0
-2
-4
-6
-8
-10
-12
-14
-16
-18
-20
-22
-24
-26
1,0
1,2
1,4
1,6
1,8
2,0
2,2
2,4
2,6
2,8
3,0
Bulk Density

MUMM monotorings point on theBCS

Box core Nr	description
BC0322_**115bis**	3 cm of very fine sand; underneath there is black muddy sand
BC0322_**130**	Bucket was completely full. 1 cm muddy sand on top with shells; 10 cm of black rather soft mu; 1 cm of muddy sand; black more consolidated mud beneath with layer of 'tubes' (2-3 mm diameter, 3-4 cm long) inside
BC0322_**230**	3 cm of mud to sandy mud, living snail on top; underneath: 10 cm of fine sand with shell fragments and shells; 10 cm black muddy sand with shell fragments and shells, living *ensys*
BC0322_**250**	surface: 3 cm fine sand; underneath: about 7 cm sand with shell fragments, lowest 10-15 cm black reduced sand with shell fragments and shells. Lot of living *ensys*
BC0322-**330**	30 cm of medium sand with lot of shell fragments and some shells, a thin mud layer inside; underneath is gravel with pebbles of 1-10 cm
BC0322_**700**	Surface: thin layer of gray silt; underneath black compact and consolidated mud with thin sandy mud layers inside
BC0322_**702**	5 cm soft silty mud above fine sand and at the bottom of the bucket black sand
BC0322_**MC5**	Fine sand with lot of shell fragments. On the surface are rather soft gray clay-pebbles of 1-5 cm. In the sand matrix some black clay-lenses were found (seperately sampled)

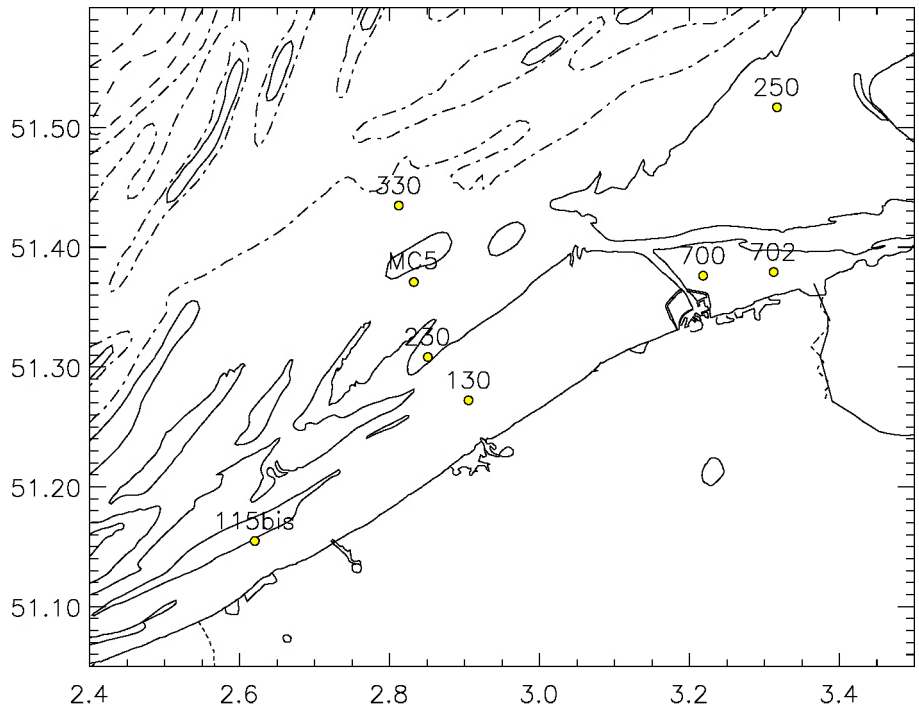

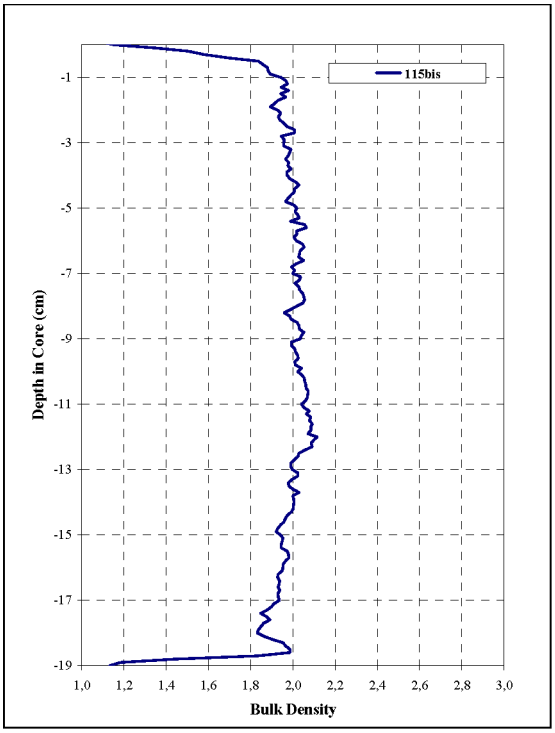
115bis
Depth in Core (cm)
-1
-3
-5
-7
-9
-11
-13
-15
-17
-19
1,0 1,2 1,4 1,6 1,8 2,0 2,2 2,4 2,6 2,8 3,0
Bulk Density

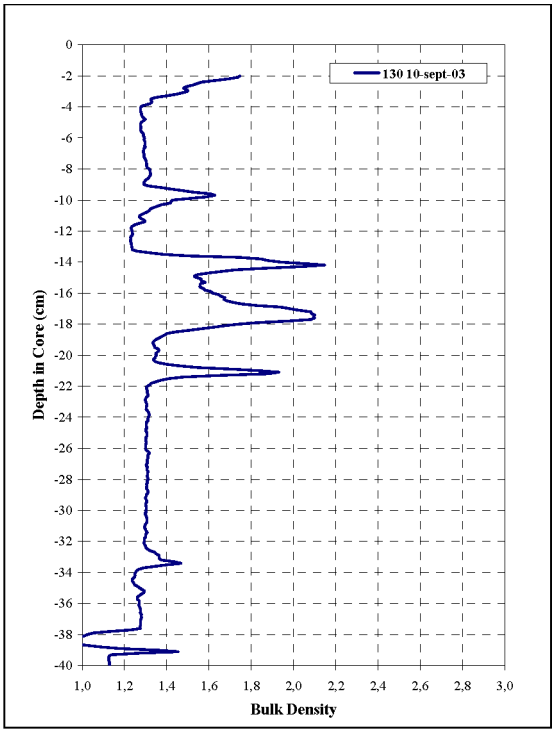
130 10-sept-03
Depth in Core (cm)
0
-2
-4
-6
-8
-10
-12
-14
-16
-18
-20
-22
-24
-26
-28
-30
-32
-34
-36
-38
-40
1,0 1,2 1,4 1,6 1,8 2,0 2,2 2,4 2,6 2,8 3,0
Bulk Density

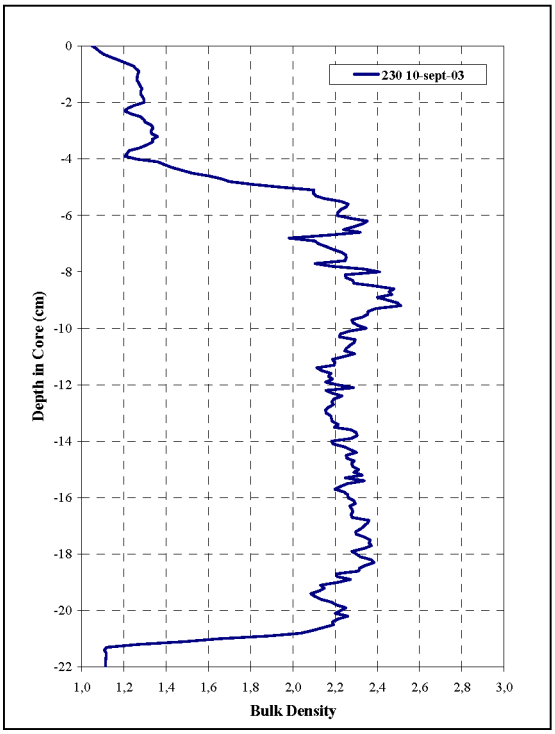
230 10-sept-03
Depth in Core (cm)
0
-2
-4
-6
-8
-10
-12
-14
-16
-18
-20
-22
1,0 1,2 1,4 1,6 1,8 2,0 2,2 2,4 2,6 2,8 3,0
Bulk Density

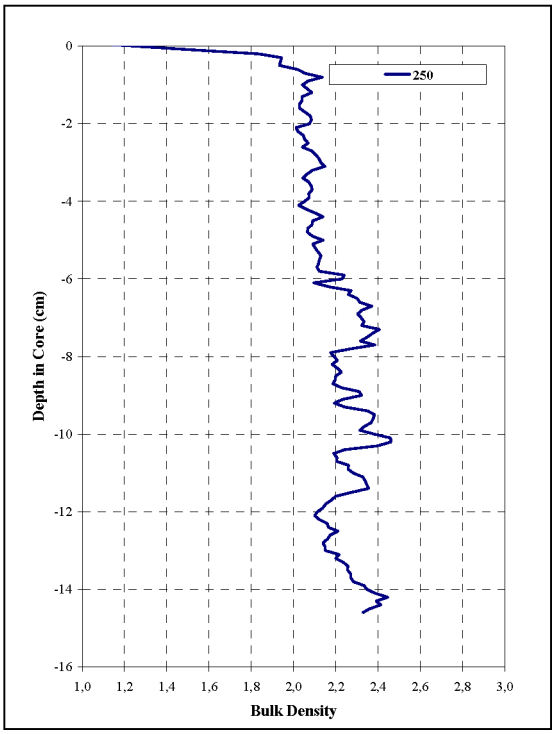
250
Depth in Core (cm)
0
-2
-4
-6
-8
-10
-12
-14
-16
1,0 1,2 1,4 1,6 1,8 2,0 2,2 2,4 2,6 2,8 3,0
Bulk Density

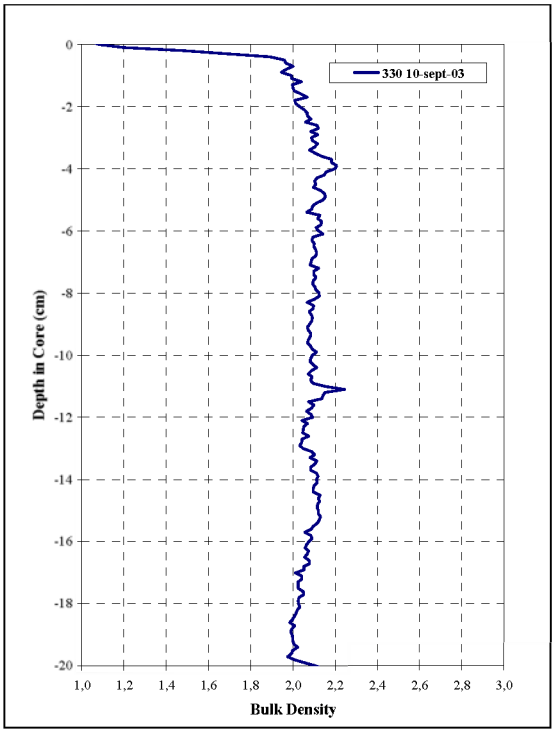
330 10-sept-03
Depth in Core (cm)
Bulk Density

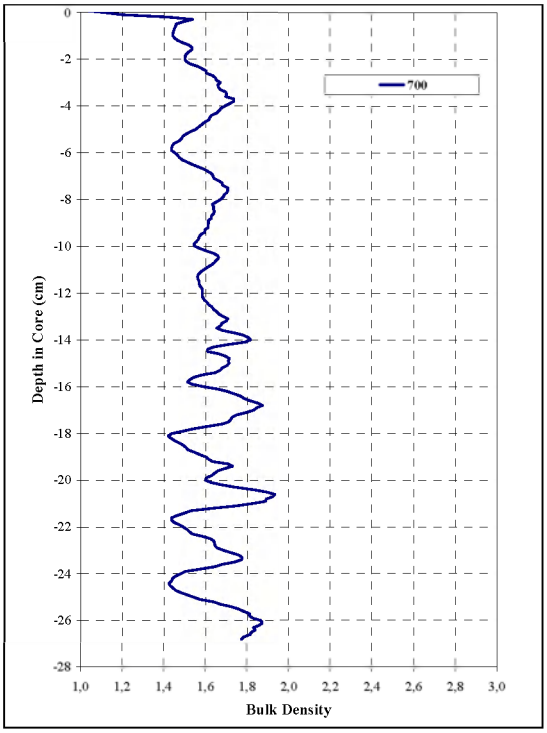
700
Depth in Core (cm)
Bulk Density

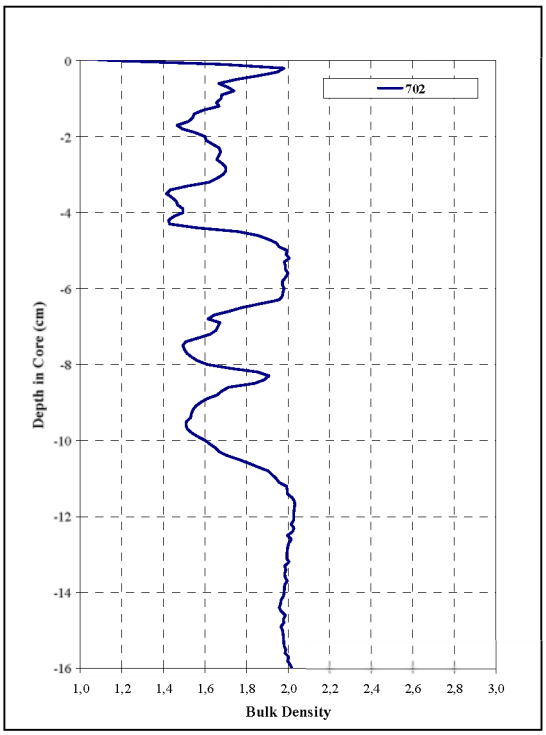
702
Depth in Core (cm)
Bulk Density

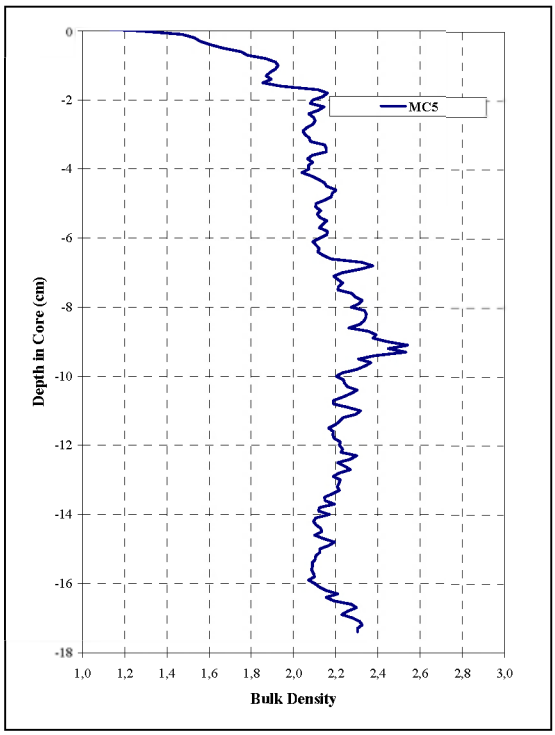
MC5
Depth in Core (cm)
Bulk Density